

UNCLASSIFIED

AD NUMBER
AD824657
NEW LIMITATION CHANGE
TO Approved for public release, distribution unlimited
FROM Distribution authorized to U.S. Gov't. agencies and their contractors; Critical Technology; OCT 1967. Other requests shall be referred to Air Force Flight Dynamics Laboratory, Attn: FDDA, Wright-Patterson AFB, OH 45433.
AUTHORITY
AFFDL ltr dtd 29 Oct 1973

THIS PAGE IS UNCLASSIFIED

AD-824 657

AFFDL-TR-67-97

BOUNDARY LAYER PRESSURE FLUCTUATIONS AND STRUCTURAL RESPONSE

DEANE R. BLACKMAN
DUNCAN M. CLARK
GEORGE J. McNULTY
JOHN F. WILBY

UNIVERSITY OF SOUTHAMPTON
HAMPSHIRE, ENGLAND

TECHNICAL REPORT AFFDL-TR-67-97

OCTOBER 1967

This document is subject to specific export controls and each transmittal to foreign governments or foreign nationals may be made only with prior approval of AFFDL (FDDA).

AIR FORCE FLIGHT DYNAMICS LABORATORY
RESEARCH AND TECHNOLOGY DIVISION
AIR FORCE SYSTEMS COMMAND
WRIGHT-PATTERSON AIR FORCE BASE, OHIO

FILE COPY

20070919134

NOTICES

When Government drawings, specifications, or other data are used for any purpose other than in connection with a definitely related Government procurement operation, the United States Government thereby incurs no responsibility nor any obligation whatsoever; and the fact that the Government may have formulated, furnished, or in any way supplied the said drawings, specifications, or other data, is not to be regarded by implication or otherwise as in any manner licensing the holder or any other person or corporation, or conveying any rights or permission to manufacture, use, or sell any patented invention that may in any way be related thereto.

Copies of this report should not be returned to the Air Force Flight Dynamics Laboratory unless return is required by security considerations, contractual obligations, or notice on a special document.

BOUNDARY LAYER PRESSURE FLUCTUATIONS AND STRUCTURAL RESPONSE

*DEANE R. BLACKMAN
DUNCAN M. CLARK
GEORGE J. McNULTY
JOHN F. WILBY*

*UNIVERSITY OF SOUTHAMPTON
HAMPSHIRE, ENGLAND*

This document is subject to specific export controls and each transmittal to foreign governments or foreign nationals may be made only with prior approval of AFFDL (FDDA).

FOREWORD

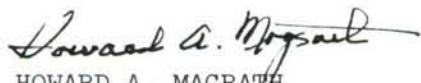
This report was prepared by the Institute of Sound and Vibration Research at the University of Southampton, England, for the Aero-Acoustics Branch, Vehicle Dynamics Division, Air Force Flight Dynamics Laboratory, Wright-Patterson Air Force Base, Ohio under Contract AF61(052)-756. This research is part of a continuing effort to obtain advanced data and techniques for defining vibration and acoustic phenomena in flight vehicles under the Air Force System Command's exploratory development program. The Project Number is 1471 "Aero-Acoustic Problems," and Task Number 147102 "Prediction and Control of Noise." Mr. P. H. Hermes and later Mr. D. L. Smith of the Aero-Acoustics Branch were task engineers.

The contract was administered by the Air Force Flight Dynamics Laboratory through the European Office of Aerospace Research (OAR), United States Air Force.

The period covered by this contract is from 1 November 1963 to 30 November 1966. This report which discusses a complete phase of the research work is one of two reports generated under the contract. These reports conclude the work on Contract AF61(052)-756. The Laminar-Turbulent Transition Region investigation, initiated under Contract AF61(052)-358, was carried out by Dr. D. R. Blackman, the Wind Tunnel Noise investigation was undertaken by Mr. D. M. Clark and the Structural Response work was undertaken by Mr. G. J. McNulty. The last two investigations were carried out in association with Mr. J. F. Wilby. The assistance of Professor E. J. Richards, Dr. D. J. Mead and Dr. M. K. Bull during the overall investigation is gratefully acknowledged.

Manuscript released by the authors in April 1967 for publication.

This technical report has been reviewed and is approved.



HOWARD A. MAGRATH
Chief, Vehicle Dynamics Division
AF Flight Dynamics Laboratory

ABSTRACT

Investigations of the pressure fluctuations under a turbulent boundary layer, and the resultant vibration of simple panels, have been extended to consider the vibration of stringer-panel arrays and the intermittent pressure field in the boundary layer transition region.

The response of multi-panel arrays to turbulent boundary layer excitation has been measured for a flow speed of 320 ft./sec. Displacement spectra for the first band of modes, measured at the bay centres, have been compared with results due to acoustic excitation at grazing incidence. The vibration in the lower order modes is greater for the acoustic excitation but the converse is true for the higher order modes. Displacement cross correlation measurements show the presence of standing waves for distances up to three bay lengths but the wave system breaks down over larger distances.

A comparison of random techniques used in structural damping measurements shows the autocorrelation decay method to be the most reliable.

Using specially constructed gating apparatus, pressure measurements in the laminar-turbulent transition region show that the turbulent spots are autonomous regions of turbulent boundary layer, with similar pressure spectra. In addition there are low frequency pressure fluctuations due to the disturbances produced by the pressure steps on the mean flow.

The background noise levels in the wind tunnel have been measured.

CONTENTS

	Page
1. Introduction	1
1.1 General Survey	1
1.2 Structural Vibration	2
1.3 Tunnel Noise	3
1.4 Laminar-Turbulent Transition Region	4
2. Pressure Fluctuations In The Laminar-Turbulent Transition Region	6
2.1 Introduction	6
2.2 Instrumentation	6
2.3 Mean Flow Parameters	7
2.4 Distribution of Turbulent Spot Periods	8
2.5 Statistical Properties of the Fluctuating Wall Pressures	10
2.6 Discussion	16
2.7 Conclusions	17
3. Wind Tunnel Noise	19
3.1 Introduction	19
3.2 Theoretical Considerations	20
3.3 Experimental Investigation	22
3.4 Summary	27
4. The Vibration of Panels With Additional Damping	28
4.1 Introduction	28
4.2 Experimental Equipment	28
4.3 Modal Damping	32
4.4 Panel Displacement	43
4.5 Conclusions	46

CONTENTS (Contd)

	Page
5. The Response of Multi-Panel Arrays to Random Excitation	48
5.1 Introduction	48
5.2 Experimental Equipment	48
5.3 Panel Normal Modes	50
5.4 Response Spectra	53
5.5 Response Correlation Measurements	56
5.6 Conclusions	57
6. General Conclusions	59
References	61

LIST OF PLATES

No.		Page
1.	Fixed aerofoil and microphone	65
2.	Probe microphone and aerofoil	66
3.	Panel with single stiffener	67
4.	Exciter-probe	68
5.	Side plate suspended freely for damping measurements	69
6.	Eight-bay array mounted in boundary layer tunnel	70
7.	Eight-bay array suspended for mode shape measurement	71

ILLUSTRATIONS

FIGURE		PAGE
1.	Arrangement of low speed wind tunnel	72
2.	Comparison of overall noise in the transition region in fan and induction tunnels	73
3.	Phase and amplitude response at station 1	74
4.	Mean velocity profiles in the fully turbulent boundary layer	75
5.	"Wake" function in the fully turbulent boundary layer	76
6.	Static pressure distribution in the working section	77
7.	Comparison of measured spectra of wall pressure fluctuations with results of Bull (1)	78
8.	Measured pressure-velocity correlations	79
9.	Variation of $R(\tau)_{\max} - R(\tau)_{\min}$ across turbulent spots	80
10.	Relation between correlation time delay and local mean velocity	81
11.	General arrangement of 9 inch x 6 inch boundary layer wind tunnel	82
12.	Noise spectrum in tunnel settling chamber	83
13.	Noise measured in settling chamber when probe microphone is inserted in working section	84
14.	Frequency response of probe microphone	84
15.	Variation of sound pressure level along tunnel working section centre line	85
16.	Variation of sound pressure level across the tunnel working section	86
17.	Noise spectra in tunnel working section	87
18.	Noise amplification through inlet contraction	88
19.	Effect of tunnel inlet condition on noise field	89
20.	Boundary layer and tunnel noise spectra	90
21.	Mode shapes and frequencies for stiffened panel	91
22.	Exciter-probe calibration with Wayne Kerr meter on normal scale	92

ILLUSTRATIONS (Contd)

	Page
23. Effect of polarising current on panel response	93
24. Schematic diagram of instrumentation for cross-correlation measurement of damping using exciter-probe	94
25. Effect of excitation bandwidth on cross correlation between excitation and response	95
26. Excitation-response cross power spectrum: medium damping	96
27. Excitation-response cross power spectrum: light damping	97
28. Displacement spectra for undamped panel: $\delta^X = 0.06$ in.	98
29. Displacement spectra for undamped panel: $\delta^X = 0.167$ in.	99
30. Displacement spectra for damped panel: $\delta^X = 0.06$ in.	100
31. Displacement spectra for damped panel: $\delta^X = 0.167$ in.	101
32. Mode shapes for 8-bay array	102
33. Measured mode shapes for 4-bay array	103
34. Response spectra for 4-bay array: boundary layer excitation	104
35. Response spectra for 8-bay array: boundary layer excitation	105
36. Response spectra for 8-bay array: boundary layer and acoustic excitation	106
37. Measured variation of modal response with boundary layer thickness: 8-bay array	107
38. Noise spectrum in the siren tunnel	108
39. Theoretical response of 8-bay array to acoustic excitation	109
40. Displacement cross correlation coefficient for 8-bay array: datum bay 3	110
41. Displacement cross correlation coefficient for 8-bay array: datum bay 3.	111
42. Displacement cross correlation coefficient for 8-bay array: datum bay 6	111
43. Displacement cross correlation coefficient for 8-bay array: one bay separation	112
44. Displacement cross correlation coefficient for 8-bay array: four bay separation	113

ILLUSTRATIONS (Contd)

Figure		Page
45.	Displacement cross power spectrum for bays 3 and 4 of 8-bay array: boundary layer excitation	114
46.	Displacement cross power spectrum for bays 3 and 5 of 8-bay array: boundary layer excitation	115
47.	Displacement cross power spectrum for bays 3 and 6 of 8-bay array: boundary layer excitation	116
48.	Displacement cross power spectrum for bays 3 and 7 of 8-bay array: boundary layer excitation	117

TABLES

Table		Page
I	Wall Shear Stress	9
II	Period and Angle of Spread of Turbulent Spots	9
III	Measured Overall Root Mean Square Pressures	11
IV	Comparison of Damping Estimates for Modes with Medium and Light Damping	37
V	Modal Damping of the 4.0 in. x 2.75 in. Panel	37
VI	Modal Damping of the 4.0 in. x 2.75 in. Panel with Additional Damping	38
VII	Modal Damping of the Stiffened 4.0 in. x 2.75 in. Panel	39
VIII	Modal Damping of the Stiffened 4.0 in. x 2.75 in. Panel with Additional Damping	40
IX	Natural Frequencies and Modal Damping of Multi- Panel Arrays	52

SYMBOLS

A	Panel area
$C_p(\underline{x}', \underline{x}'', \omega)$	Real part of $S_p(\underline{x}', \underline{x}'', \omega)$
C_w	Constant
D	$\frac{Eh^3}{12(1-\sigma^2)}$
E	Young's modulus
f	Frequency cycles/second
f_c	Cut-off frequency of horn
f_e	Excitation frequency
$f_{1,1}$	Natural frequency of mode (1 - 1)
h	Panel thickness
$H_\alpha(\omega)$	Transfer function
$H_\alpha^*(\omega)$	Complex conjugate of $H_\alpha(\omega)$
i	$\sqrt{-1}$
K	Value of excitation power spectral density when assumed to be constant
K_w	Constant = 0.4
L_1	Panel dimension in x_1 direction
L_3	Panel dimension in x_3 direction
m	Mode order in x_1 direction
M_o	Free stream Mach number
M_α	Generalised mass in mode α
n	Mode order in x_3 direction
p	Fluctuating pressure
p'	Root mean square pressure
p_n	Fluctuating pressure due to noise
p_s	Fluctuating pressure due to pressure step
p_T	Fluctuating pressure due to turbulence
q	Dynamic pressure $\frac{1}{2}\rho_\infty U^2$

SYMBOLS (Contd)

$R(\tau)$	Autocorrelation function
$R_p(\tau)$	Autocorrelation function of pulse signal
$R_1(\tau)$	Observed autocorrelation function; equation (2.4)
$R(p(\underline{x}'), w(\underline{x}''), \tau)$	Pressure-displacement cross correlation function
R_θ	Reynolds number based on momentum thickness
s	Length of turbulent spot
$S_d(\omega)$	Displacement power spectral density function
$S_p(\omega)$	Pressure power spectral density function
$S_p(\underline{x}', \underline{x}'', \omega)$	Pressure cross power spectral density function
$S(p(\underline{x}'), w(\underline{x}''), \omega)$	Pressure-displacement cross power spectral density function
t	Time variable
u	Fluctuating velocity component in x_1 direction
u^*	Friction velocity = $(\tau_w / \rho_a)^{1/2}$
U	Mean velocity in x_1 direction
U_o	Free stream velocity
w	Panel displacement in x_2 direction
$w(x_2/\delta)$	Wake function
x_1, x_2, x_3	Cartesian coordinate systems, direction of flow along positive x_1 axis
$\underline{x} \equiv (x_1, x_3)$	Position vector in plane of the wall
Z_α	Function defined by equations (4.4) and (4.5)
α	Panel mode order $\alpha \equiv m, n$
β	Panel mode order
γ	Intermittency
δ	Boundary layer thickness
δ_α	Damping ratio for mode α
δ_A	Damping ratio measured by autocorrelation method
δ_C	Damping ratio measured by cross power spectrum method
δ_D	Mean damping ratio measured by discrete frequency excitation
δ_{D1}	Damping ratio measured by discrete frequency excitation using amplitude-phase method

SYMBOLS (Contd)

δ_{D2}	Damping ratio measured by discrete frequency excitation using amplitude response method
ν	Hysteretic loss factor
$\Pi(x_1)$	Wake function parameter
ρ	Density of panel
ρ_a	Density of air
σ	Poisson's ratio
τ	Time delay parameter
τ_w	Wall shear stress
$\Phi_D(\omega-\omega^1)$	Spectral window function for Fourier transformation
$\psi_\alpha(\underline{x})$	Mode shape of order α
ω	Angular frequency
ω_α	Angular frequency of mode α
ω_1, ω_2	Lower and upper frequencies of ideal rectangular filter
$\Delta\omega$	Frequency bandwidth

1. INTRODUCTION

1.1 General Survey

Since the advent of space flight and high speed civil flight there has been considerable interest in the random pressure field produced by a turbulent boundary layer. Topics of interest have included the statistical properties of the wall pressure field, the vibration of adjacent structures, and the acoustic radiation caused directly by the pressure fluctuations or indirectly by the structural vibration. As part of the general investigation, a series of projects has been undertaken at the University of Southampton, the work being based mainly on the specially constructed boundary layer wind tunnel in the Institute of Sound and Vibration Research. Certain items in the investigation have been concluded and reported. Bull (1) studied the statistical properties of the wall pressure field associated with a fully developed boundary layer. The response of single panels to boundary layer pressure fluctuations was investigated and discussed by Wilby (Reference 12).

Further results of the investigation are discussed in this report. The structural work has been continued to include the vibration of single panels when additional damping treatment has been applied. Also the response of more complicated structures, composed of multi-panel arrays, is discussed. When these larger structures are used there is a tendency for the natural frequency range to be extended to lower frequencies, unless the structural stiffness is controlled, and problems can arise due to interference from low frequency noise in the tunnel. With a view to the possible reduction of the acoustic field, noise measurements have been made in the wind tunnel and the results are presented in the report. Finally the work of Bull has been extended by investigating the pressure fluctuations in the laminar-turbulent transition region.

The instrumentation necessary for the investigation has been discussed in Reference 1, but the experimental results are contained in the present report.

1.2. Structural Vibration

A brief survey was made by Wilby (Ref. 12) of theoretical and experimental work by other authors on the vibration of structures exposed to turbulent boundary layer pressure fields. It was shown that there was only a limited number of experimental studies, and in only one of these was the multi-panel array considered. Thus the measurement of the vibration of stringer-panel arrays, when exposed to boundary layer excitation, forms a logical extension of the single panel measurements discussed in Ref 1. The more complicated structures are, for obvious reasons, more representative of practical structures than in the single isolated panel, and it is easier therefore to extrapolate the results of laboratory experiments to include conditions encountered in practice.

The measurements on a single panel do not show the way in which the structural vibration and acoustic radiation are affected when the structure is composed of a series of connected panels. To investigate this it is necessary to consider the scale of the excitation pressure correlations relative to the panel bay dimensions and to measure the vibration correlation between pairs of adjacent and separated panel bays. The noise radiated by the panel array will depend on the degree of correlation of the panel vibration, and on this will depend also the manner in which the results for single panels can be extrapolated to full-scale conditions.

The size of the experimental panels is limited by the dimensions of the boundary layer wind tunnel working section, and by the requirement that the boundary layer conditions should be approximately uniform over the surface of the structure. These limitations mean that only model, rather

rather than full-scale, structures can be used in the experimental study.

The structural investigation reported in Reference 12 included a study of the use of random techniques in the measurement of modal damping, with reference to the measurement of damping in the presence of an airflow. Under these conditions the use of discrete frequency excitation is not possible and the random methods provide suitable alternatives. It was found that, for the lightly damped panels when the narrowest filters available had bandwidths which were greater than the resonance bandwidths, the response autocorrelation decay method provided the most reliable estimate of the modal damping. However, before general conclusions can be drawn, it is necessary to consider the relative accuracy of the methods for a range of values of the frequency ratio, defined by the ratio of the filter bandwidth to the bandwidth of the resonant peak. This can be done by varying the filter bandwidth when the damping is constant, or by varying the damping when the filter bandwidth remains constant. The second alternative has been chosen for the present investigation because it permits also the measurement of the effect of damping on the boundary layer induced vibration. The structures chosen are single panels which are similar in design to those used in the earlier work.

1.3. Tunnel Noise

The noise in conventional wind tunnels has been measured by several authors with a view to the silencing of the noise from the propulsive unit. In the present investigations the wind tunnel has been specially designed to have low noise and vibration characteristics in the working section but even so, in common with other boundary layer wind tunnel facilities, it is found that significant low frequency noise is present. There is very little experimental or theoretical information regarding the relative importance of possible noise sources: tunnel inlet noise, noise radiated by the turbulent boundary layer, or noise transmitted from the injector through the subsonic boundary layer. Hence a project was started, to measure the

noise distribution in the tunnel subsonic working section, with the intention of identifying the most important sources. Not until the sources are positively identified can attempts be made to reduce the acoustic interference field and extend the available frequency range for future boundary layer investigations.

1.4. Laminar-Turbulent Transition Region

The measurement of wall pressure fluctuations and structural vibrations discussed by other authors and, previously, in the investigations in the Institute have been concerned with fully developed turbulent boundary layers. Little attention has been paid to the transition region which precedes the fully developed turbulence and no measurements have been made of the fluctuating pressures which will occur on the wall beneath such a region of intermittent turbulence. From a practical point of view the transition region is of interest because it is not known whether the pressure fluctuations cause greater acoustic radiation or panel vibration than in the regions of fully developed turbulence.

Transition in the present context is the name given to the change of regime which occurs in most practical flows; it is a change from an ordered and systematic flow to a disordered one which can be described only in statistical terms. It is possible to show theoretically that the flow becomes unstable at a critical Reynolds number but beyond this stage the analytical solution becomes too complex and recourse is to experiment. The instability leads to the appearance of a spot of turbulence which is convected downstream, diffusing and mixing with other spots which appear with random incidence in a limited streamwise region of the flow, i.e. in the transition region. Eventually the boundary layer flow consists entirely of intermingled spots and forms the fully developed turbulent boundary layer further downstream. The incidence of the spots

follows a probability distribution and appears effectively on the surface as an ever increasing probability, past a certain point, of finding turbulent flow. Moving down the surface presents, on the average, a continuous change from all laminar, through varying proportions of turbulent, to fully turbulent flow.

While an adequate theory is available for predicting the onset of the instability, almost nothing is known of the way in which a spot appears, or of the way the structure of the spot is related to the fully developed turbulent flow. To what extent the turbulent boundary layer merely has the properties of mixed turbulent spots is unknown. Thus the aim of the present work was to study the pressure fluctuations associated with intermittently turbulent flow found in the transition region, to relate them if possible to other features of the transition process, and to make comparisons with other fairly well established results for the wall pressure field of the turbulent boundary layer. It was not intended to investigate the transition mechanism itself, for which the measurement of such a complex parameter as the wall pressure is probably much less appropriate than the refined techniques developed by Schubauer, Klebanoff and others at the National Bureau of Standards.

It was found in preliminary measurements that the boundary layer wind tunnel at the Institute did not provide suitable conditions for the transition region measurements and this investigation, unlike all the others undertaken in the overall program at the Institute, was carried out in a low speed wind tunnel. However the results can be compared with those of Bull measured in the boundary layer wind tunnel under fully turbulent conditions. The Reynolds number, based on the boundary layer momentum thickness, was 5,000 to 50,000 for the measurements of Bull, and 800 to 1,500 for the present transition region measurements.

2. PRESSURE FLUCTUATIONS IN THE LAMINAR-TURBULENT TRANSITION REGION

2.1. Introduction

The investigation of the pressure fluctuations in the laminar-turbulent transition region of a boundary layer was carried out as an extension of the work of Bull (1) in the fully developed turbulent boundary layer. In keeping with this concept no attempt has been made to extend the work to cover the mechanism of transition itself, for which there are more powerful methods available already. A considerable proportion of the work in this investigation has been concerned with the development of instrumentation which is suitable for the unusual flow under examination. This development work has been described previously (Reference 1) so that detailed descriptions of the instrumentation need not be given here. The discussion in this chapter will be restricted mainly to the results of the investigation.

2.2. Instrumentation

The investigation was carried out in a low speed wind tunnel which was adapted to reduce the ambient noise levels as much as possible. A new working section made from acoustically inert fibre board was fitted to the tunnel, and existing areas of sheet metal construction were coated with a damping material. The general arrangement of the tunnel is shown diagrammatically in Figure 1. The working surface was formed by a 0.25 inch thick brass plate, highly polished and with a 6° wedge cut under the leading edge. Transition was controlled by altering the pressure gradient by means of flexible tunnel liners.

The desirability of using low speed flow for this investigation is evident when a general study is made of the conflicting requirements involved. Referring to Figure 2 it is clear that at low speeds, whilst the signal-to-noise ratio (as shown by the vertical separation between the lines for $0.006 q$ and for tunnel noise)

improves, there is a lower limit set by the instrument noise. Tunnel airspeeds of approximately 70 ft./sec. were chosen for this investigation. The requirements are even more restrictive when consideration of the frequency spectrum of the various signals is included. Improvements on the frequency range used for these experiments will probably come from lower speed investigations in a specially muted tunnel.

The wall pressure fluctuations were measured using a pin-hole microphone which was constructed by placing a Bruel and Kjaer $\frac{1}{2}$ inch diameter microphone behind a 0.030 inch diameter hole in the brass plate. (See Reference 1). The system had an adequate sensitivity but suffered from frequency limitations which occurred when the pin-hole cavity acted as a Helmholtz resonator. The effects on phase were even more severe, typical calibration curves being shown in Figure 3. Turbulence measurements were made using a hot wire anemometer constructed from tungsten wire with a diameter of 5 microns.

The gating apparatus, which forms the centre of the experimental method, has been described in detail in Reference 1. The operation of the instrument is difficult when the signal-to-noise ratio is poor (< 10 dB), and experience in using the apparatus is necessary if meaningful results are to be obtained.

2.3. Mean Flow Parameters

The values of some of the mean flow parameters measured in the laminar layer have been presented in Reference (1). In addition, measurements and calculations relating to the fully turbulent boundary layer have been made with a view not only to confirming the existence of a turbulent boundary layer with characteristics close to those normally found, but of estimating the wall shear stress in the turbulent spots.

Measurements of the mean flow parameters were made using a pitot tube in conjunction with a static tapping on the wall. The

results at the three measuring stations are shown in Figures 4 and 5, plotted in terms of Coles' form (2) for the velocity profile

$$\frac{U}{u^*} = \frac{1}{K_w} \log_e \frac{x_2 u^*}{\nu} + C_w + \frac{\Pi(x_1)}{K_w} w(x_2/\delta)$$

where $K_w = 0.4$, $C_w = 5.1$ and $\Pi(x_1)$ is a parameter determined by the flow conditions. The agreement is seen to be satisfactory.

Calculation of the wall shear stress has been made using Buri's method (3), with the measured pressure distribution in the tunnel shown in Figure 6. The resulting values for $\frac{u^*}{U_0}$, for the pressure gradients corresponding to turbulent and laminar flow at the measuring station are shown in Table I, together with the measured values from Figure 4. It is seen that there is good agreement between the results, and there is little variation in the wall shear stress over the range of pressure gradient encountered in changing the intermittency.

2.4. Distribution of Turbulent Spot Periods

In order to correct for the effect of the intermittent nature of the flow on the measured frequency power spectra it is necessary to measure the distribution of the periods of the turbulent spots. The method used to do this is based on the use of the gating apparatus (1) to produce an electrical pulse of length equal to that of the turbulent spot, and an auxiliary piece of apparatus which operates in the following manner.

Imagine a counting unit which will count to 16 only. This is so constructed that upon reaching 16 no further counting occurs but one output pulse is produced. This unit is supplied with a periodic signal which has passed through the gate of the gating apparatus. At the end of each turbulent spot, when the gate is closed, a zero pulse is used to return the counter to zero. If now the

TABLE I
Wall Shear Stress

Position	1	2	3
Distance from leading edge (inches)	7	16	25
Measured:-			
$\frac{u^*}{U_o}$ (Profile)	0.0426	0.0467	0.0446
Calculated:-			
$\frac{u^*}{U_o}$ (Turbulent)	0.0494	0.0468	0.0436
$\frac{u^*}{U_o}$ (Laminar)	0.0494	0.0463	0.0400

TABLE II
Period and Angle of Spread of Turbulent Spots

Position	1	2	3
Preferred period (seconds)	0.0036	0.0070	0.0220
Angle of Spread (degrees)	3.3	2.8	5.8
R_θ	336	410	570

frequency of the periodic signal is 1600 c.p.s. (for example), when a spot passes the microphone the gate opens and the unit starts counting. If the duration of the spot is, say, 0.009 second then 14 complete cycles will be counted but as this does not exceed 16 no output is produced. If the duration of the spot was 0.015 second, a total of 24 complete cycles would be passed by the gate, although only the first 16 would be counted, and a single output pulse produced. By repeating with a number of different frequencies, the integral distribution of spot lengths can be built up. The probability density is found by differentiating this distribution.

The results show that there is a preferred period associated with each measuring station, and that most of the spots have a duration which is fairly close to this period. For each measuring station, the preferred periods are shown in Table II.

The most probable explanation for the preferred period is that most of the spots originate at the leading edge of the plate. If this is assumed, and it is also assumed that the geometry of the spots is the same as that described by Schubauer and Klebanoff (4), then the corresponding angle of spread in each case has the value shown in Table II. It is seen that the rate of spread is increased at station 3; the value of 5.8° is the average of spreading at about 3° followed by spreading at a greater rate. If it is assumed that the greater rate of spread starts just downstream of station 2, the true local angle at station 3 is 11° .

These results for the rate of transverse contamination agree with the results of Schubauer and Klebanoff (4) obtained from an examination of photographs of the hot wire signal in the transition region.

2.5. Statistical Properties of the Fluctuating Wall Pressures

2.5.1. Variation of Pressure Intensity with Intermittency

The pressure was measured using a pin-hole microphone

TABLE III

Measured Overall Root Mean Square Pressures

Station	1	2	3
Resolution Correction	2.6	1.30	1.23
p'/τ_w	6.65	2.35	2.07
R_θ	800	1100	1500

mounted in the surface of the flat plate under test, and the intensity was determined, using the apparatus described in Reference (1), by squaring and integrating the pressure signal. Before analysis the pressure signal was filtered to remove low frequency interference, so that an acceptable signal-to-noise ratio could be achieved.

Because of the design of the wind tunnel used for the experiments, variations in the flow conditions external to the boundary layer occur when changing from laminar to turbulent flow over the measuring station. These variations have associated with them changes in the surface shear stress in turbulent spots, and hence in the observed intensity of the pressure fluctuations. An estimate of the variation of the intensity is obtained from the variation in shear stress, and it is shown in Table I that the latter change is small.

Subject to certain statistical restrictions described by Corrsin (5), the observed mean square pressure p^2 of a signal which consists of a continuous noise component p_n^2 and a component which contributes p_T^2 intermittently, is

$$p^2 = \gamma p_T^2 + p_n^2 \quad (2.1.)$$

where the intermittency γ is the fraction of the time for which p_T is present. If p_T^2 is constant then, from equation (2.1) there is a linear relationship between the observed mean square pressure and the intermittency. The present measurements of p^2 and γ do not show such a linear variation and this may be due to a functional relationship between p_T and γ , as has been suggested previously (1). Alternatively it is suggested here that the major part of the non-linearity is due to the effect of the disturbance of the external flow by the turbulent spot which takes the form of a static pressure step.

The magnitude of the pressure step effect, p_s^2 , will

depend on the length to thickness ratio of the spot, and on the differences in velocity between the spot and the external flow, but the effect on the observed mean square pressure is similar to associating a static pressure increase with the spot. The mean square pressure observed with an A.C. coupled meter is then, after Corrsin (5),

$$p^2 = \gamma p_T^2 + p_n^2 + p_s^2 \gamma (1-\gamma) \quad (2.2.)$$

Direct measurements of this effect have been made by introducing a series of known D.C. shifts into the pressure signal of each turbulent spot, and correlating these signals in turn with a reference signal which is non-zero only during the passage of a spot, when it has some constant value. The results of these measurements agree with the observed departure from linearity of the $p^2:\gamma$ graphs, and show that the effect contributes an extra 25% to the observed intensity or r.m.s. pressure at intermittencies of 0.5 (where the effect is greatest). Whereas the intensity of the turbulence is proportional to the wall shear stress, the magnitude of the pressure step is governed by the free stream velocity and the geometry of the spot.

The magnitude of the intensity is very difficult to estimate accurately in these experiments due to:-

- (a) background noise, which accounts for 50% of the total observed signal,
 - (b) limited microphone response, which underestimates the high frequency contribution.
- and
- (c) limited microphone resolution, which can be allowed for, in part, by a correction factor such as used by Bull (1, Part I), but the magnitude of the factor becomes very large in the present case.

The best estimate of the root mean square pressure p' in terms of the wall shear stress τ_w , is shown in Table III, together

with the estimated resolution correction and the associated Reynolds number R_θ based on the momentum thickness. With the exception of station 1, the results are in good agreement with those for other experiments (e.g. Reference 1, Part I Figure 25).

2.5.2. Pressure Power Spectral Density

The power spectral density of the wall pressure fluctuations in the laminar-turbulent transition region of the boundary layer was determined from pressure measurements analysed in third-octave bands using a Bruel and Kjaer Spectrometer Type 2112. The results have been reduced to non-dimensional form using wall shearing stress τ_w , free stream velocity U_o , boundary layer thickness δ and intermittency γ .

The observed spectrum is the result of contributions from not only the wall pressure fluctuations, but also the acoustic noise in the tunnel. Moreover the spectrum of the wall pressure fluctuations is disturbed by the intermittent flow.

The contribution from the tunnel noise is confined mainly to the low frequency part of the spectrum and the components could be attenuated by means of a filter. For this reason the spectra are quoted for a frequency range such that the associated Strouhal numbers are greater than about 2.

In order to compensate for the distortion of the spectrum by the intermittent nature of the signal, it is necessary to measure the relative proportions of spots of a particular length, as discussed in Section 2.4. It may be shown (6) that the correlation coefficient $R_p(\tau)$ of the pulse signal corresponding to the incidence of the turbulent spots, is

$$R_p(\tau) = \int_{\tau}^{\infty} \frac{s-\tau}{s} ds \quad (2.3.)$$

where s is the probability density function for the turbulent spot length. Then the correlation coefficient $R_1(\tau)$, which will be

observed in an intermittent signal, is related to the fully turbulent correlation coefficient $R(\tau)$ by

$$R_1(\tau) = R_p(\tau) R(\tau). \quad (2.4.)$$

If the Fourier transform of $R_1(\tau)$ is determined, the degree of distortion of the spectrum may be deduced, and it is found that for the distributions described in Section 2.4, the error in the observed spectra is negligible for the frequency range of interest.

Spectra measured at each of the stations are shown in Figure 7, and it is seen that, within the restricted frequency bands, reasonable consistency exists between the present results and those of Bull (1) for fully developed turbulent boundary layers. The frequency band is limited at the lower end by the unfavourable signal-to-noise ratio, and at the upper end, at the indicated Strouhal numbers, by the inadequacy of the measuring microphone system. However the results suggest that the turbulence in the spots in the transition region is similar to that in fully developed turbulent flow.

2.5.3. Pressure-Velocity Correlations

Measurements have been made of the correlation between the wall pressure and the longitudinal component of velocity, denoted as the p-u correlation function. The role of this particular function in the pressure generation process is an indirect one; the interest in the present case however is not so much concerned with this process as with the comparison between the present results and the form this correlation function is observed to take in the fully turbulent layer.

Measurements of p-u correlations in the fully developed turbulent boundary layer have been made previously (1,7,8) and the features of the curves have been established, e.g. a zero crossing at a time delay related to the position of the hot wire anemometer in the layer. The degree of correlation is characterised by the difference between the greatest positive and negative values.

Severe bandwidth restrictions were necessary in the present case due to tunnel noise at the low frequency end of the spectrum and the phase change in the microphone system (Figure 3) at high frequencies. The frequency band was limited, therefore, to $2 < \frac{\omega \delta}{U_0} < 3.5$. It is not easy to estimate the change this filtering makes to the magnitude of the correlation function. The best that can be said of the present results from this point of view is that the results obtained in the fully turbulent layer are consistent with those obtained in the intermittent flow of the transition region (see Figure 8).

The way in which the magnitude varies across the layer is shown in Figure 9, which compares favourably with results quoted in (1,7,8). The variation of the time delay with local mean velocity (Figure 10) shows that the convection speed of the pressure disturbance is in fact the local mean velocity, again in keeping with other results from fully developed layers.

2.6. Discussion

It has been shown that the behavior of the various parameters of the wall pressure fluctuations observed in the transition region is very similar to that observed in the fully developed turbulent layer. This is true not only for comparison with the fully turbulent layers in this investigation, but also with the equivalent measurements by other investigators. There are reservations in using the p-u correlation measurements, for the reasons discussed in Section 2.5.3., but the spectra measurements, which cover a range of disturbances ranging from about 0.5 to 5 times the spot thickness, are significant. If the extrapolation is made, using the spectra of Bull (1), to frequencies above those measured, the conclusion drawn is that the spots look like pieces of a turbulent boundary layer.

This picture is not entirely consistent with the

accepted view of the structure of turbulent wall flow since it poses difficulties in introducing mean flow energy into the turbulence. These difficulties can be countered if it is supposed that the trailing edge of the spot is responsible for the energy extraction. There is a priori evidence for this in that the spot is growing by extending its trailing edge. Similar behaviour has been observed by Lindgren (9) in pipes.

2.7. Conclusions

From the results of this investigation it has been concluded that:-

- (a) Two states exist in the growth of turbulent spots in a laminar layer. For Reynolds numbers (based on laminar momentum thickness) less than 500 the lateral spread is about 3° , above this Reynolds number, it is about 11° . A similar result has been obtained by Schubauer by a method different from the present one.
- (b) In addition to the wall pressure fluctuations contributed by the turbulence, there is an added component in the transition region due to disturbance of the mean flow by the turbulent spots, amounting to an intensity p'/q of about 0.005 when the length:thickness ratio of the spots is not less than 15. This could give rise to localized structural excitation, but at frequencies well below those arising from turbulence.
- (c) Within the frequency band for which the Strouhal number $\frac{\omega \delta}{U_0}$ is between 2 and 20, the spectrum of the wall pressure fluctuations within the spots scales in the same way as in the fully turbulent layer. The Reynolds numbers in these experiments were between 800 and 1500.
- (d) Within the frequency band for which the Strouhal number is between 2 and 3.5 the correlation between the wall pressure fluctuations and the longitudinal component of velocity is similar to that in the fully developed turbulent boundary layer.
- (e) On the basis of the close similarity between the nature

of the pressure fields it is suggested that the turbulent spots act like small autonomous pieces of turbulent boundary layer. A model of the energy transfer mechanism consistent with these conditions is proposed.

3. WIND TUNNEL NOISE

3.1. Introduction

Experimental investigations of the turbulent boundary layer pressure field in wind tunnels have been carried out by several authors and the measured spectra show large differences at low frequencies, where the measured pressure spectral density may change rapidly with frequency. These variations are not characteristic of the turbulent boundary layer pressure fluctuations and the phenomenon has been attributed to the presence of background acoustic noise in the tunnel. The acoustic disturbances distort the measured boundary layer pressure spectrum and introduce errors in the measurement of the overall root mean square boundary layer pressure. Furthermore, when the tunnel is used for the study of structural response, or for the study of the noise radiated by the excited structures, the low frequency vibration and noise radiation will be influenced by the tunnel acoustic field.

In the investigation of boundary layer pressure fluctuations, the background noise can be eliminated if the pressure spectrum is measured only in the frequency range above the range of interference, by the use of high pass filters. However, corrections have to be made to the overall root mean square pressure. In structural vibration measurements, the filtering technique was used by Baroudi (10) when interference occurred in the frequency range containing the lower order panel natural frequencies, but the method suffered from the disadvantage that valuable information was lost. The problem can be minimised if the experimental structures are designed so that the lowest natural frequency is above the frequency range of acoustic interference. This method was adopted by Maestrello (11) and Wilby (12), but it places a restriction on the structural specimens which is difficult to maintain for larger structures, unless the structural stiffness is controlled.

The noise levels in general purpose wind tunnels have been measured by several authors (e.g. 13, 14), where the problems were

associated with reducing the noise of the propulsive units. Measurements of acoustic radiation from the boundary layer in a supersonic wind tunnel have been carried out by Laufer (15) using hot wire anemometers to detect the acoustic disturbances in the free stream. Laufer showed that the overall root mean square pressure in the radiation field could be related to the wall shear stress, but the magnitude of the pressure was an order of magnitude lower than at the wall surface. The non-dimensional spectra showed that the energy in the acoustic field was predominantly low frequency when compared to the wall pressure field. Measurements by Bull (16) in the boundary layer wind tunnel at Southampton showed the existence of a background noise field but the noise sources were not identified. The noise was predominantly low frequency, in agreement with Laufer. The present experimental investigation of the noise level inside the boundary layer tunnel was carried out to determine the noise distribution in the tunnel and to attempt to identify the noise sources.

3.2. Theoretical Considerations

3.2.1. Noise Sources

There are several possible sources of noise in a wind tunnel and usually the most important is the fluid propulsive unit. The form of the unit, and hence the noise spectrum, will vary with the type of tunnel. In general the tunnel will be fan driven or operate from a compressed air supply as a blow-down tunnel or an injector tunnel. In the present investigation the tunnel is of the induced flow type and fan noise will not occur. The radiation of noise from the injector into the tunnel working section has been reduced by the insertion of a sonic choke between the subsonic section and the injector, but noise can still be transmitted through the subsonic boundary layer.

The noise levels in the tunnel may arise also from the amplification of disturbances by the tunnel inlet contraction, or from the acoustic radiation from the turbulent boundary layer itself.

3.2.2 Boundary Layer Radiated Noise

The radiation of noise from a turbulent boundary layer has been

studied theoretically by several authors, and it is of interest to consider the results in relation to the present experimental conditions.

The work of Lighthill, on the generation of aerodynamic noise by turbulence in the absence of solid boundaries, was extended by Curle (17) to include the more general case when solid boundaries were present. Curle separated the acoustic radiation into two components, one component having the quadrupole-type properties associated with the unrestricted flow (although effects due to the solid boundaries were included), and the other having the form associated with dipole radiation. Under the assumptions that the surface dimensions of the solid boundary were small compared to the acoustic wavelengths, and that the observer was sufficiently far from the surface for free field conditions to be valid, Curle showed that the dipole radiation was the more important. Then the radiated acoustic power was proportional to the sixth power of the free stream velocity.

The importance of the dipole term will decrease when the surface dimensions increase, and under such conditions the quadrupole-type contribution has to be included. The case of large surfaces has been considered by several authors, including Powell (18) and Williams and Lyon (19), who have shown that the dipole source strength vanishes on infinitely large, flat surfaces. The result does not apply, however, to plates with surface curvature, or to finite plates where edge effects may become significant. In both of these exceptions, dipole contributions have to be considered.

On a dimensional analysis Williams and Lyon showed that the far field acoustic radiation intensity from a turbulent boundary layer on an infinitely large, flat plate, exhibited the U_o^8 law associated with quadrupole radiation. However the relative importance of the dipole and quadrupole radiation from a finite plate is difficult to establish, even in the far field. For example, the dimensional analysis requires a knowledge of the constants of proportionality, and the magnitude of the constants is in dispute, suggested values differing by several orders of magnitude.

A survey of the current theoretical results suggests that the intensity of the boundary layer radiated noise inside a wind tunnel will

follow a velocity law which is intermediate between U_o^6 and U_o^8 . However the theoretical results apply to far field conditions only, the near field case having been omitted due to the greatly increased complication of the analysis. The experimental results of Laufer (15) in a supersonic wind tunnel indicate that, for a constant Reynolds number, the radiated intensity is proportional to the square of the free stream dynamic pressure.

3.2.3 Tunnel Inlet Noise

The general shape of the settling chamber and contraction in the tunnel inlet is similar to that of an acoustic horn. Figure 11 shows that the contraction has a zero rate of change of area at that junction with the tunnel working section, so that it can be represented, in the ideal case, by a catenoidal horn. From Morse (20), using Rayleigh's law of reciprocity. (21), the contraction can be considered as a hearing trumpet, with a predicted cut-off frequency of 91.9 c.p.s. Theoretically the transmission coefficient at the cut-off frequency f_c is infinite. At frequencies below f_c there is zero transmission and at frequencies greater than f_c the transmission coefficient falls quickly to an asymptotic value of unity.

3.3 Experimental Investigation

3.3.1. Instrumentation

The noise measurements were carried out in the 9 inch x 6 inch subsonic working section of the boundary layer wind tunnel at the University of Southampton. The general arrangement of the tunnel is shown in Figure 11, and the construction and operation of the tunnel have been described briefly in (12) and in detail in (1, 16). The microphone and supporting aerofoil were mounted on a 6 inch diameter plug which could be inserted in a series of measuring positions along the length of the tunnel working section.

The most important problem in the measurement of the noise in the tunnel is that of designing a measuring probe which will not change the noise field when the probe is inserted into the airflow. It was found that this condition was not satisfied completely by any of the microphone systems used, but the two systems finally adopted were those which created the minimum

disturbances. The acoustic disturbances created by the microphone systems in the presence of the airflow were measured by means of a flush mounted microphone in the wall of the tunnel settling chamber.

In the preliminary measurements, Bull (16) used a $\frac{1}{2}$ inch diameter Bruel and Kjaer condenser microphone which was mounted in a rigid aerofoil. The aerofoil was carefully faired into the tunnel side wall (Plate 1), but the microphone could not be traversed across the tunnel working section. The microphone diaphragm was enclosed in a nose cone so that a smooth fairing was presented to the airflow, the microphone pointing in the upstream direction. The aerofoil did not affect the low frequency noise in the tunnel, the noise being monitored in the tunnel inlet, but the noise level increased at frequencies greater than 1,000 c.p.s., as is shown in Figure 12.

Similar microphone-aerofoil systems were constructed using $\frac{1}{2}$ inch and $\frac{1}{4}$ inch diameter microphones which could be traversed across the tunnel working section. However to achieve this movement the fairing on the aerofoil had to be reduced considerably and the aerofoil mounting became less rigid. These changes resulted in an increase in the acoustic disturbances which prohibited the use of the systems for tunnel noise measurement. Thus a second system, shown in Plate 2, was constructed. The microphone and nose cone mounting shown in Plate 1 was replaced by a microphone probe tube, with an outside diameter of 0.08 inch, approximately, and a length of 5 inches. The tube was inserted along the span of a thin aerofoil, the open end of the tube being flush with the hole in the tip of the aerofoil, and the system produced an acceptably low change in the tunnel noise field (Figure 13). The probe tube was calibrated, following the procedure recommended by Bruel and Kjaer, by means of a noise source in a small cavity, and fine wire wool was inserted in the tube to obtain optimum damping of the acoustic resonances. The final calibration curve is shown in Figure 14. At frequencies greater than 2,000 c.p.s. the probe response falls rapidly, but the present investigation is concerned mainly with frequencies below 1,000 c.p.s. so the frequency response is acceptable.

Under operating conditions the static pressure in the boundary layer wind tunnel is below atmospheric pressure. This does not create difficulties in the operation of the fixed aerofoil because the microphone capsule and cathode follower are contained within the tunnel working section. However, difficulties did arise with the probe microphone, where the capsule and cathode follower were mounted externally to the tunnel. It was found that air leaks occurred, via the cathode follower, into the capsule, and a pressure differential was created which reduced the sensitivity of the probe when the tunnel was in operation. The problem was overcome by placing the microphone capsule and cathode follower in an enclosure whose pressure could be equalised with that in the tunnel working section.

3.3.2. Noise Measurements

The noise field in the wind tunnel has been measured at two flow speeds of 329 ft./sec. and 540 ft./sec., with nominal Mach numbers of 0.3 and 0.5 respectively. Noise levels were measured at positions along the tunnel centre line, and traverses across the tunnel were made at four positions along the working section.

Figure 15 shows the noise levels measured along the tunnel centre line using the fixed aerofoil microphone and the probe tube microphone. At the downstream measuring positions the two microphone systems show good agreement but at the upstream positions the probe microphone indicates higher noise levels than does the fixed aerofoil system. The difference may be due to turbulence in the probe orifice, or to directional properties of the fixed aerofoil microphone if sound waves are propagated in the upstream direction, but it was not possible to identify the main cause of the differences. None of the results in the figure shows the presence of a standing wave system in the wind tunnel working section.

Both sets of results in Figure 15 show an increase in noise level in the downstream direction, the increase measured by the fixed aerofoil being 9 dB approximately, whereas the increase measured by the probe tube microphone was only 1 dB approximately. However both microphones show a similar variation in noise level with flow speed, the change being 7.5 dB for the probe tube results and 8 dB for the fixed aerofoil. This compares with an 8 dB increase in

the total intensity of the boundary layer pressure field. In terms of velocity alone, the variation implies that the noise intensity is proportional to U^n where the mean value of n is $n = 3.6$. If the change in air density is taken into consideration, the noise intensity can be expressed in terms of q^k where q is the free stream dynamic pressure and k has a mean value $k = 1.95$. Thus the overall pressure fluctuations measured by the microphones are proportional to the dynamic pressure and hence to the boundary layer fluctuating pressures. This result is in agreement with the experimental results of Laufer (15) but in contradiction to the theoretical predictions based on the far field radiation. However, the results of Laufer showed that the noise field was 19 dB to 26 dB below that of the boundary layer pressure field, whereas the results in Figure 15 show a difference of 15.5 dB, based on the fixed aerofoil measurements, or 11.5 dB based on the probe tube microphone measurements.

Typical noise traverses, measured across the tunnel working section by the probe tube microphone, are shown in Figure 16. The noise level is a minimum on the tunnel centre line and increased markedly when the probe enters the turbulent boundary layer. The increase does not indicate, necessarily, a change in the acoustic field, since the microphone will react to hydrodynamic pressure fluctuations in the boundary layer. At the wall the measured pressures are about 4 dB higher than the levels measured by Bull (1) using flush mounted transducers. The difference will be due, at least in part, to the increased disturbance made by the aerofoil, which did not make a flush surface with the tunnel wall. Analysis of the measurements does not show the presence of standing waves across the tunnel working section.

Noise spectra measured by the two microphone systems are compared in Figure 17. The spectrum measured by the fixed aerofoil is similar in shape to that measured by the probe microphone, although there is a slight deviation at the higher frequencies. When the probe microphone is withdrawn towards the tunnel wall there is a general increase in the spectral density level, without the appearance of any frequency dependent variations which would indicate selectivity due to resonances.

3.3.3. Tunnel Inlet Noise

It has been suggested that the low frequency noise level in the tunnel may be due to amplification of low frequency disturbances in the tunnel inlet, and it has been shown in Section 3.2.3 that the inlet contraction could act, in theory, as an amplifier of low frequency acoustic disturbances in the range of 92 c.p.s. to 300 c.p.s. approximately

The acoustic amplification due to the contraction was measured in the absence of airflow. A loudspeaker was placed in front of the inlet to the tunnel and the noise levels were measured in the tunnel settling chamber and in the working section. The resulting spectra are shown in Figure 18 and it is seen that amplification occurs within a frequency range of about 50 c.p.s. to 500 c.p.s., which is similar to that predicted for the very idealised system in section 3.2.3. The maximum amplification measured is 13 dB at frequencies in the neighborhood of 110 c.p.s.

Noise spectra measured in the tunnel settling chamber and working section are shown in Figure 19 for several different inlet conditions. The honeycombs and gauzes were fitted in the tunnel inlet to provide low turbulence conditions in the tunnel working sections. The noise measurements in Figure 19 show that the screens did not affect the tunnel noise levels significantly, either in the settling chamber or in the working section. The difference in the spectral density level between the settling chamber and the working section varies from 25 dB at a frequency of 100 c.p.s. to 21 dB at 500 c.p.s. This change is larger than that associated with the amplification measured in Figure 18 and the results indicate that the noise level in the working section does not arise from the magnification of disturbances at the tunnel inlet.

3.3.4. Comparison with Boundary Layer Spectra

The effect of the tunnel noise field on the wall pressure field can be estimated by combining the pressure power spectra for the two sources. This can be performed directly if it is assumed that the noise field at the centre of the tunnel is not altered significantly when passing through the boundary layer, and that the boundary layer spectrum can be extended to low

frequencies by the use of the empirical non-dimensional spectrum. Measured acoustical and estimated boundary layer spectra are combined in Figure 20 for a Mach number $M_0 = 0.3$ at a position 41.6 inches downstream from the tunnel datum. The combined spectrum is found to be very similar to that measured by Bull at the tunnel wall. This provides confirmatory evidence that the noise levels measured in the tunnel are essentially those present before the insertion of the microphone, and are not purely self-induced by the airflow over the microphone.

3.4 Summary

Noise levels have been measured in the working section of the boundary layer wind tunnel, but no evidence of standing wave systems has been found in either the streamwise or lateral directions. In the lateral direction the measured noise levels were a minimum on the tunnel centre line, but they increased closer to the wall due to the combined effect of the acoustic field and the turbulent hydro-dynamic field in the boundary layer. When the measured acoustic spectra and the predicted boundary layer spectra are combined the resulting spectra are similar to those measured by Bull using flush mounted transducers in the tunnel wall.

The tunnel inlet honeycombs and gauzes have no measurable effect on the noise levels in the working section. The acoustic horn effect, or rather the hearing trumpet effect, of the inlet settling chamber and contraction amplifies acoustic signals in the frequency range 50 c.p.s. to 500 c.p.s. but the amplification is not sufficient to account for the noise levels in the working section.

The source of the noise in the wind tunnel has not been located with certainty and further measurements will be necessary before the relative importance of the acoustic radiation from the boundary layer and the injector can be established. However, the overall acoustic pressure in the tunnel is proportional to the free stream dynamic pressure and to the boundary layer root mean square pressure, whereas the acoustical radiation from the injector should be independent of the flow velocity in the subsonic section. This suggests that the noise levels are associated with radiation from the turbulent boundary layer.

4. THE VIBRATION OF PANELS WITH ADDITIONAL DAMPING

4.1 Introduction

The response of lightly damped single panels to random excitation has been discussed previously in Reference 12. The investigation was concerned mainly with the vibration due to turbulent boundary layer excitation, which introduced the problem of measuring panel damping in the presence of an airflow. Random techniques can be used and there are at least three possible alternatives; direct response spectrum analysis, response autocorrelation decay, and excitation - response cross spectrum analysis. For the particular experimental conditions, and for the available equipment, the displacement autocorrelation method was found to be the most accurate. However, the method suffered from the disadvantage that it could be applied to only a limited number of modes.

The investigation has been extended to include a range of damping coefficients, the panel damping being increased by the addition of an unconstrained damping layer. The change in damping allows the methods of damping measurement to be compared for a range of values of the ratio of filter bandwidth to resonance bandwidth. The range of application of the individual methods can then be determined. Also the vibration measurements will show the effect of increased damping on the response of the panels to boundary layer excitation.

4.2 Experimental Equipment

4.2.1 Boundary Layer Wind Tunnel

The experimental programme was carried out in the boundary layer wind tunnel at the University of Southampton. The tunnel, which has been described in detail by Bull (16), has a subsonic working section which is 10 feet in length, and a supersonic section. A general arrangement of the tunnel is shown in Figure 11. The panel vibration investigation was carried in the subsonic section at flow Mach numbers of 0.3 and 0.5.

The characteristic properties of the flow in the tunnel were measured by Bull and are presented in Reference 16. The measurements were

used to specify the aerodynamic conditions at the panel measuring positions. The values of the most important parameters are listed in Reference 12.

4.2.2. Experimental Panels

In the investigation, two panels of rectangular planform were considered. The panels were similar to one of the specimens discussed in (12), and were mounted on 6-inch diameter plugs which could be placed at several locations along the tunnel working section. The basic panel dimensions were 4.0 in. \times 2.75 in. \times 0.015 in., but one of the panels was modified by the addition of a stiffener along the major axis, as shown in Plate 3. The stiffener was of simple rectangular cross section with a height of 0.875 inch and a thickness of 0.1 inch. It was bonded to the panel surface using an epoxy resin, and both ends were fixed.

Each panel could be enclosed in the pressure equalising box described in (12), so that the static pressure differential present during tunnel operation could be eliminated across the experimental panels.

The vibration characteristics of the panels were measured by subjecting the panels to discrete frequency excitation. The modal patterns were identified in the first instance by sprinkling fine sand over the plate surface, the mode shapes then being measured by traversing the displacement measuring probe across the panel. Approximate mode shapes for the stiffened panel are shown in Figure 21. Due to the high stiffness of the stringer, the mode shapes and natural frequencies are essentially those associated with two fully fixed panels, of half the basic panel area.

The damping of the panels was increased by the addition of an unconstrained damping layer to the panel surface which was not exposed to the airflow. The damping layer was bonded to the panel face.

4.2.3. Exciter-probe System

The excitation-response cross power spectrum method involves either the direct measurement of the cross power spectrum, or the measurement of the excitation-response cross correlation function from which the cross power spectrum can be obtained by Fourier transformation. The latter method was adopted in this investigation.

Experimental difficulties prevent the monitoring of the boundary layer pressure field on the panels, and a second exciting force, provided by means of an electromagnet, was used as a datum. Cross correlation between the electromagnet excitation and the panel vibration eliminates the vibration due to the boundary layer pressure field, because the electromagnetic and boundary layer excitations are uncorrelated, but the effects of flow speed on modal damping are retained.

To allow the positioning of the measuring probe and the electromagnetic exciter in the pressure equalising box, a special combined exciter-probe, shown in Plate 4, was designed for use with the Wayne Kerr Vibration Meter B731A. The exciter probe consists of a central core which acts as a measuring probe and on which are wound two coils of wire. The core is non-magnetic and one coil is required to supply a D.C. bias to the magnetic field, which would otherwise be provided by the permanent magnetic core of the standard exciter. The permanent magnetism is required to minimise the frequency doubling effect which can arise when the vibrating element has no permanent magnetism. The second coil on the probe carries the alternating current associated with the exciting force.

During the development stages, combinations of up to six coils mounted on formers were used to determine the optimum construction. It was found that any increase in excitation efficiency was countered by increased problems of coil over-heating and eddy currents. In the arrangement chosen finally the eddy current losses were negligible but heating of the probe core could occur when operating for long periods.

The balance of the vibration meter measuring circuit is affected by the combined capacitance of the probe and connecting cable. At the time of investigation the maximum possible capacitance was 130pF. The capacitance of the exciter-probe was approximately 95pF so that a connecting cable with a length of only 3 feet was used in place of the 10 feet long cable fitted to the standard probe. The shorter cable connecting the probe and the meter system was found to be acceptable for the measuring positions in the tunnel.

The probe was calibrated using a simple vibration rig and a microscope with a vernier eyepiece. The system has been described in (12). The calibration curve for the probe is shown in Figure 22, and it is seen that the response is linear for the range of conditions shown. The sensitivity of the probe is 1.75×10^{-4} inch/volt which is similar to the calibration of 1.66×10^{-4} inch/volt for the standard Wayne Kerr C Type Probe. The sensitive element of the exciter-probe has a diameter of 0.14 inch, which is similar to that of the Wayne-Kerr C probe, but the surrounding guard ring is larger in the exciter-probe to provide an increased heat sink.

The effect of the D.C. polarisation is shown in Figure 23. In the absence of the direct current the panel does not distinguish between magnetic attraction and repulsion, and it vibrates at twice the frequency of excitation. The polarising current introduces a vibration component at the frequency of excitation, and this component increases in importance as the degree of polarisation increases. The phenomenon is most important when the excitation frequency f_e is half the value of a natural frequency.

The response at frequencies $f_{1,1}$ and f_e , where $f_e = 0.5f_{1,1}$ and $f_{1,1}$ is the panel fundamental natural frequency, shown in Figure 23 was measured using narrow band filters. Curves of this type were used to determine the polarisation current necessary to obtain a sufficiently large vibration ratio at the frequencies f_e and $2f_e$. The effect of the frequency doubling on the excitation-response cross correlation coefficient has been shown in (12). In the damping measurements the excitation was restricted in general to a frequency range in the neighbourhood of a natural frequency, and the limitations were much less severe than those suggested by Figure 23.

4.2.4. Instrumentation for the Cross Power Spectrum Method

A schematic diagram of the excitation and response measuring circuits is shown in Figure 24. The broad band output of the White Noise Generator was passed through a filter with a variable bandwidth. The polarising current to the coil was adjusted to the required value by means of a variable resistance. The panel vibration was measured using a standard Wayne Kerr Vibration Meter connected to the exciter-probe and the output signal from the Meter

was recorded on one channel of a twin track tape recorder. The voltage across the exciting coil was recorded simultaneously on the second channel of the recorder, and the excitation and vibration signals were cross correlated using the correlator at the University of Southampton (22). When necessary the vibration signal could be used alone to determine the autocorrelation coefficient.

To test the accuracy of the cross power spectrum method, a preliminary investigation was carried out under zero airflow conditions. The tunnel side plate carrying the experimental panel was suspended freely as shown in Plate 5. Bandwidth limited white noise excitation was used and the effect of the bandwidth on the excitation-response cross correlation coefficient was measured. Figure 25, taken from (12), shows the variation of correlation coefficient with excitation bandwidth for three conditions. The maximum correlation coefficient increases as the bandwidth is reduced but never exceeds a value of 0.2. Hence, in subsequent work, a narrow filter having a bandwidth of 4.5% at the half-power point has been used. Maximum cross correlation coefficients greater than 0.5 were then obtained, but errors could be introduced when the panel damping is heavy and the resonance peaks have bandwidths greater than 4.5%.

4.3 Modal Damping

4.3.1. Theory

The use of random techniques in the determination of modal damping has been investigated in (12), where the practical limitations were discussed. The modal damping can be determined directly from the resonance peaks of the measured displacement spectrum if the filter bandwidth is smaller than the resonance bandwidth. In many cases it is not possible to satisfy this condition, particularly when the damping is very light. When the filter bandwidths are too wide for direct spectrum analysis, displacement autocorrelation or excitation-response cross power spectral density methods offer possible alternatives. In (12) it was found that, for light damping and for the experimental conditions chosen, the displacement

autocorrelation method, when its use was valid, gave a more accurate estimate of the modal damping than did the cross power spectrum method. The purpose of this investigation is to extend the work to include higher modal damping whilst maintaining the same excitation conditions.

From (12) the excitation-response cross power spectral density function can be expressed as

$$S(p(\underline{x}'), w(\underline{x}'), \omega) = \sum_{\alpha} \psi_{\alpha}(\underline{x}') H_{\alpha}(\omega) \int_A \psi_{\alpha}(\underline{x}) S_p(\underline{x}, \underline{x}', \omega) d\underline{x} \quad (4.1)$$

where $S_p(\underline{x}, \underline{x}', \omega)$ is the excitation cross power spectral density, $H_{\alpha}(\omega)$ is the transfer function or receptance, and $\psi_{\alpha}(\underline{x})$ is the mode shape for the mode of order α . The modal damping can be estimated when $S(p(\underline{x}'), w(\underline{x}'), \omega)$ is plotted in the complex plane, in a manner similar to that of Kennedy and Pancu (23) for discrete frequency excitation. In practice the excitation-response cross power spectral density function is obtained by transforming the corresponding cross correlation function, and a spectral window function $\phi_D(\omega - \omega')$ is introduced because of the impossibility of achieving infinite time delays in practice. The measured cross power spectral density function is:

$$S'(p(\underline{x}'), w(\underline{x}'), \omega) = \sum_{\alpha} \psi_{\alpha}(\underline{x}') \frac{1}{2\pi} \int_A \psi_{\alpha}(\underline{x}) \int_{-\infty}^{\infty} \phi_D(\omega - \omega') H_{\alpha}(\omega') S_p(\underline{x}, \underline{x}', \omega') d\omega' d\underline{x} \quad (4.2)$$

For single point excitation, with spectral density $S_p(\omega)$,

$$S'(p(\underline{x}'), w(\underline{x}'), \omega) = \sum_{\alpha} \psi_{\alpha}(\underline{x}') \psi_{\alpha}(\underline{x}') K \frac{1}{2\pi} \int_{-\infty}^{\infty} \phi_D(\omega - \omega') H_{\alpha}(\omega') d\omega' \quad (4.3)$$

where it is assumed that the excitation power spectral density is independent of frequency, i.e. $S_p(\omega) = K$.

The error introduced by one particular form of spectral window has been investigated by Clarkson and Mercer (24), and corrections for truncation can be applied to the measured results.

When the autocorrelation method is used, it is shown in (12) that the displacement autocorrelation function is given approximately by the equation

$$R_d(\tau) = \sum_{\alpha} \psi_{\alpha}^2(\underline{x}) \frac{\pi e^{-\delta_{\alpha} \omega_{\alpha} \tau}}{2 M_{\alpha}^2 \omega_{\alpha}^2 \delta_{\alpha}^2} \cos \omega_{\alpha} \tau \int_A \int_A \psi_{\alpha}(\underline{x}') \psi_{\alpha}(\underline{x}'') C_p(\underline{x}', \underline{x}'', \omega_{\alpha}) d\underline{x}' d\underline{x}'' \quad (4.4)$$

where $C_p(\underline{x}', \underline{x}'', \omega_{\alpha})$ is the real part of the pressure cross power spectral density function evaluated at $\omega = \omega_{\alpha}$. For a multidegree of freedom system it is assumed in equation (4.4) that the natural frequencies are well separated and the damping is small. Taking τ as the independent variable

$$R_d(\tau) \approx \sum_{\alpha} Z_{\alpha} e^{-\delta_{\alpha} \omega_{\alpha} \tau} \cos \omega_{\alpha} \tau \quad (4.5)$$

where Z_{α} is independent of τ . Thus the approximate form of the autocorrelation coefficient is a series of exponentially decaying cosines. The method is of use in cases where the vibration in all but one mode can be effectively excluded by the use of filters. The filtered signal will then have an autocorrelation coefficient in the form of a single exponentially decaying cosine.

It has been shown in section 4.2.4 that, in order to obtain a reasonably high excitation-response cross correlation coefficient, the excitation bandwidth had to be limited so that effectively only one mode was excited. Thus the problem is reduced to that of a single degree of freedom system, and, for single point excitation, the excitation-response cross coefficient function is

$$R(p(\underline{x}'), w(\underline{x}''), \tau) \approx 2 \psi_{\alpha}(\underline{x}') \psi_{\alpha}(\underline{x}'') K \int_{\omega_1}^{\omega_2} H_{\alpha}(\omega) \cos \omega \tau d\omega \quad (4.6)$$

where ω_1 and ω_2 are the lower and upper cut off frequencies of an ideal rectangular filter of bandwidth $\Delta\omega = \omega_2 - \omega_1$, centred at the natural frequency ω_{α} of the mode. The excitation power spectral density is

assumed to be constant over this frequency range and to have a value K . If $\Delta\omega$ is large relative to the bandwidth of $H_\alpha(\omega)$, increases in $\Delta\omega$ will have a negligible effect on the value of the integral and hence on the correlation function. However the cross correlation coefficient will be inversely proportional to the square root of the filter bandwidth. An optimum will be reached when the excitation bandwidth is sufficiently narrow to give a high cross correlation coefficient, but when it is sufficiently wide for changes in bandwidth to have a negligible effect on the cross correlation function. The requirement for a high cross correlation coefficient arises from the need to obtain a correlation coefficient which retains a value greater than the value associated with correlator instrument error, over a time delay range which is large enough for the truncation errors to be reasonably small when applying the Fourier transformation. The practical limitations of the method will depend on the optimum conditions for the excitation. The effect of the limitations can be shown by varying the damping of the vibrating system when the excitation bandwidth is maintained at a constant value, or by varying the excitation bandwidth when the damping remains constant. The former method has been adopted in the present investigation.

4.3.2. Damping Measurements

Damping measurements have been made on lightly damped panels by Wilby (12). Similar measurements have been made on panels with greater damping (which will be referred to as "medium" damping), and the damping coefficients have been increased further by the addition of an unconstrained damping layer ("heavy" damping). The results for the three ranges of damping can be compared for excitation which was white noise, restricted to a 4.5% frequency bandwidth for the cross power spectrum method.

Figure 25 shows the measured excitation-response cross correlation coefficient for a mode with medium damping. The maximum value of the

coefficient is approximately 0.8. The cross-power spectral density obtained from the transformation of the coefficient is shown also in the figure and, from (24), the damping coefficient is estimated to be 0.0179. This is 17% larger than the discrete frequency value shown in Table IV. In Figure 26, similar data is presented for a lightly damped mode but in this case the maximum correlation coefficient is only 0.25 and the coefficient decays, within a short time delay, to values which are comparable to correlator error. The damping coefficient estimated from the cross power spectrum is an order of magnitude greater than the discrete frequency value (Table IV). In the lightly damped case the errors due to the small cross correlation coefficient, or to the short time delay, are so large that the resulting damping estimate is extremely inaccurate.

The excitation bandwidth in the two cases was 4.5%, but the effect of the bandwidth can be shown more clearly if it is expressed in terms of the bandwidth of the resonance peak of the structure. The resonance bandwidth will be determined by the half-power points and can be obtained approximately from twice the value of the damping coefficient. Thus, for the data in Figure 25 the ratio of excitation bandwidth to resonance bandwidth was 1.47 and in Figure 26 the ratio was 10.6.

Further data presented in Table IV shows that the autocorrelation method gave damping estimates which were within $\pm 16\%$ of the discrete frequency values, and the autocorrelation method was unaffected by the ratio of excitation bandwidth to resonance bandwidth.

Damping measurements for the unstiffened and stiffened panels are shown in Tables V and VII respectively. In zero airflow conditions the damping coefficients were obtained from amplitude-phase (δ_{D1}) and amplitude (δ_{D2}) methods using discrete frequency excitation. The mean damping coefficient, δ , is also shown in the tables, and has values in the range $0.0068 \leq \delta_D \leq 0.029$. The damping coefficients obtained from discrete frequency excitation can be compared in the tables with values obtained from the excitation-response cross power spectrum method (δ_C)

TABLE IV

Comparison of Damping Estimates for Modes with Medium and Light Damping

Method of Estimation	Damping Coefficient δ_a	
	Medium Damping	Light Damping
Discrete Frequency	0.0153	0.00212
Cross Power Spectrum: from narrow band excitation	0.0179	0.0367
Autocorrelation Coefficient: from narrow band excitation	0.0157	0.00203
Autocorrelation Coefficient: from filtered response to broad band excitation	---	0.00253

TABLE V

Modal Damping of the 4.0 in. \times 2.75 in. Panel

Mode	1 - 1		2 - 1		1 - 2		2 - 2	
Frequency c.p.s.	488		744		1396		1900	
Air flow ft./sec.	0	320	0	320	0	320	0	320
δ_{D1}	0.0163	-	0.0093	-	0.0070	-	0.0069	-
δ_{D2}	0.0153	-	0.00745	-	0.0068	-	0.0067	-
δ_D	0.0158	-	0.0084	-	0.0069	-	0.0068	-
δ_C	0.0179	0.0210	0.0092	0.0098	0.0085	0.0091	0.0098	0.0083
δ_A	0.0159	0.0160	0.0068	0.0061	0.0080	0.0041	0.0070	0.0051
δ_C/δ_D	1.132	-	1.095	-	1.231	-	1.441	-
δ_A/δ_D	1.006	-	0.810	-	1.158	-	1.029	-

TABLE VI

Modal Damping of the 4.0 x 2.75 in. Panel with Additional

Damping

Mode	1 - 1		2 - 1	
Frequency c.p.s.	540		920	
Airflow ft./sec.	0	320	0	320
δ_{D1}	0.053	-	0.053	-
δ_{D2}	0.056	-	0.058	-
δ_D	0.055	-	0.056	-
δ_C	0.049	0.063	0.049	0.051
δ_A	0.071	0.071	0.069	0.068
δ_C/δ_D	0.924	-	0.924	-
δ_A/δ_D	1.340	-	1.301	-

TABLE VII

Modal Damping of Stiffened 4.0 x 2.75 in. Panel

Mode Order*	1		2		3		4		5		6		7
Frequency c.p.s.	1720		1935		2072		2543		3035		3722		4665
Airflow ft./sec.	0	320	0	320	0	320	0	320	0	320	0	320	0
δ_{D1}	0.029	-	0.025	-	0.013	-	0.018	-	0.021	-	0.017	-	0.009
δ_{D2}	0.028	-	0.019	-	0.013	-	0.019	-	0.019	-	0.019	-	0.009
δ_D	0.029	-	0.022	-	0.013	-	0.019	-	0.019	-	0.018	-	0.009
δ_C	0.039	0.037	0.035	0.041	0.020	0.027	0.029	0.030	0.025	0.028	0.023	0.021	0.023
δ_A	0.032	0.030	0.021	0.029	0.018	0.020	0.023	0.027	0.028	0.027	0.028	0.031	0.021
δ_C/δ_D	1.345	-	1.591	-	1.538	-	1.526	--	1.250	-	1.278	-	2.558
δ_A/δ_D	1.103	-	0.955	-	1.384	-	1.210	-	1.400	-	1.555	-	2.334

*See Figure 2

TABLE VIII

Modal Damping of Stiffened 4.0 in. × 2.75 in. Panel
with Additional Damping

Mode*	1		2		3		4	
Frequency c.p.s.	1730		1900		2010		2520	
Airflow ft./sec.	0	320	0	320	0	320	0	320
δ_{D1}	0.098	-	0.081	-	0.078	-	0.075	-
δ_{D2}	0.092	-	0.087	-	0.081	-	0.083	-
δ_D	0.095	-	0.084	-	0.080	-	0.079	-
δ_C	0.083	0.112	0.073	0.076	0.079	0.083	0.078	0.079
δ_A	0.057	0.088	0.069	0.057	0.059	0.065	0.060	0.061
δ_C/δ_D	0.874	-	0.870	-	0.987	-	0.987	-
δ_A/δ_D	0.600	-	0.822	-	0.737	-	0.759	-

* See Figure 2

and from the response autocorrelation method (δ_A). The random excitation was narrow band white noise with a 4.5% bandwidth, so that the ratio of excitation to resonance bandwidth was in the range of 3.31 to 0.78. The results show that in general the random excitation methods over estimate the damping and that the cross power spectrum method has the greater error. However the errors are much smaller than those which arise when the damping is very light (Table IV).

When the unconstrained damping layer was added to the panels, the damping coefficients measured by discrete frequency excitation increased by factors of 3 to 6. Results for the two panels are contained in Tables VI and VIII. Random techniques were again applied in the measurement of damping, the excitation bandwidth being 4.5%. Under these conditions the ratio of excitation bandwidth to resonance bandwidth lies in the range of 0.24 to 0.41. The results in Tables VI and VIII show that, in general, the cross power spectrum and autocorrelation methods now underestimate the modal damping, and that the autocorrelation method has the largest errors.

The damping coefficients shown in Tables V and VIII can be considered in relation to the assumptions used to establish the methods theoretically. In the cross power spectral density method it is assumed that for single point excitation, the exciting force has a constant power spectral density over the frequency range of interest. This is necessary if the resonance curve in the complex response plane (23) is to be used directly, and it is assumed also in the derivation of equation (4.3). The assumption is not necessary in the autocorrelation method, but equation (4.5) depends on the assumptions that the natural frequencies are well separated and the damping is small.

For an ideal rectangular filter the assumption of constant excitation spectral density will be satisfied fairly well when the ratio of excitation bandwidth to resonance bandwidth is greater than 1.5 approximately. In the case of a practical filter the assumption will be

less accurate if the same bandwidth ratio is used, but the above bounding value can be taken as a guide. On this basis the assumption of a constant excitation spectral density is valid for both the modes in Table IV, but for only some of the modes in Tables V and VII. It is not valid for the modes in Tables VI and VIII and in this case the assumption of small damping used in the autocorrelation method is also invalid. From the filter characteristics, the cross power spectrum method would be expected to underestimate the modal damping significantly when the bandwidth ratio is less than 1.5 approximately.

When the assumptions are clearly satisfied, the ratio of excitation bandwidth to resonance bandwidth being of the order 10, the cross power spectrum method overestimates the modal damping by an order of magnitude, but the autocorrelation method is reasonably accurate. When the assumptions are satisfied only marginally, with a bandwidth ratio of approximately 1.5, the cross power spectrum method overestimates the damping but the error is only a factor of 1.5 to 2.0. The autocorrelation method is still the more accurate, for the modes which satisfy the conditions on the method. Under conditions for which the theoretical assumptions are no longer valid, with bandwidth ratios less than unity, and high damping, it appears that the cross power spectrum method predicts the modal damping with reasonable accuracy, and the autocorrelation method is in error. The accuracy of the cross power spectrum method in these conditions is surprising but it is due, probably, to the combination of two opposing effects. It has been observed above that the cross correlation technique tends to overestimate the damping. However if the variation of excitation spectral density caused by the filter characteristic is large in the neighbourhood of the natural frequency, it will have the effect of underestimating the damping, unless corrections are made. The two effects will provide a certain amount of cancellation, and this may explain the apparent improved performance of the cross correlation method.

The results indicate that the excitation-response cross power

spectrum method, when used through the associated cross correlation function, is of very limited application and tends to be less accurate than the autocorrelation method when the necessary conditions are satisfied for each method. The limitation on the use of the cross power spectrum method, to conditions in which the ratio of excitation bandwidth to response bandwidth is approximately unity, suggests that more reliable results may then be obtained if the available filters are used in the direct analysis of the resonance peak, and the peak bandwidth is measured.

4.3.3. Effect of Airflow

The effect of an airflow velocity of 320 ft./sec. on the modal damping of the panels is shown in Tables V to VIII. Because of problems discussed above, the results for the heavily damped panels should be treated with caution, but, with one exception, all the modes show only a small change of damping with flow velocity, the changes being of the same order of magnitude as the experimental error. When the structural damping is large, the acoustic damping will form only a small fraction of the total and the flow parameters would be expected to have a very small effect on the total modal damping. The results agree with those in (12), where significant changes in the lightly damped panels were observed for the lowest order modes only.

4.4. Panel Displacement

4.4.1. Measured Response

The effect of the increased damping on the panel response has been observed when the panels were exposed to an airflow velocity of 320 ft./sec. in the boundary layer wind tunnel. The panel displacement spectra were measured for the undamped and damped conditions so that the results could be compared.

The displacement of the panels was measured by means of a Wayne Kerr capacitance probe, as discussed in (12). The output signal from the meter was recorded on magnetic tape and analysed using the 2% bandwidth filters of the Muirhead Pametrada Wave Analyser. The filtered signal was integrated for 50 seconds to obtain a statistically reliable result.

Displacement power spectra for the undamped and damped panels are

shown in Figures 28 to 31, where the response is expressed in terms of the displacement for unit excitation. This is given by the ratio of the displacement power spectral density to the excitation pressure power spectral density. The measuring probe position (x_1, x_3) is related to the Cartesian coordinate system with the origin at the upstream lower corner of the panel, the x_1 and x_3 directions being parallel to the panel major and minor axes, respectively, and the positive x_1 direction in the flow direction. Measured response spectra for the undamped 4.0 x 2.75 in. panel are shown in Figures 28 and 29 for two boundary layer thicknesses. Measured spectra for the damped panel under similar flow conditions are shown in Figures 30 and 31. The results have not been corrected for resolution loss, but the errors will be small because the filter bandwidth is equal to, or less than, the bandwidths of the peaks.

4.4.2. Theoretical Response

The theoretical prediction of the response of simple panels to turbulent boundary layer excitation has been discussed in (12) using the normal mode approach, and it was seen that there was generally good agreement between the predicted and measured responses. However the theory tended to overestimate the panel displacement.

Using the notations of (12), the displacement power spectral density function $S_d(\omega)$ at position \underline{x} , is given by the following equation; which is similar to that of Powell (25).

$$S_d(\omega) = \sum_{\alpha} \sum_{\beta} \psi_{\alpha}(\underline{x}) \psi_{\beta}(\underline{x}) H_{\alpha}^*(\omega) H_{\beta}(\omega) \int_A \int_A \psi_{\alpha}(\underline{x}') \psi_{\beta}(\underline{x}'') S_p(\underline{x}', \underline{x}'', \omega) d\underline{x}' d\underline{x}'' \quad (4.7)$$

where $\psi_{\alpha}(\underline{x})$ is the mode shape of the mode of order α

$H_{\alpha}(\omega)$ is the complex response function for the mode of order α

$H_{\alpha}^*(\omega)$ is the complex conjugate of $H_{\alpha}(\omega)$

and $S_p(\underline{x}', \underline{x}'', \omega)$ is the excitation pressure cross power spectral density function.

For viscous damping, δ_α , the response function is

$$H_\alpha(\omega) = \frac{1}{M_\alpha((\omega_\alpha^2 - \omega^2) + 2i\delta_\alpha\omega\omega_\alpha)}$$

where M_α is the generalised mass and ω_α is the natural frequency. The pressure cross power spectrum can be obtained empirically from Bull (1, 16) and analytic representations of the excitation field are summarised in Appendix A of (12).

The displacement spectral density function has been determined analytically in (12), with the assumption that the mode shapes are similar to those of a simply supported panel. That is,

$$\psi_\alpha(\underline{x}) = \sin \frac{m\pi x_1}{L_1} \sin \frac{n\pi x_3}{L_3} \quad (4.8)$$

where L_1, L_3 are the panel dimensions in the x_1, x_3 directions respectively. The results can be used to estimate the response of the medium and heavily damped panels, although assumptions of light damping in the theoretical work may not be completely valid. Because of the high stiffness of the central stiffener, the stiffened panel can be considered, approximately, as two fully fixed panels.

In (12) it was shown that the cross terms in equation (4.7), i.e. terms for which $\alpha \neq \beta$, could be neglected for the lightly damped panels. This is not necessarily true for the present structures where the damping is high, and the contributions from the cross terms have to be considered.

Displacement spectra have been calculated for the experimental panels, under the experimental conditions shown in Figures 28 to 31. The spectra, based on the joint terms ($\alpha = \beta$) only, are shown in the appropriate figures. In Figures 29 and 31 the cross term contributions have been estimated and the combined spectra are shown. In Figure 29 it is seen that the cross terms make only a small contribution to the total displacement spectral density, but in Figure 31, where there is heavy damping, the

cross terms have a significant effect, even though the natural frequencies are well separated.

4.4.3. Discussion

The results in Figures 28 to 31 show that, with the exception of the 1-2 mode in Figure 29, the theory predicts the response to a reasonable degree of accuracy. The presence of the damping treatment increases the panel natural frequencies slightly, but the main effect shown is that of the reduced level of vibration, particularly at the natural frequencies. The measured and estimated spectra show that the presence of the damping changes the resonant peak spectral density by factors of 10^{-2} , approximately, but as is to be expected the change in response at the frequencies of the spectral troughs is much less marked. The theoretical spectra have been calculated using measured natural frequencies in the undamped and damped cases, so that the results will not show any predicted variation of natural frequency with damping. Otherwise the theory predicts fairly accurately the variation of the response spectra with damping.

4.5. Conclusions

From the investigation into the vibration of undamped and damped panels, conclusions can be drawn regarding the methods of measuring modal damping, and the effect of damping on boundary layer induced vibration.

(a) Consider conditions specified by the frequency ratio which is defined as the ratio of the filter bandwidth to the bandwidth of the resonant peak, both bandwidths being measured at the half-power point.

When the frequency ratio is large relative to unity (i.e. of the order of 10) the excitation-response cross spectral density method, through the cross correlation function, overestimates the damping excessively (by a factor of 10 for the conditions investigated). When the ratio is of the order of unity the method still overestimates the damping but to a much smaller degree of error (factor of 2). Finally, when the ratio is less than unity the method appears to give a reasonable estimate of the damping, but this may be fortuitous because of the cancelling effect of two opposing errors (Section 4.3.2.).

(b) In all cases where the modes could be separated into single degree of freedom systems, and the damping was not too large, the displacement autocorrelation method gave reliable estimates of the modal damping.

(c) Based on the results of the present investigation, and the results in (12), the following recommendations are proposed for the use of random techniques in the measurement of damping.

- (i) When the frequency ratio of filter bandwidth to the measured bandwidth of the resonant peak is less than 0.25, then the damping be estimated from the measured bandwidth of the peak.
- (ii) When the frequency ratio is greater than 0.25, when the natural frequencies are well separated, and when the resonant peaks are large relative to the neighbouring spectral troughs, then the response autocorrelation method be used.
- (iii) When conditions (i) and (ii) are not satisfied, the structure shall be excited by narrow band white noise, and the excitation-response cross power spectrum method, through the cross correlation function, be used.
- (iv) The alternative method to (iii), using the direct measurement of the excitation-response cross power spectral density, has not been investigated. This method may be more accurate than method (iii), in which case it might provide an alternative to method (ii).

(d) The measurements show no significant variation of panel damping with flow velocity or boundary layer thickness.

(e) The effect of damping on the vibration of simple panels exposed to turbulent boundary layer excitation is similar to that predicted from the normal mode approach. As predicted, the greatest change of response occurs at the panel natural frequencies. When the damping is heavy, cross term contributions to the theoretical response spectra become significant and have to be included.

5. THE RESPONSE OF MULTI-PANEL ARRAYS TO RANDOM EXCITATION

5.1. Introduction

The vibration of simple panels exposed to random excitation in the form of a turbulent boundary layer pressure field or acoustics plane waves, is discussed by Wilby in Reference 12.

In the discussion it was observed that the simple panels were not very representative of practical structures and that it would be advisable to consider the vibration of more complicated structures in the form of multi-panel arrays.

Two multi-panel arrays, constructed by the bonding of stiffeners to the basic panels, have been investigated. The vibration has been measured when the arrays were exposed to the turbulent boundary layer pressure field in the wind tunnel and, for one array, comparative measurements were carried out for excitation composed of grazing incidence acoustic plane waves. In all cases the displacement power spectral density was measured for one or more panel bays, and, for boundary layer excitation, displacement cross correlation measurements were made between several bays of the array. In addition the panels were excited at discrete frequencies in order to identify the normal modes of the structures.

In the presentation of the results it has been possible to make comparisons with theoretical predictions but, at the present stage, this is limited mainly to the determination of natural frequencies and normal mode shapes. Future work at the Institute will enable estimates to be made of the vibration due to the random excitation, and comparisons will be made with the measurements.

5.2. Experimental Equipment

5.2.1. Panels

The experimental panel arrays were made by bonding thin sheets of steel to frames which had the same dimensions as the side plates of the boundary layer wind tunnel. The frames surrounded 22 inch x 6 inch

rectangular apertures which formed the effective area of the basic panels. For constructional reasons the plate length was chosen to be within the longitudinal dimension of a tunnel side plate, and for aerodynamic reasons the length was restricted so that the boundary layer characteristics did not change appreciably over the panel surface. The panel width was restricted so that the panel surface was not affected by the three-dimensional boundary layer in the corners of the tunnel working section. Each panel had a thickness of 0.015 inch.

The stiffeners were bonded to the panel surface and secured at the ends by means of clamps. The stiffeners were parallel to the 6 inch side of the basic panel, and were 0.015 inch thick. The stiffeners had "L" shaped cross sections, each arm of the "L" being 0.25 inch in length.

Two panel arrays were tested, one having four bays of dimensions 5.5 in. x 6.0 in. x 0.015 in., and the second having eight bays with dimensions 2.75 in. x 6.0 in. x 0.015 in. In each case the 6.0 inch dimension was perpendicular to the direction of flow in the tunnel. The eight-bay array is shown mounted in the tunnel side wall in Plate 6.

5.2.2. Pressure Equalising Facility

As described previously (e.g. Volume I) the static pressure in the wind tunnel is below atmospheric pressure when in operation. The static pressure differential across the single panels was eliminated by enclosing one face in a small box which could be equalised to the tunnel static pressure. The box could not be used for the panel array but a large chamber with dimensions 16 ft. x 12 ft. x 8 ft. was constructed around the tunnel working section to serve the dual purpose of pressure equalisation and a noise measuring environment. The chamber is of double wall construction with sand filling the intermediate volume. It can be partially evacuated to provide a receiving volume which is at the same static pressure as the tunnel working section. The evacuation is achieved by means of a vacuum pump, fine control being provided by manual operation of a series of valves.

5.2.3. Vibration Measuring Equipment

The panels used in the investigation were too thin to permit the attachment of measuring instruments without significantly altering the vibrational characteristics of the structures. Hence a non-contacting Wayne Kerr capacitance probe was used, and the panel vibration was measured in terms of the panel displacement.

The probe could be mounted on a traverse gear which allowed movement over the entire panel surface. The traverse gear had provision for the simultaneous use of several probes at different positions on the panel array, and two probes were used for the correlation measurements of the panel displacement. The complete side plate with the panel array, traverse gear and probe system could be placed in four positions along the tunnel working section, or could be removed from the tunnel for discrete frequency excitation in free space, or for random acoustic excitation in the siren tunnel. The signals from the capacitance probes were recorded on magnetic tape and analysed on a Muirhead Pametrada Wave Analyser, using filters of 1.2% bandwidth, when the displacement spectra were required, or on the Institute correlator when the displacement correlation coefficient was being measured.

5.3 Panel Normal Modes

5.3.1. Discrete Frequency Excitation

Plate 7 shows the multi-stiffened panel array in position for the identification of the mode shapes using discrete frequency excitation, which was produced by means of an electromagnet. When measuring the mode shapes two probes were used and these could be traversed across the panel surface so that the amplitude and relative phase of the displacements at two positions could be measured. In general one probe was placed at a reference point on one of the bays and the second probe was placed at several positions on the same bay and on other bays. Measured mode shapes are shown in Figures 32 and 33.

5.3.2. Damping Measurements

The damping in each mode was measured from amplitude-response

curves drawn on an X-Y Plotter, but in certain cases where the resonance peaks could not be identified easily the damping measurements were carried out using a Resolved Components Indicator with the excitation signal as the reference.

The damping in the boundary layer tunnel in the presence of the airflow was measured using the special exciter probe described in Section 4. This latter method involved the use of the excitation-response cross power spectrum, determined from the Fourier transform of the associated cross correlation function and, as indicated in Section 4, it is liable to over estimate the damping by a significant factor. The displacement autocorrelation method, which often provides the most reliable estimates of the damping, could not be used because of the close proximity of the structural natural frequencies.

Measured values of the modal damping ratios are shown in Table IX for several conditions.

5.3.3. Calculated Frequencies and Normal Modes

The natural frequencies and mode shapes of multi-stiffened panels have been calculated by Lin (26), Mercer (27), and Mercer and Seavey (28). Based on the equation of motion of a single bay of the panel array

$$\text{i.e.} \quad \nabla^2 \nabla^2 w = - \frac{hp}{D} \frac{d^2 w}{dt^2}$$

Lin determined the upper and lower bounding modes, designated as the stringer bending and torsional modes respectively, for a given band of modes. The work of Mercer and Seavey has enabled the calculation of the natural frequencies and mode shapes of the intermediate modes for either regularly or irregularly spaced stiffeners, and the method has been used to calculate mode shapes and natural frequencies for the experimental panel arrays. Theoretical mode shapes for the eight-bay array are shown in Figure 32. In some cases the predicted mode shapes differ from those measured. This is due, probably, to errors in manufacture of the arrays creating non-identical panel bays.

Measured and predicted natural frequencies are contained in Table IX.

TABLE IX

Natural Frequencies and Modal Damping of Multi-Panel Arrays

8-Bay Array						4-Bay Array		
Mode	Natural Frequency c.p.s.		Damping ratio δ_a			Mode	Natural Frequency c.p.s.	
	Calculated	Measured	(a)	(b)	(c)		Calculated	Measured
1 (Torsion)	325	285	0.013	0.039	0.014	1	101	126
2	332	320	0.008	0.049	0.022	2 (Torsion)	121	147
3	342	340	0.009	0.058	-	3	128	155
4	353	370	0.022	0.041	0.025	4 (Bending)	143	160
5	362	385	-	0.038	0.024			
6	368	395	-	-	-			
7	-	-	-	-	-			
8 (Bending)	-	420	0.0095	0.031	0.027			

Damping ratio (a) Wind tunnel, no airflow.

(b) Wind tunnel, airflow 329 ft./sec.

(c) Siren tunnel.

5.4 Response Spectra

5.4.1. Boundary Layer Excitation

The response of the four-bay and eight-bay arrays to boundary layer excitation has been measured at a flow velocity of 329 ft./sec. (Plate 6) and typical spectra are shown in Figures 34 to 36. The measurements for the eight-bay array are shown for the values of the boundary layer thickness which occur at the extremes of the range available, and at one boundary layer thickness response spectra are shown for two different bays. In all cases interest was centred mainly on the first band of natural frequencies, the band being bounded by the first stringer torsional and bending modes, so the displacement was measured at the centres of the bays. The spectrum for the four bay array shows four resonant peaks, but only seven resonant peaks were measured for the eight-bay array. In the latter case there was no measurable response at the eighth natural frequency in the band.

Theoretical response spectra have not been calculated for the experimental panels but, as a first approximation, the response in the stringer torsional mode has been estimated using the theory developed for the single panel. (See Ref 12) In this case it is assumed that the mode shape is the same as that for a mode (m, n) of a simply supported single panel where m , the number of modal half wavelengths along the panel length, is equal to the number of bays in the panel array, and n is taken to be unity. Thus for the eight-bay array, the equivalent simply supported mode of order $(8, 1)$ was considered. In this approximate method the measured natural frequency is used, but otherwise the effects of the finite mass (12% of the panel mass) and dimensions of the stiffeners are neglected.

The calculated response in the stringer torsional mode is shown in each of the Figures 34 to 36 and it is seen that there is a certain amount of agreement (the measured resonance peaks have not been corrected for loss of resolution) but the theory over estimates the response in all cases. This follows the trend shown in Ref. 12 for the single panels and,

as discussed in the earlier results, errors of this nature can arise because of the assumed mode shapes. Close agreement between experiment and theory can not be expected, so that the results, especially for the eight-bay array, are satisfactory. The associated boundary layer pressure spectra are shown in Reference 12.

When the measured spectra for the two boundary layer conditions in Figures 35 and 36 are compared it is seen that below 400 c.p.s., i.e. for the five lowest order modes, the response to unit excitation is greater for the thinner boundary layer. For the two highest order modes shown, the response is greater when the panel array is exposed to the thicker boundary layer. The measured variation of modal response with boundary layer thickness is shown in Figure 37, where the displacement power spectral density is plotted for the natural frequencies of the panel array.

When considering the lowest order (stringer torsional) mode the simplified theory predicts a change in response spectral density with boundary layer thickness which is very similar to that measured.

5.4.2. Siren Excitation

The vibration of the eight-bay array has been measured when exposed to siren excitation, which is composed of random acoustic plane waves at grazing incidence. The panel side plate was mounted in the opening of the working section of the siren tunnel, the remaining open area being blocked by heavy wooden boards. The structural modal damping was measured under these experimental conditions because the radiation impedance differed from that in the boundary layer wind tunnel. The measured damping coefficients are contained in Table IX.

The noise spectrum measured in the siren tunnel is shown in Figure 38 and it is seen that the frequency range is limited, effectively, to the range 100 c.p.s. to 1,000 c.p.s. However the present investigation is restricted to bands of natural frequencies which lie in the range of 150 c.p.s. to 400 c.p.s. so that the results will not be affected by siren tunnel limitations. A response spectrum, for the frequency range of interest, is shown in Figure 36.

5.4.3. Comparison of Response Spectra

When the panel response spectrum in Figure 36 for acoustic excitation is compared with response spectra to boundary layer excitation, shown in Figures 35 and 36 for the same position on the panel array, it is seen that the acoustic excitation produces the largest response in the three lowest order modes whilst the boundary layer excitation causes the largest response in the highest order modes in the band. In all cases the response is taken to be the displacement power spectral density for unit excitation spectral density, so that the comparison excludes the effect of excitation power spectral density. Thus the observed variations are due to changes in the excitation correlation pattern, or to changes in the modal damping.

When the experimental damping coefficients associated with the two excitation conditions are compared in Table IX, it is seen that the modal damping measured in the boundary layer wind tunnel when the airflow is present exceeds that measured in the siren tunnel. The difference between the damping ratios is greater for the lower order modes than it is for the higher order modes. This variation will contribute to the change in spectrum shape with type of excitation but the measured spectrum change is much greater than that associated solely with the damping change. Thus the effects of the excitation correlation pattern will have to be included before a complete discussion of the spectra is possible.

The shape of the displacement spectrum for the centre of the fourth bay of the eight-bay array has been estimated from (29) for acoustic excitation. As a first approximation it was assumed that the damping was independent of frequency and typical stiffener characteristics were assumed. The spectrum (Figure 39) is similar in shape to that measured, in so far as there is no mode which dominates the response. The assumed damping was higher than that measured so that the estimated resonance peaks are not as prominent as those in the measured spectra.

5.5. Response Correlation Measurements

5.5.1. Displacement Cross Correlation Coefficient

The displacement cross correlation between the centres of pairs of panels has been measured for the eight-bay array and the resulting cross correlation coefficients are shown in Figures 40 to 44.

In Figures 40 and 41 displacement cross correlation coefficients are shown, over a positive time delay range, for two boundary layer thicknesses and for a series of measuring probe separation distances ξ_1 . Because the probes are placed at the centres of the bays the values of ξ_1 are integral products of the bay length of 2.75 inches. In each case bay 3, numbering from the upstream edge of the array, is taken as the datum. The measurements show the expected fall-off of correlation coefficient as the separation distance increases, but the coefficient for each probe separation shows a strong periodic component, with low frequency modulation. Figure 42 shows similar results for the measured correlation coefficient between adjacent bays, with bay 6 as the datum.

When positive and negative time delays are considered, correlation coefficients are obtained with the forms shown in Figures 43 and 44. In Figure 43, for a probe separation of one bay length (2.75 inches) the correlation coefficient shows a certain degree of symmetry about the zero time delay axis, with a maximum correlation coefficient amplitude of about 0.3. When the separation is increased to four bay lengths (11 inches) the maximum cross correlation coefficient is reduced by a factor of 2 and there is no evidence of symmetry.

A general inspection of the correlation data in Figures 40 to 44 shows that there is a degree of correlation between the panel bays which are close together, and the symmetrical shape of the coefficient about $\tau = 0$ indicates that the vibration system is predominantly one of standing waves. When the bay separation is increased there is little correlation between the bay displacements and there is no overall indication of a standing or running wave system. A preliminary analysis of the envelope of the correlation coefficient indicates the presence of an overall maximum value of

the coefficient for each separation distance, the time delay at which this maximum occurs being greater for the greater separations. If this phenomenon is interpreted as being associated with a wave velocity in the panel array, the value of the velocity is 13,500 ft./sec. approximately.

5.5.2. Displacement Cross Power Spectra

For certain experimental conditions the displacement cross correlation coefficients have been transformed to give the displacement cross power spectra, and results for bay pairs (3, 4), (3, 5), (3, 6) and (3, 7) are shown in Figures 45 to 48. The spectra in Figures 45, 46 and 48 are associated with the cross correlation coefficients in Figure 40. The cross spectra show the presence of several resonance-type loops which can be associated with the natural frequencies of the array. When one particular natural frequency is considered the cross spectrum will show the relative phase of the displacement in each bay and an estimate can be made of the associated mode shape. If a sufficient number of cross spectra are measured the presence of standing or running waves can be investigated for each of the modes.

5.6 Conclusions

The vibration of two multi-panel arrays has been measured when the arrays were exposed to turbulent boundary layer excitation. Also the vibration of the eight-bay array was measured under random acoustic excitation. However the investigation has not been completed and only tentative conclusions can be drawn at the present stage.

The response in the lower order modes of the first mode band was greater for siren excitation than for boundary layer excitation but the converse was true for the higher order modes of the band. Part of the difference in the spectrum shape is due to changes in modal damping due to the presence of the airflow in the tunnel, but account must be taken also of the changes in matching between the mode shapes and the excitation correlation patterns for the two pressure fields.

A coarse estimate of the response in the stringer torsional mode can be obtained from the single panel theory, but the theory overestimates the displacement.

Displacement cross correlation measurements between panel bays indicate that standing wave systems exist within two or three bay lengths but the waves die out over larger separation distances. The overall correlation coefficient did not show the presence of running waves. There is a fairly strong standing wave system because of the low torsional stiffness of the stringers.

6. GENERAL CONCLUSIONS

Work on several topics which can be considered separately, but which are associated with the general investigation of boundary layer pressure fluctuations and boundary layer induced vibration, has been discussed, and summaries with detailed conclusions have been presented at the end of each section. It is possible to draw now several general conclusions from the investigation as a whole.

(a) Random techniques can be used to measure the modal damping of structures, and usually the most accurate results are obtained by means of the response autocorrelation decay method. This is especially true when the response can be separated into a series of single degree of freedom systems with damping which is not too large. If filters with bandwidths which are narrow compared with the bandwidths of the resonance peaks are available, damping estimates can be obtained from the measured bandwidth of each resonant peak. The excitation-response cross power spectrum method, via the cross correlation function, is very sensitive to the accuracy of the correlator, and the method can be very inaccurate.

(b) The vibration of stringer-panel arrays exposed to boundary layer excitation shows the presence of standing wave systems extending over several bay lengths when the stringers have low torsional stiffness. The standing waves occur in spite of slight irregularities in bay dimensions which arise in manufacture. Considering the vibration in the first band of modes, the presence of the airflow has a greater effect on the damping than was the case for the smaller, single panels. However, taking the changes of damping into account, the vibration of the arrays caused by siren excitation was greater than that caused by boundary layer excitation for the lower order modes, whilst the converse was true for the higher order modes of the band.

(c) Measurements of the low frequency noise in the boundary layer wind tunnel indicate that it is not associated with the amplification of low frequency disturbances in the tunnel inlet, but it has not been possible to distinguish between acoustic radiation from the turbulent boundary layer and

injector noise propagated in an upstream direction. Thus further work is required before wind tunnels can be used for low frequency investigations of the boundary layer fluctuating pressure field and the boundary layer induced structural vibration.

(d) The growth of turbulent spots in the laminar-turbulent transition region of the boundary layer occurs in two phases, the spread of the turbulent spots being 3° , approximately, for Reynolds numbers (based on laminar momentum thickness) less than 500, and about 11° for higher Reynolds numbers. In both stages, measurements of the pressure spectra and the pressure-velocity cross correlation show that the turbulent spots act like small autonomous regions of turbulent boundary layer. This suggests that the vibration of structures beneath the transition region can be estimated from measurements in the fully turbulent region. However there will be additional low frequency vibration caused by the disturbance of the mean flow by the turbulent spots. The excitation at the low frequencies may be of similar intensity to that associated with the fully developed turbulent boundary layer.

REFERENCES

1. Bull, M.K.
Wilby, J.F.
Blackman, D.R.

Wall pressure fluctuations in boundary layer flow and response of simple structures to random pressure fields.
University of Southampton Report AASU 243 (July 1963) (Final Report on Contract No. AF61(052)-358)
2. Coles, D.

The law of the wake in the turbulent boundary layer.
J. Fluid Mechs. 1 pp 191-226 (1956)
3. Schlichting, H.

Boundary layer theory
Pergamon Press (1955)
4. Schubauer, G.B.
Klebanoff, P.S.

Contributions to the mechanism of boundary layer transition.
N.A.C.A. Report 1289 (1956)
5. Corrsin, S.
Kistler, A.L.

Free-stream boundaries of turbulent flows.
N.A.C.A. Report 1244 (1955)
6. Blackman, D.R.

Wall pressure fluctuations in the laminar-turbulent transition region of a boundary layer.
University of Southampton Ph.D. Thesis (April 1964)
7. Wooldridge, C.E.
Willmarth, W.W.

Measurements of the correlation between the fluctuating velocities and fluctuating wall pressure in a thick turbulent boundary layer.
University of Michigan Report 02920-2-T (1962)

REFERENCES (Contd)

8. Serafini, J.S. Wall pressure fluctuations and pressure-velocity correlations in a turbulent boundary layer.
A.G.A.R.D. Report No. 453 (1963)
9. Lindgren, E.R. The transition process and other phenomena in viscous flow.
Arkiv Fysik 12, 1 (1957)
10. el Baroudi, M.Y. Turbulence-induced panel vibrations
University of Toronto UTIA Report 98
(February 1964)
11. Maestrello, L. Measurement of noise radiated by boundary layer excited panels.
J. Sound Vib. 2, 2 pp 100-115 (April 1965)
12. Wilby, J.F. The response of simple panels to turbulent boundary layer excitation.
AFFDL-TR-67-70 (To be published)
13. Westley, R. Aerodynamic sound and pressure fluctuations in a supersonic blow-down wind tunnel.
N.R.C. of Canada Report LR-274 (January 1960)
14. Irani, P.A. Aerodynamic noise in aircraft and wind tunnels.
Iya Shidhar, K.
Nat. Aero. Lab. Bangalore, India,
Scientific Review SR-AE-2-63 (August 1963)
15. Laufer, J. Some statistical properties of the pressure field radiated by a turbulent boundary layer.
The Physics of Fluids 7, 8, pp 1191-1197
(August 1964)

REFERENCES (Contd)

16. Bull, M.K. Wall pressure fluctuations associated with subsonic turbulent boundary layer flow.
University of Southampton Ph.D. Thesis (June 1963)
17. Curle, N. The influence of solid boundaries upon aerodynamic sound.
Proc. Roy. Soc. A 231 pp 505-514 (1955)
18. Powell, A. Aerodynamic noise and the plain boundary
J.Acoust.Soc.Amer. 32, 8 pp 982-990
(August 1960)
19. Ffowcs Williams, J.E. The sound radiated from turbulent flows near flexible boundaries.
Lyon, R.H.
Bolt, Beranek and Newman Report 1054
(August 1963)
20. Morse, P.M. Vibration and Sound
McGraw-Hill Book Co. Inc. (2nd edition 1948)
21. Rayleigh, Lord The theory of sound, Volume 2 (page 145)
Dover Publications. (1945)
22. Allcock, G.A. A general purpose analogue correlator
Tanner, P.L. for the analysis of random noise signals.
McLachlan, K.R. University of Southampton Report AASU 205
(1962)
23. Kennedy, C.C. Use of vectors in vibration measurement
Pancu, C.D.P. and analysis.
J.Aero.Sci. 14, 11, pp 603-625,
(November, 1947)

REFERENCES (Contd)

- | | | |
|-----|--------------------------------|--|
| 24. | Clarkson, B.L.
Mercer, C.A. | Use of cross correlation in studying the response of lightly damped structures to random forces.
A.I.A.A. Journal <u>3</u> , 2, pp 2287-2291
(December 1965) |
| 25. | Powell, A. | On the fatigue failure of structures due to vibration excited by random pressure fields.
J.Acoust.Soc.Amer. <u>30</u> , 12, pp 1130-1135
(December 1958) |
| 26. | Lin, Y.K. | Free vibrations of continuous skin-stringer panels
J.App.Mechs. pp 669-676 (December 1960) |
| 27. | Mercer, C.A. | The response of structures to random pressures
University of Southampton Ph.D. Thesis
(May 1965) |
| 28. | Mercer, C.A.
Seavey Miss C. | Prediction of natural frequencies and normal modes of skin-stringer panel rows
To be published J.Sound Vib. <u>5</u> , 3 (1967) |
| 29. | Wilby, E.G. | The response of damped, stiffened structures to random excitation.
University of Southampton. Ph.D. Thesis in preparation. |

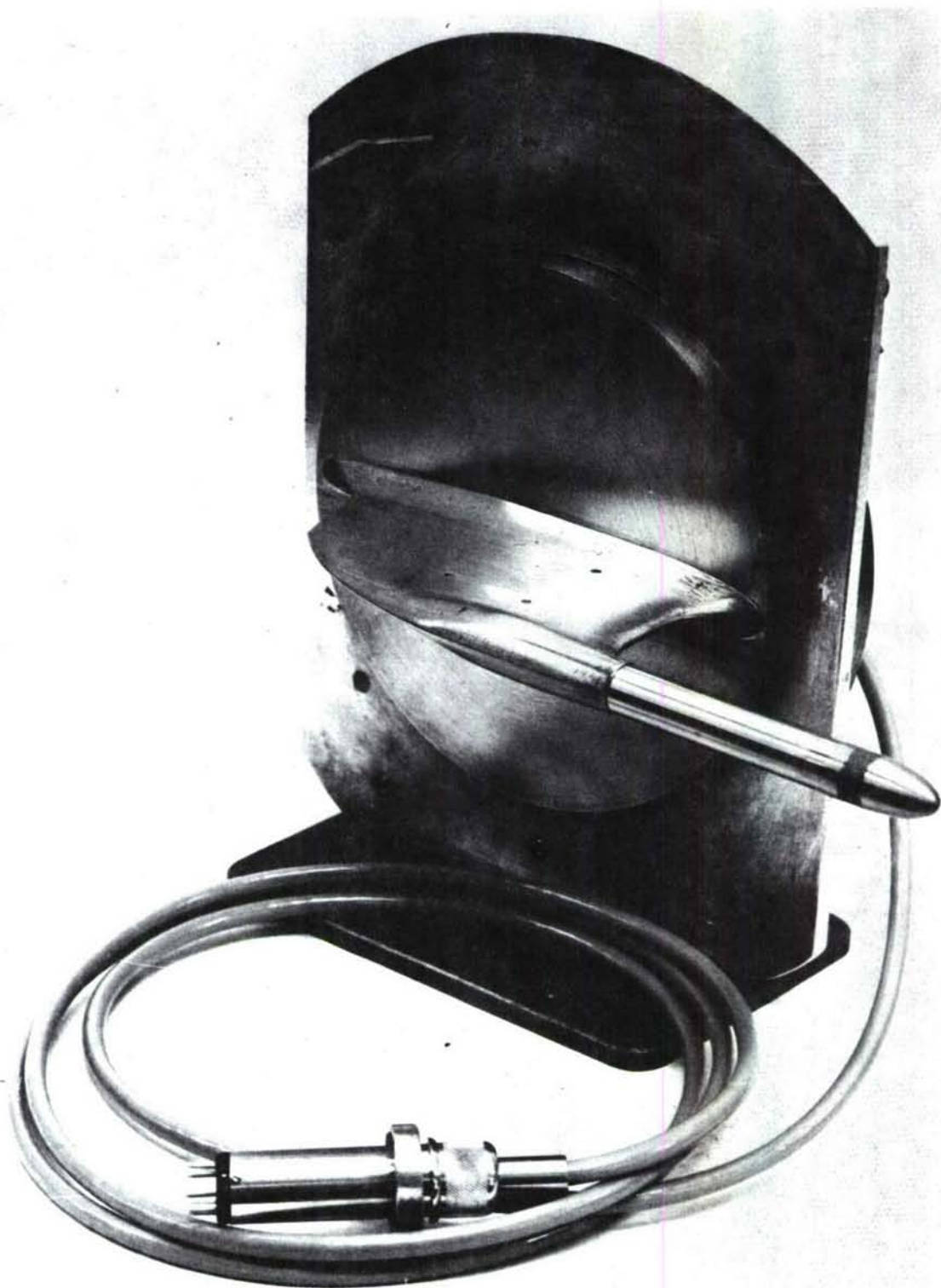


Plate 1 Fixed aerofoil and microphone.

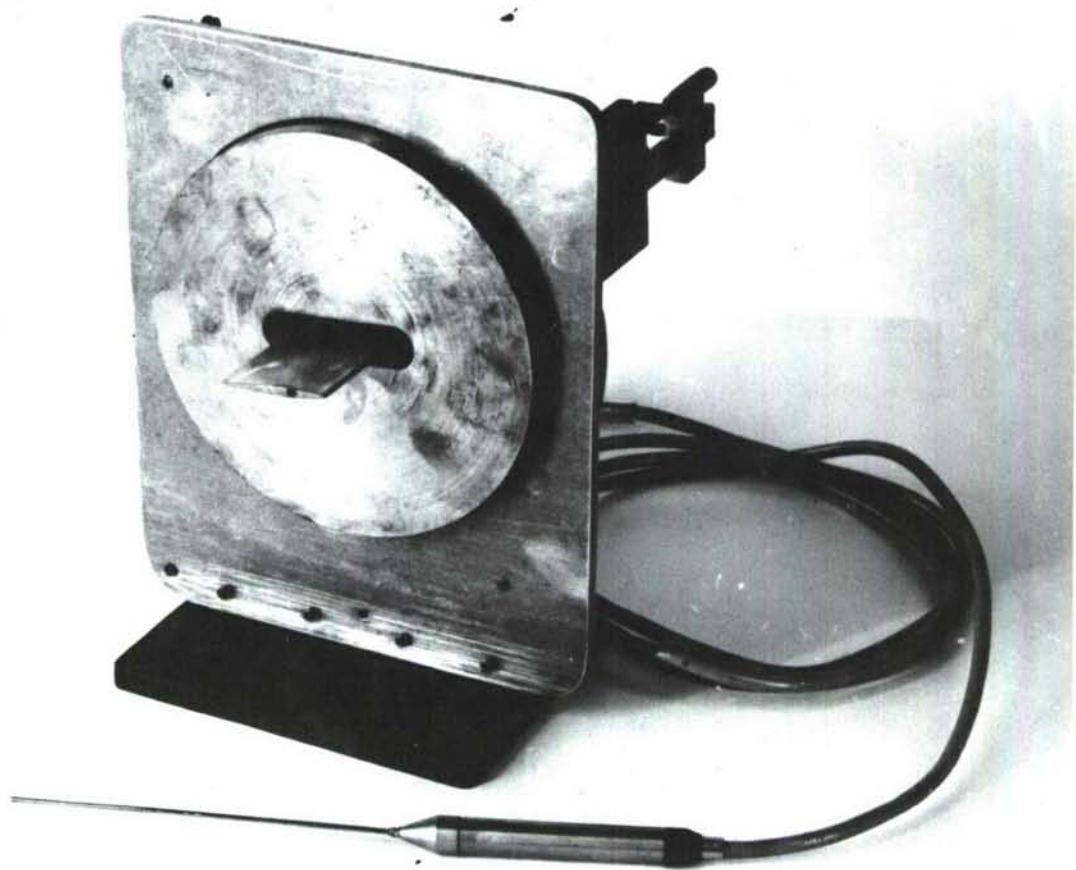


Plate 2 Probe microphone and aerofoil.

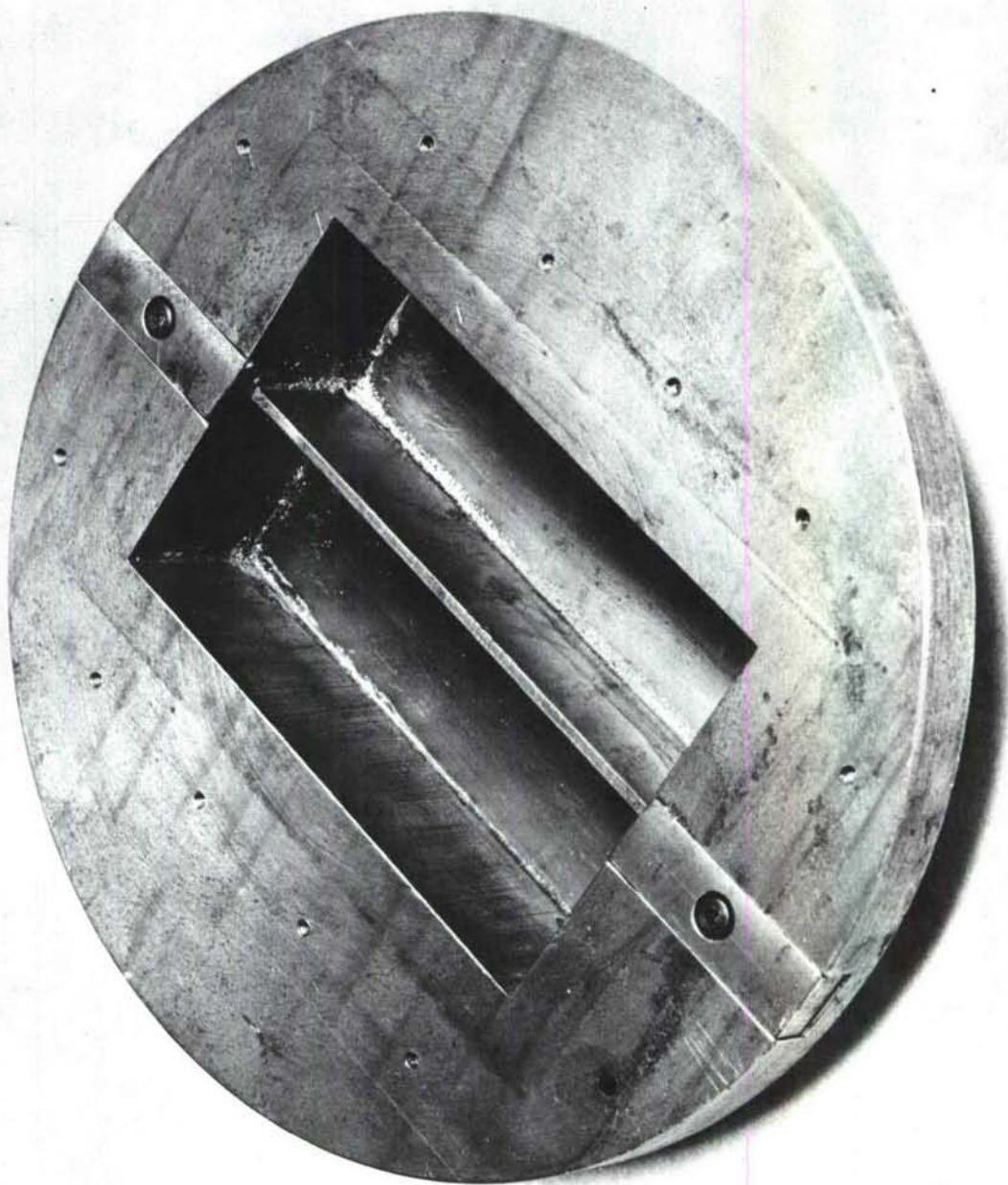


Plate 3 Panel with single stiffener.

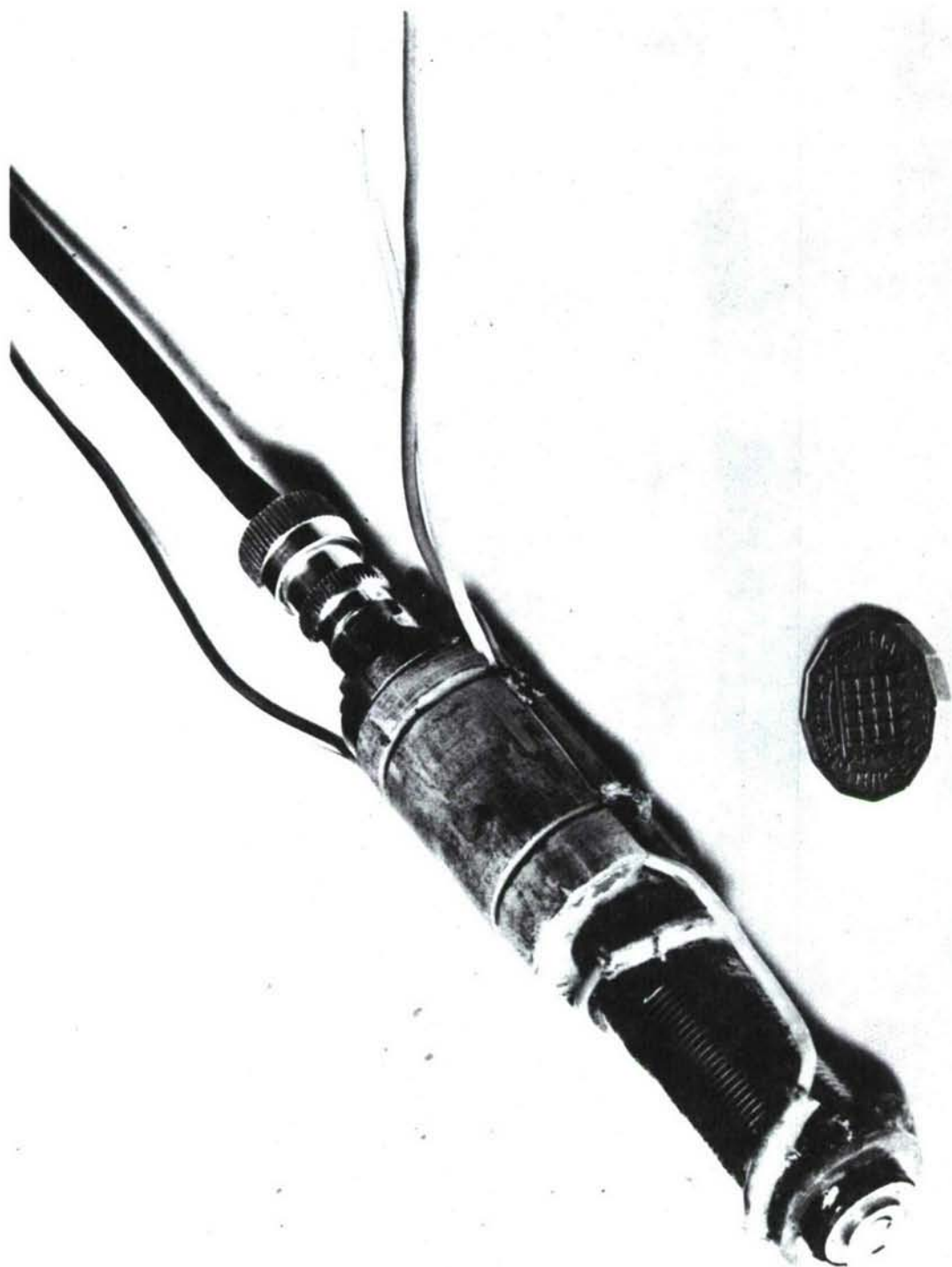


Plate 4 Exciter- probe.

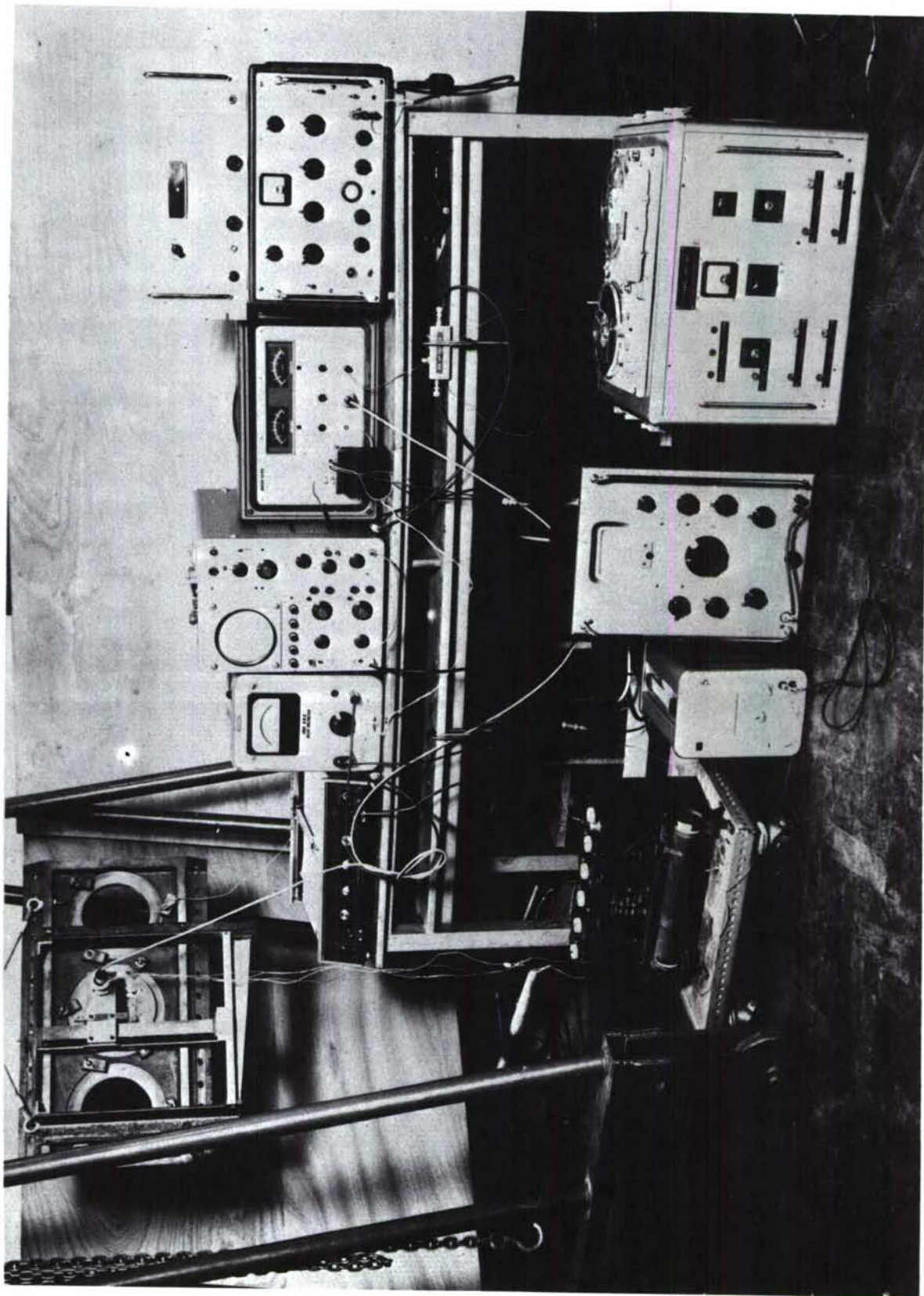


Plate 5 Side plate suspended for damping measurements.



Plate 6 Eight-bay array mounted in boundary layer tunnel.

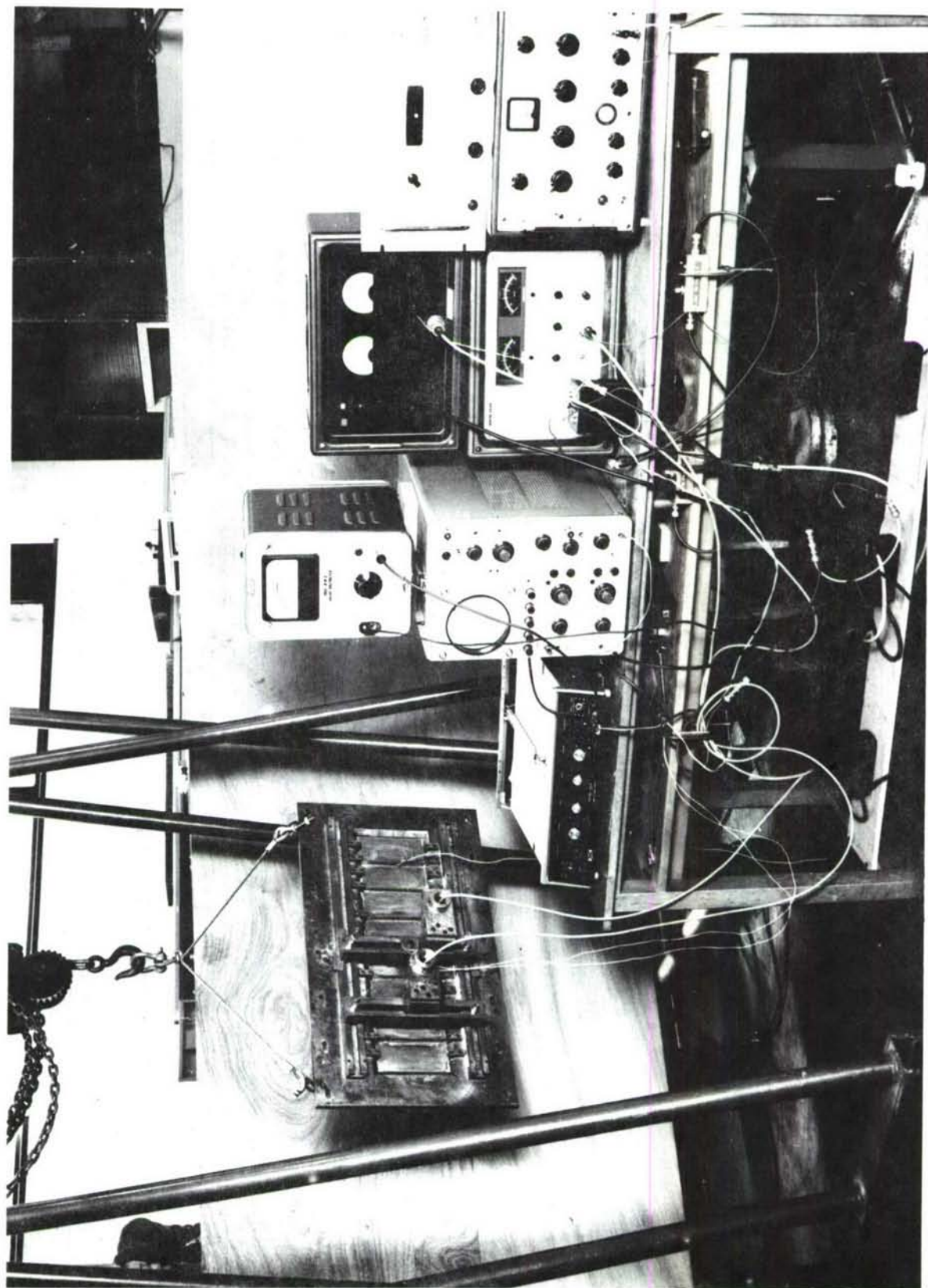
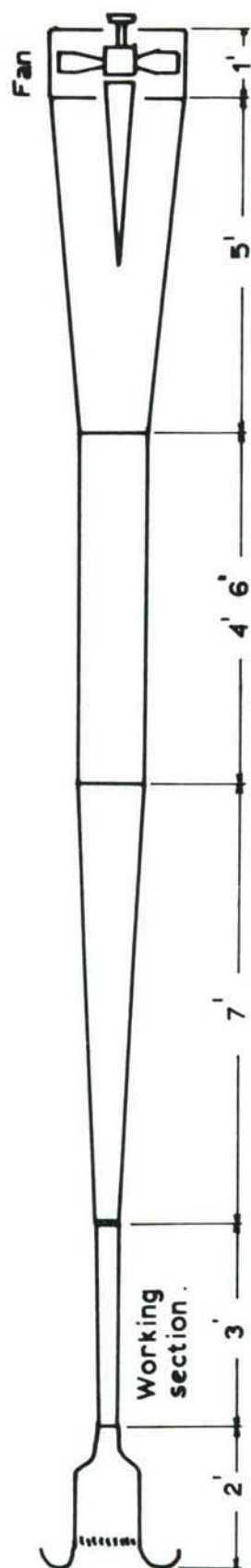


Plate 7 Eight-bay array suspended for mode shape measurement.

GENERAL ARRANGEMENT .



DETAILS OF WORKING SECTION .

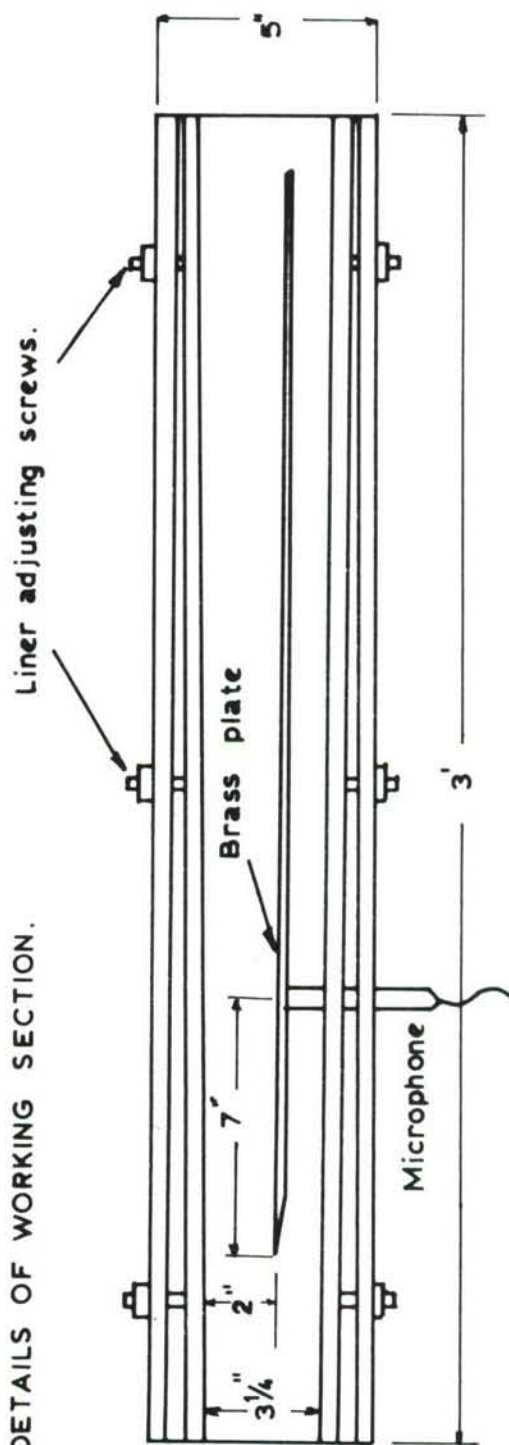


Fig. 1. Arrangement of low speed wind tunnel .

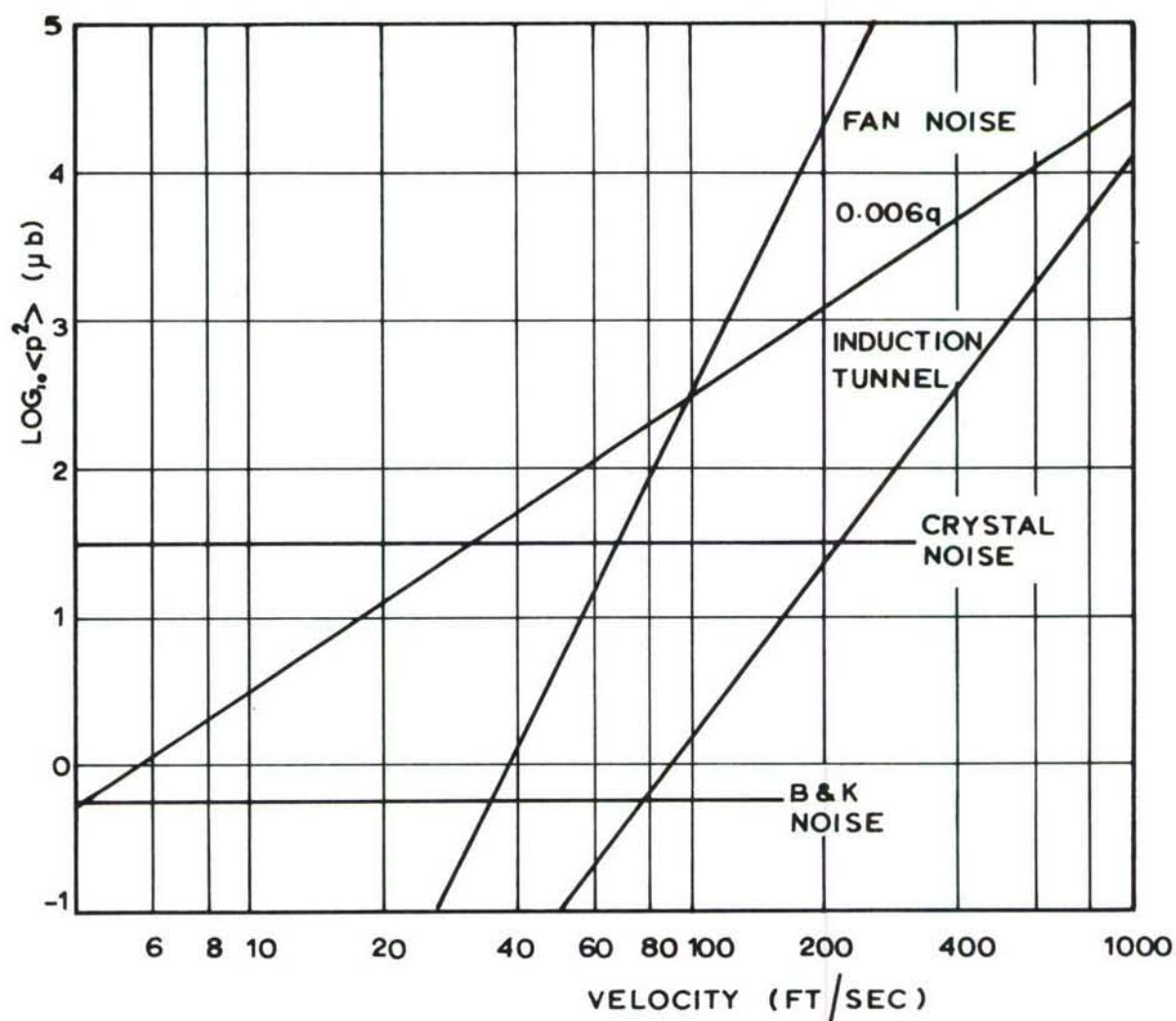


Fig. 2. Comparison of overall noise in the transition region in fan and induction tunnels.

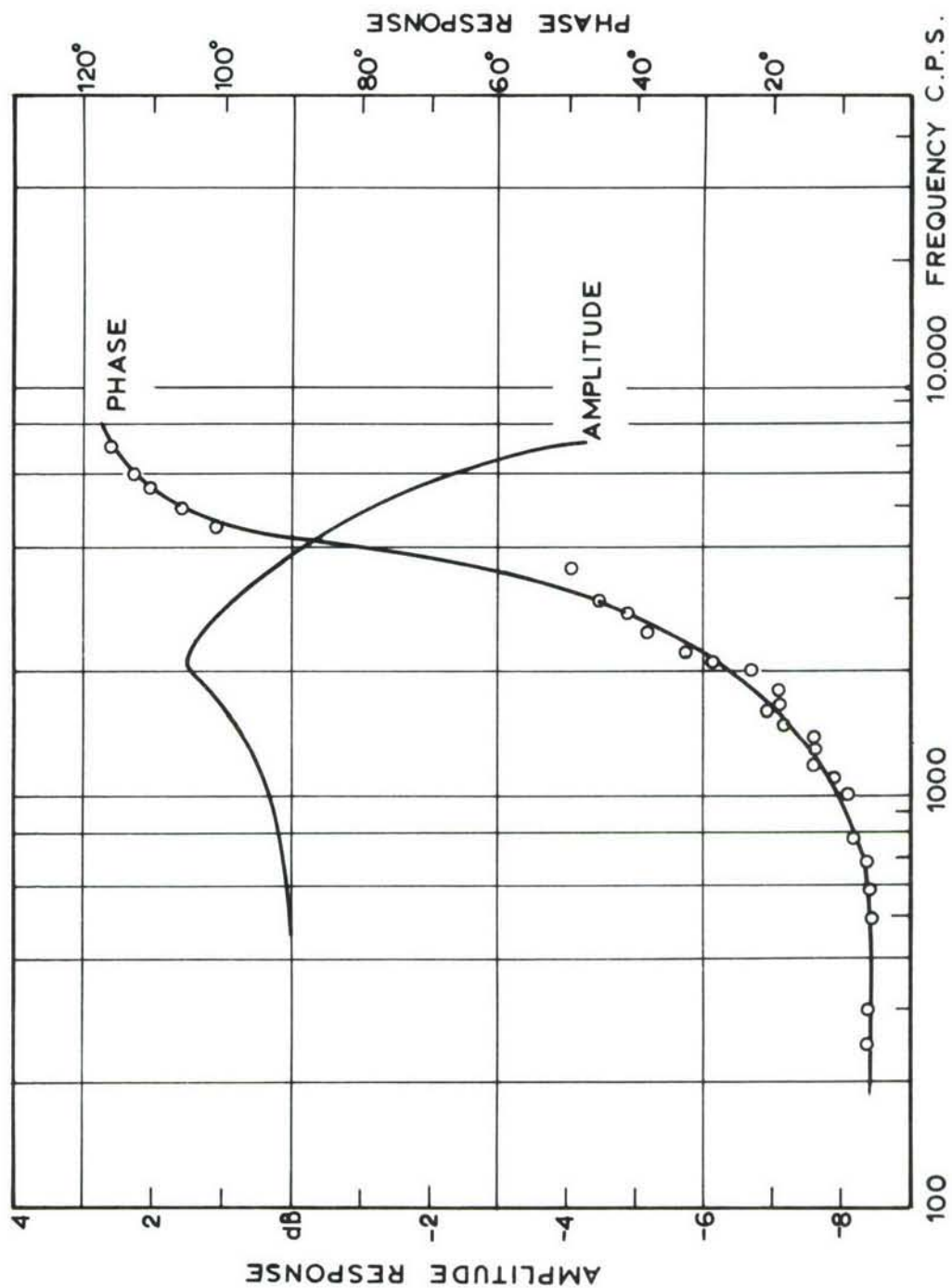


Fig.3. Phase and amplitude response at station 1

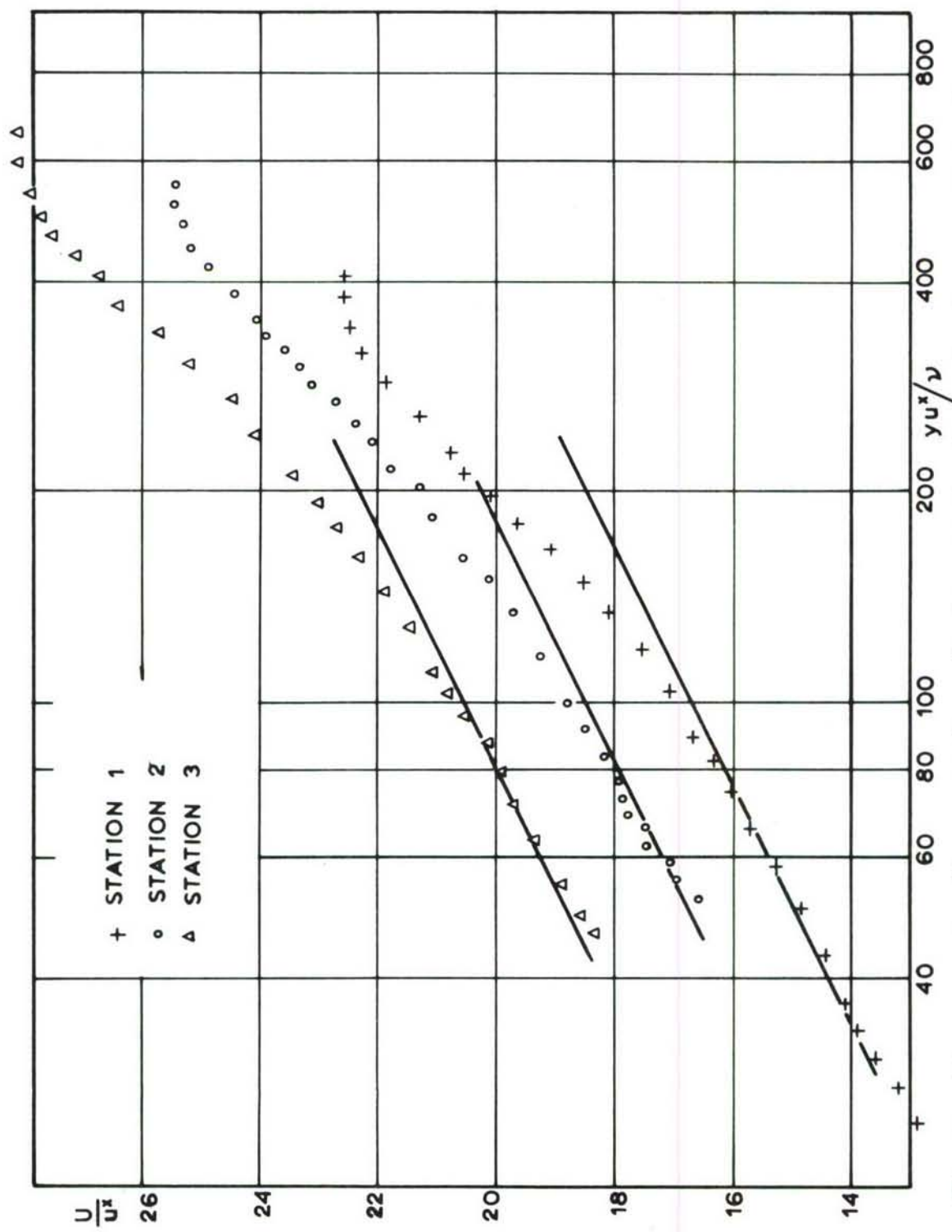


Fig. 4. Mean velocity profiles in the fully turbulent boundary layer.

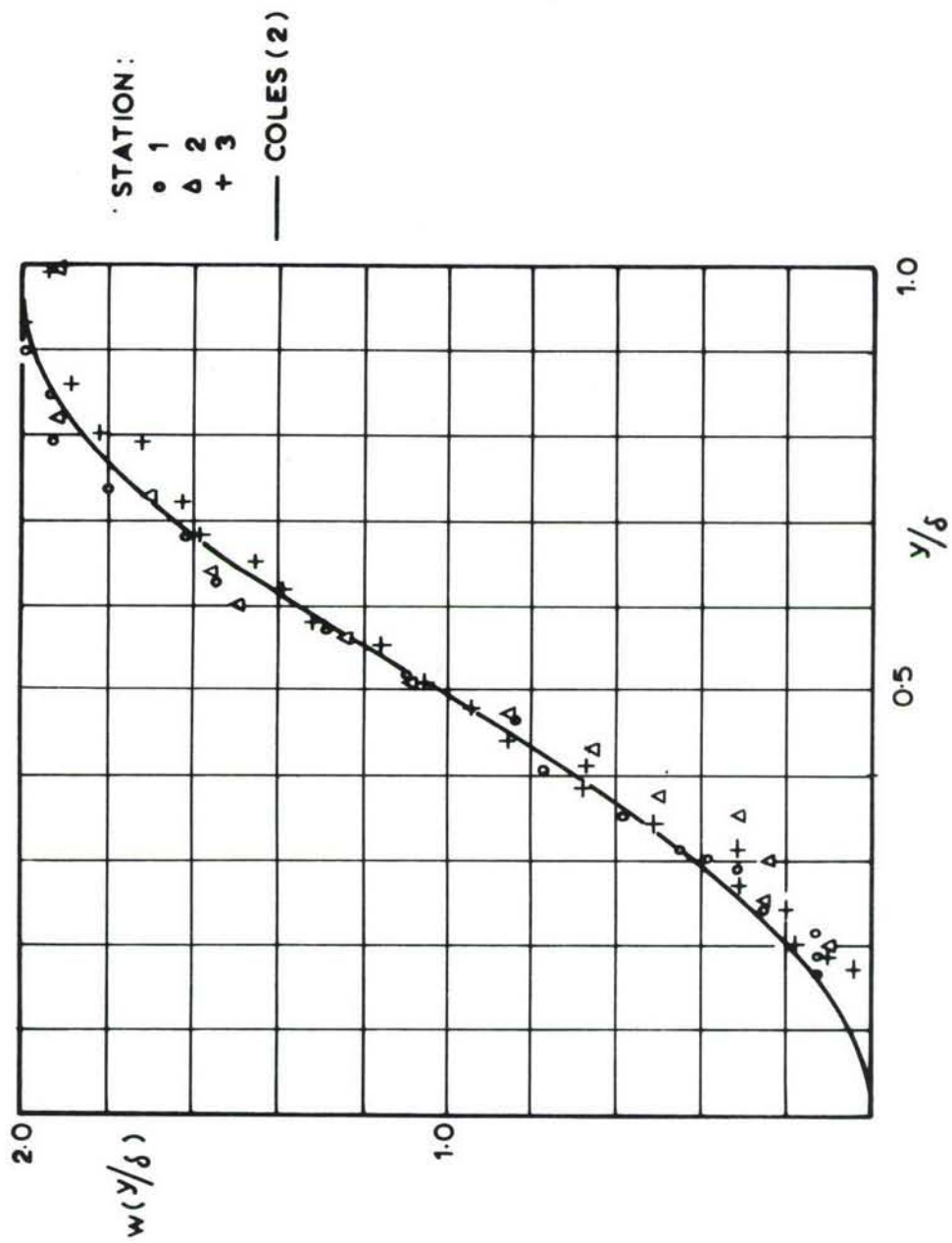


Fig. 5. 'Wake' function in the fully turbulent boundary layer.

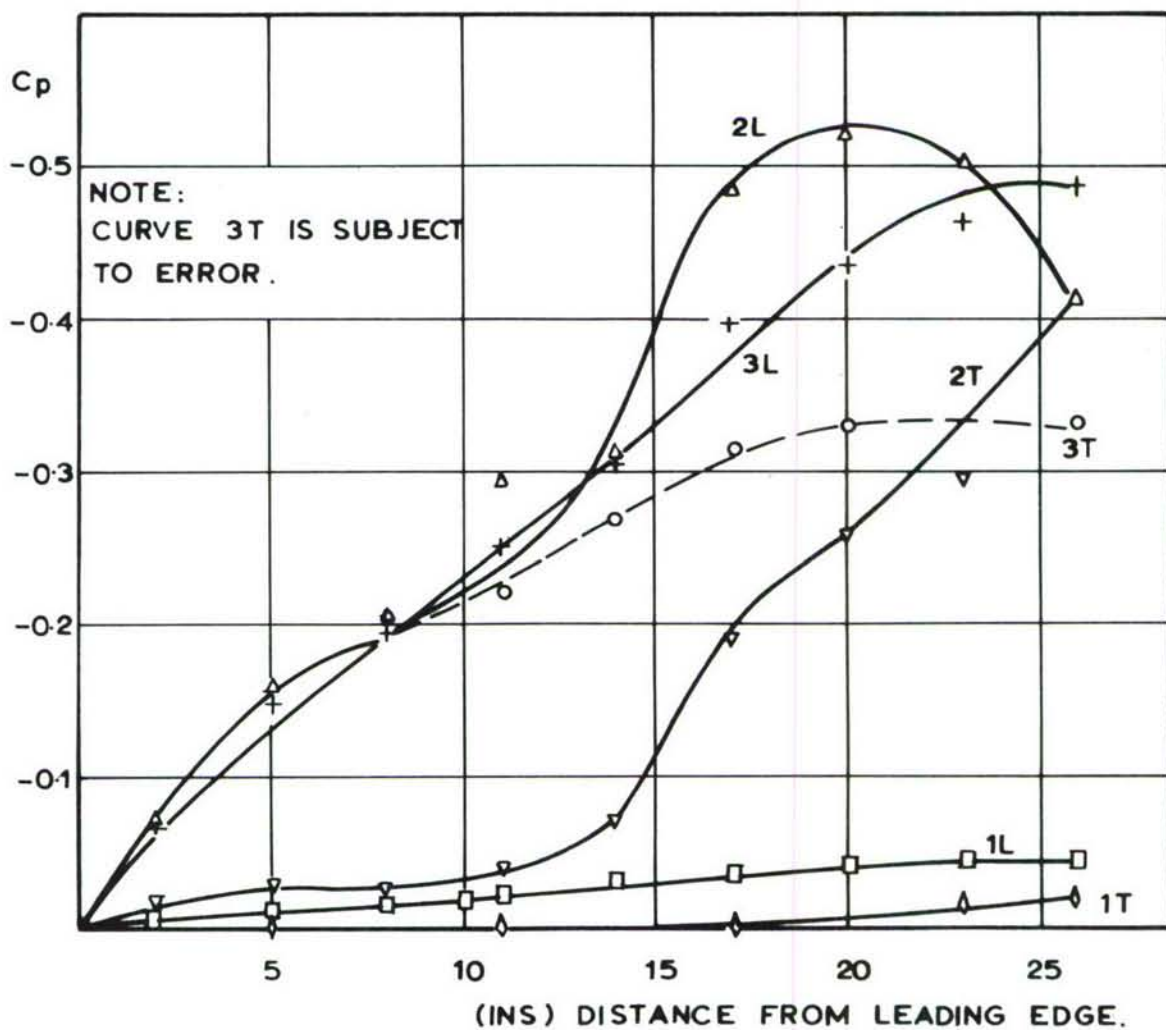


Fig. 6. Static pressure distribution in the working section.

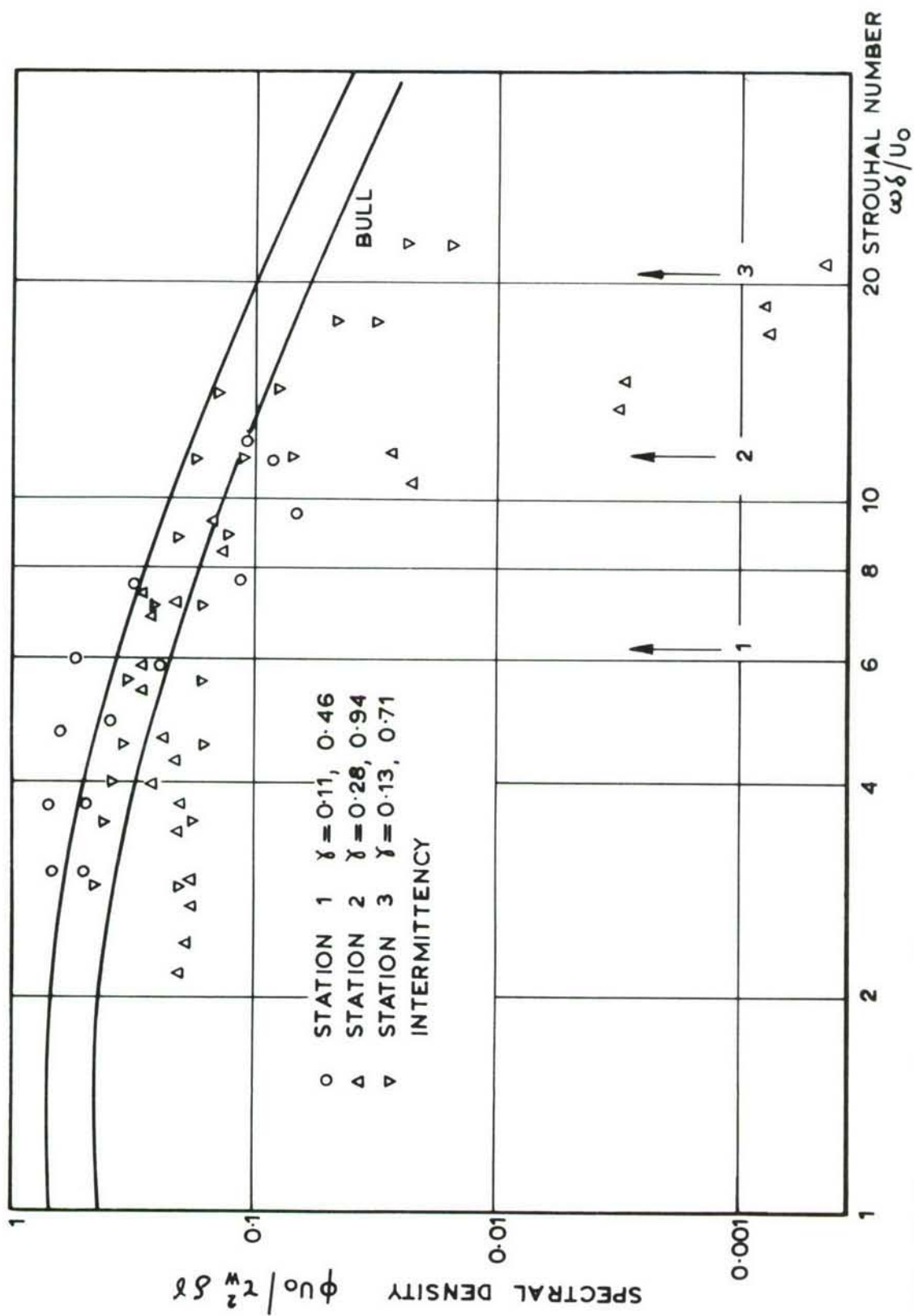


Fig.7. Comparison of measured spectra of wall pressure fluctuations with results of Bull. (1)

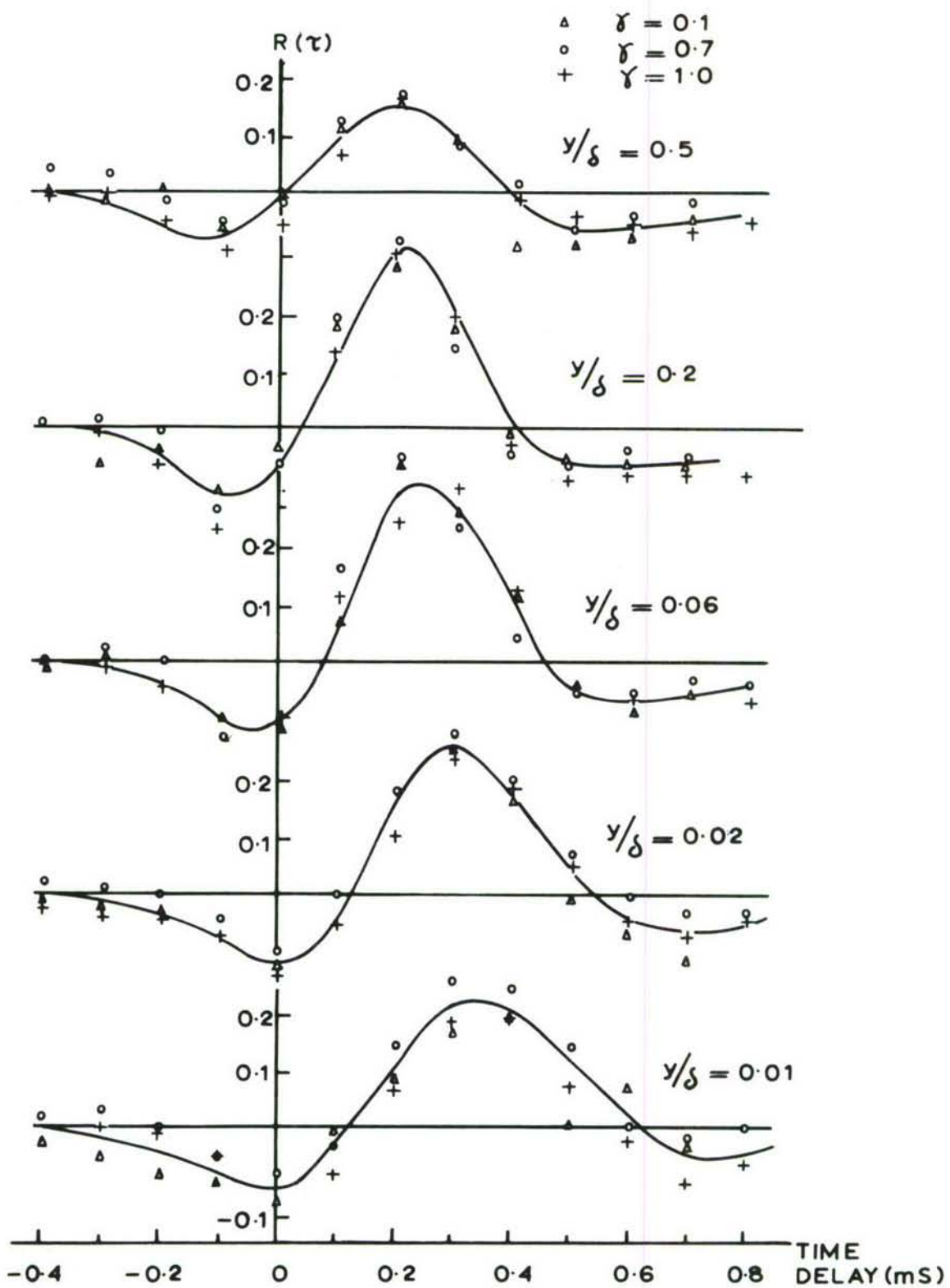


Fig.8. Measured pressure - velocity correlations

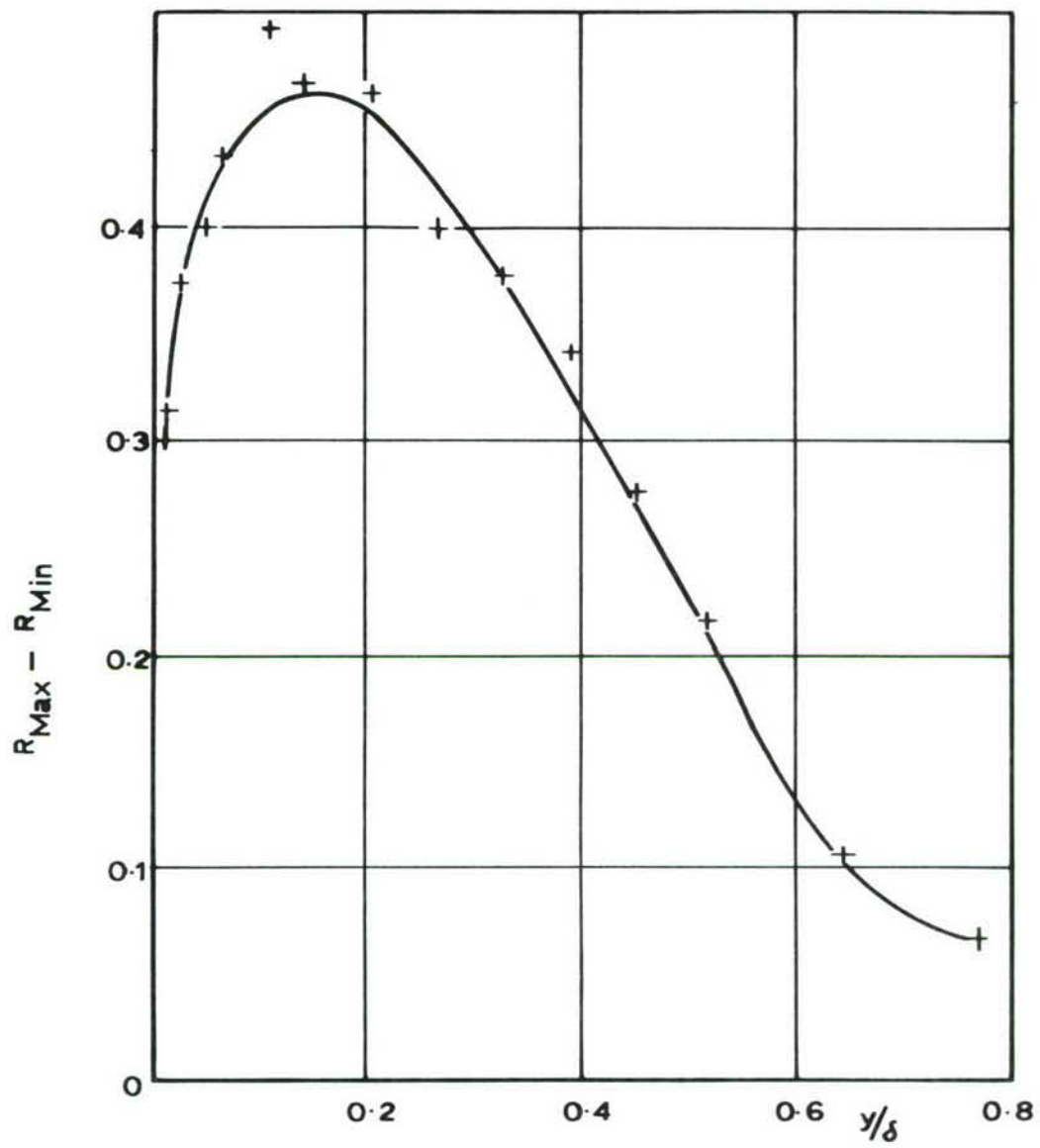


Fig. 9. Variation of $R(\tau)_{\text{Max}} - R(\tau)_{\text{Min}}$ across turbulent spots.

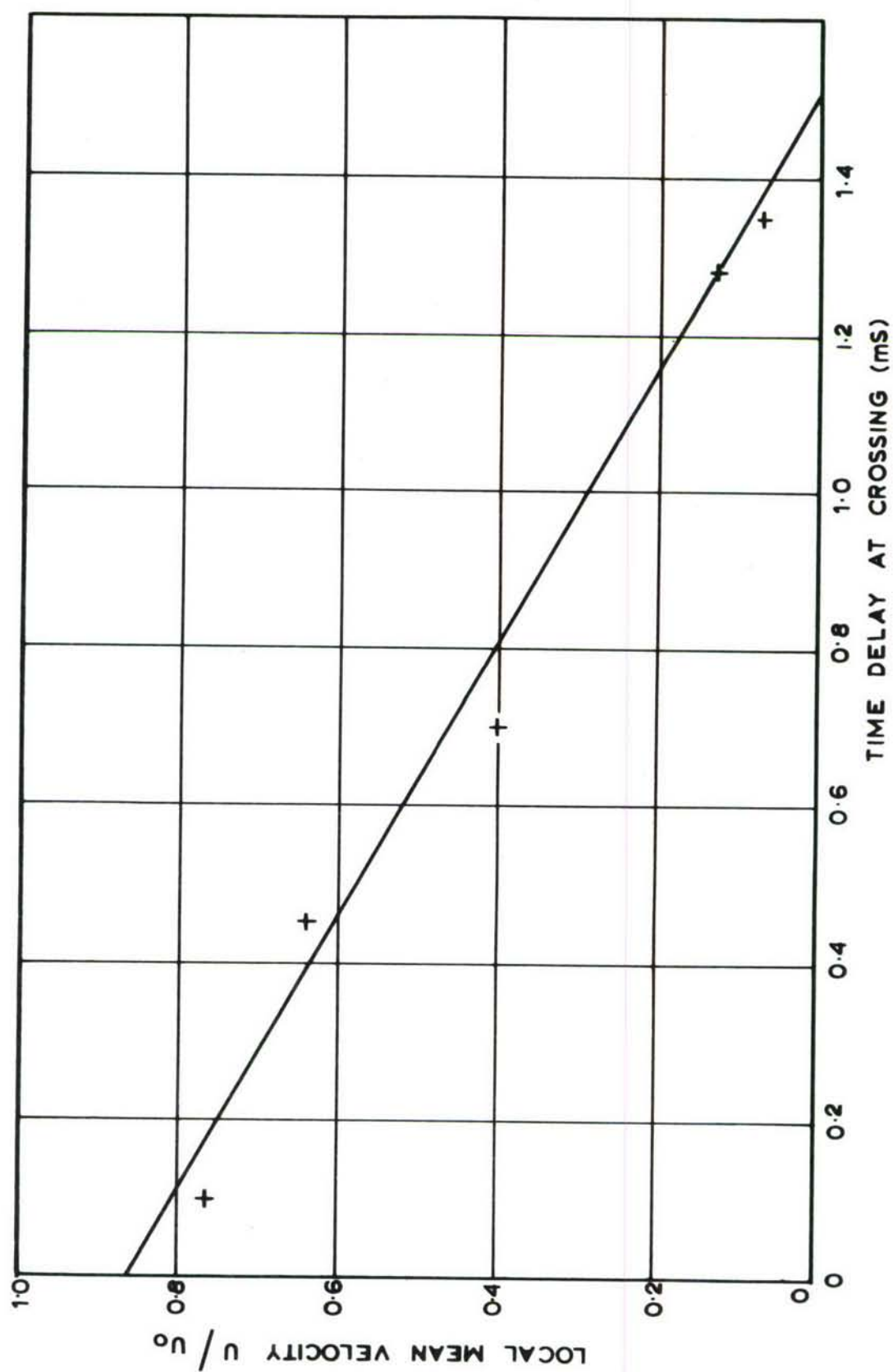


Fig. 10. Relation between correlation time delay and local mean velocity.

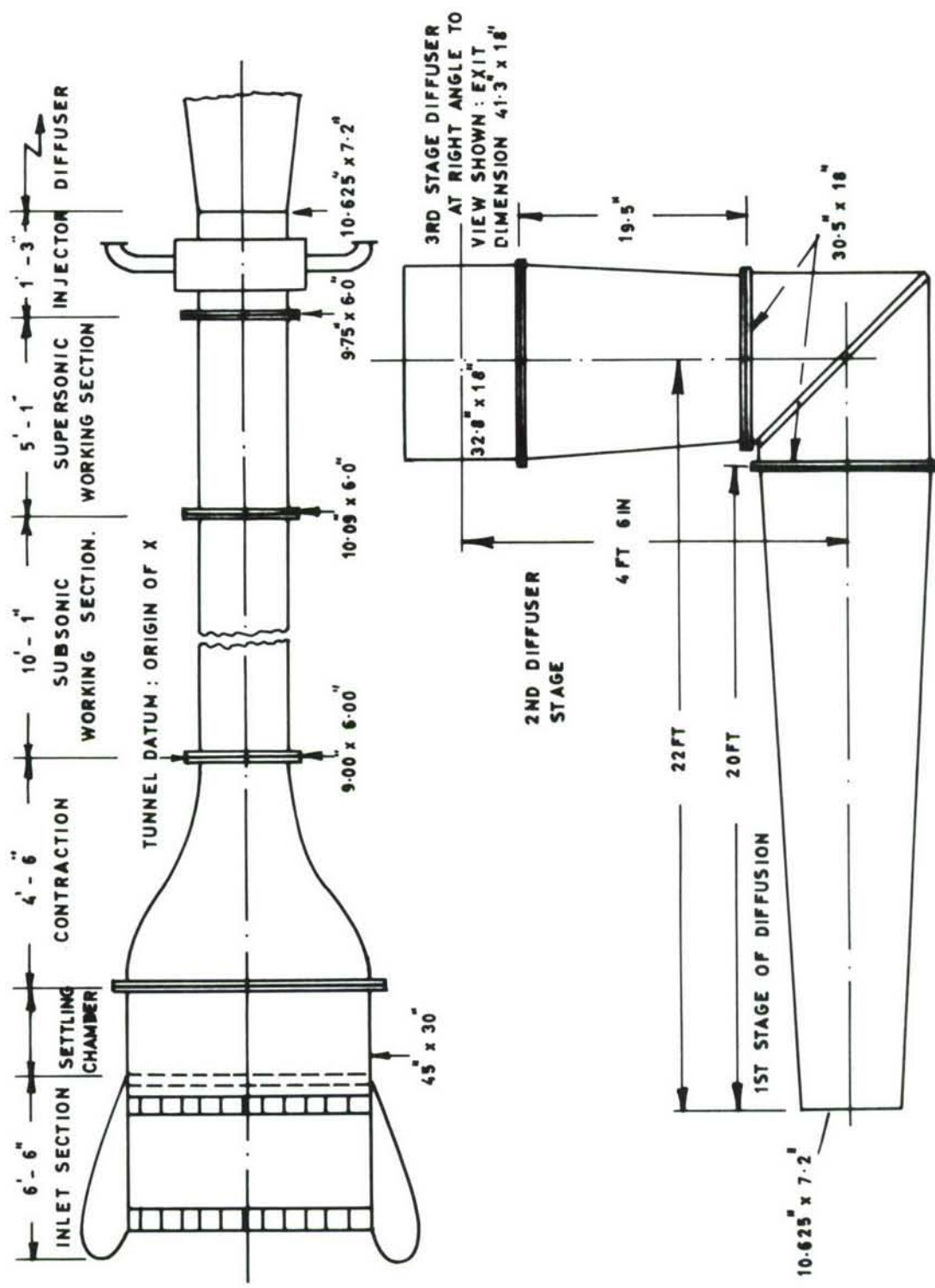


Fig.11. General arrangement of 9 in x 6 in boundary layer wind tunnel.

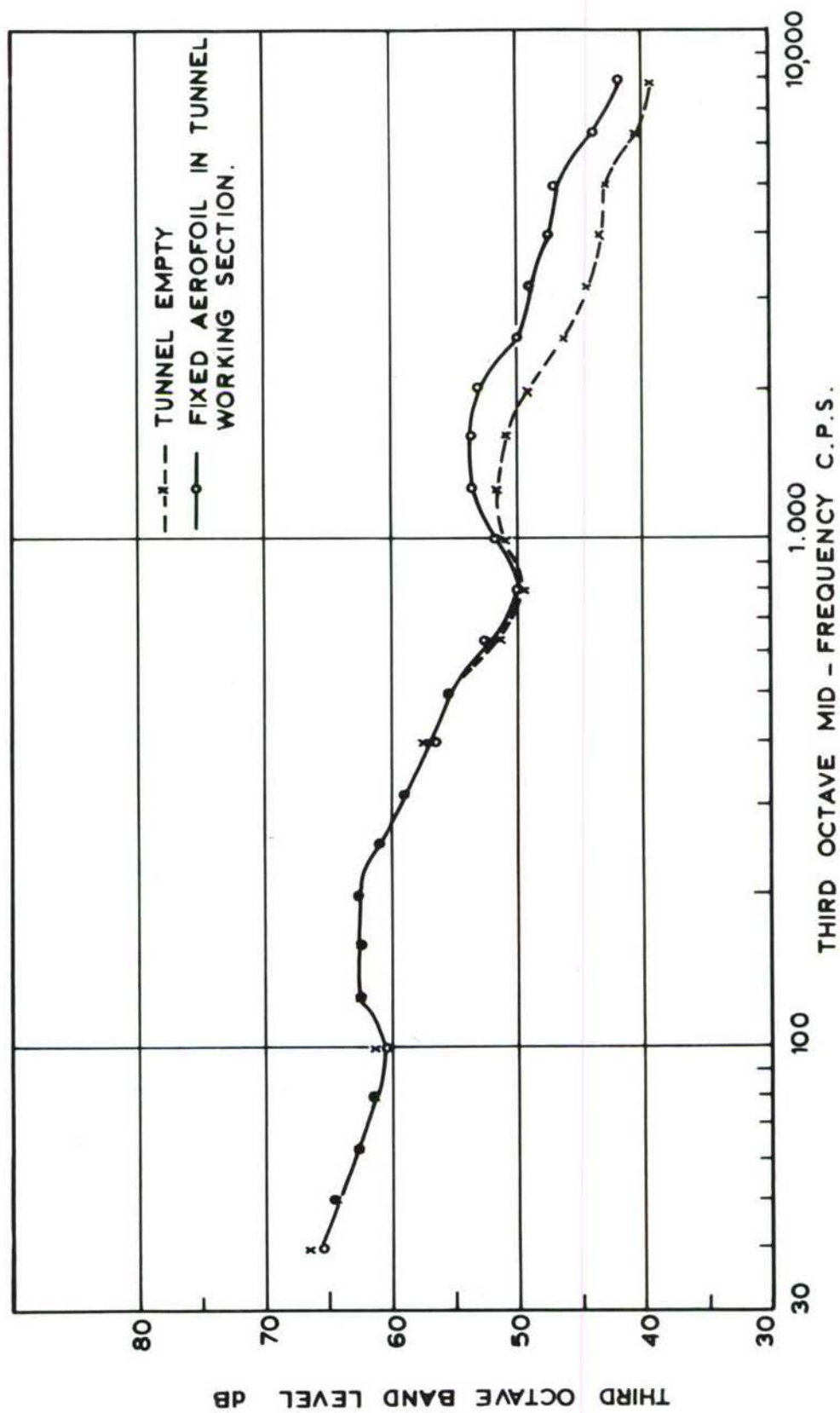


Fig. 12. Noise spectrum in tunnel settling chamber.

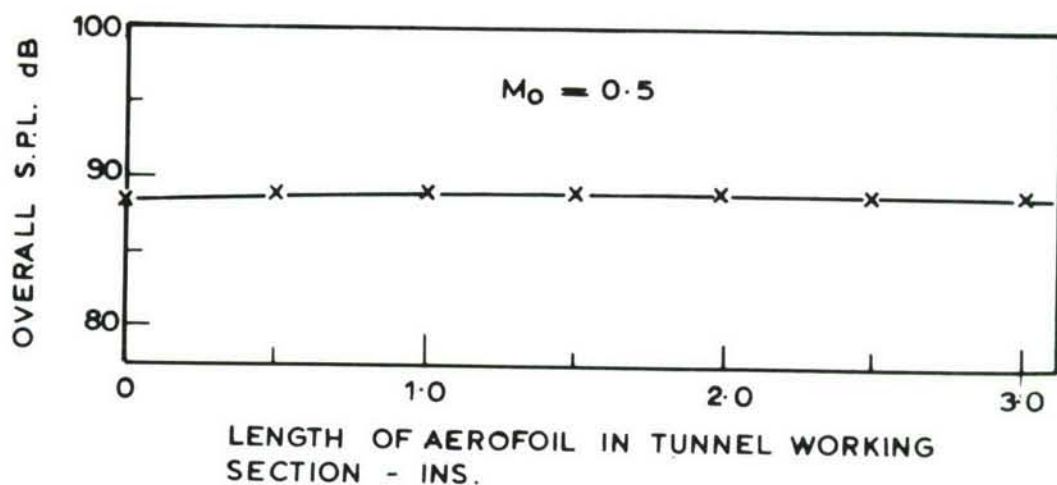


Fig. 13. Noise measured in settling chamber when probe microphone is inserted in working section.

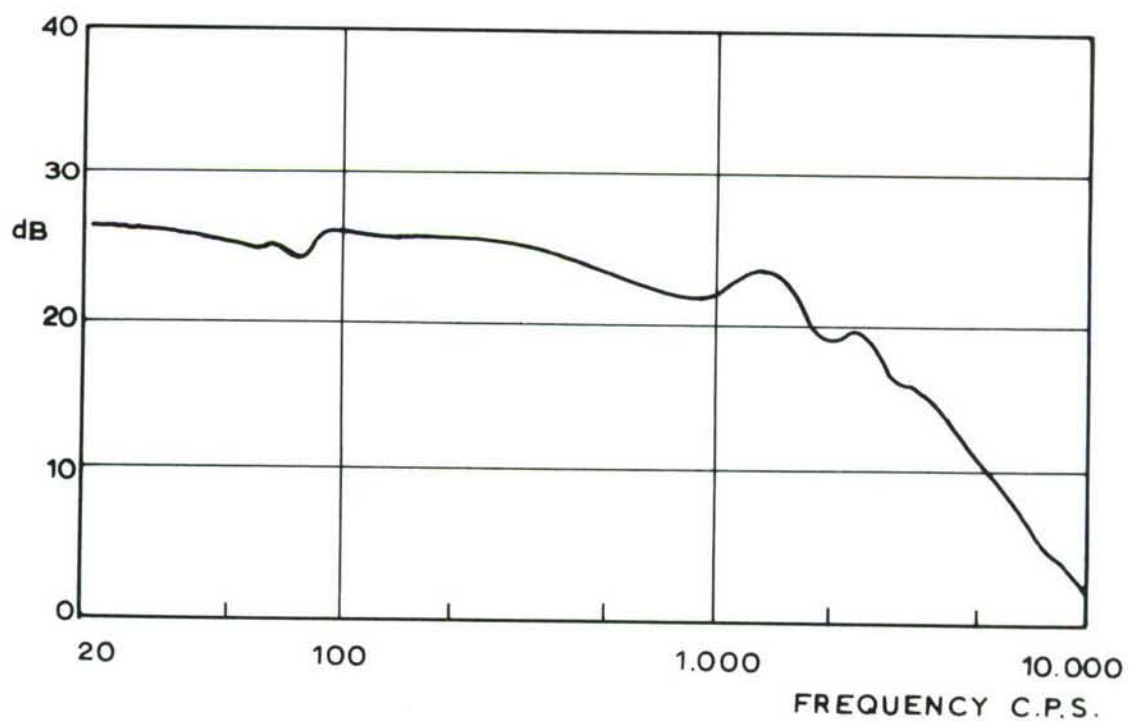


Fig. 14. Frequency response of probe microphone.

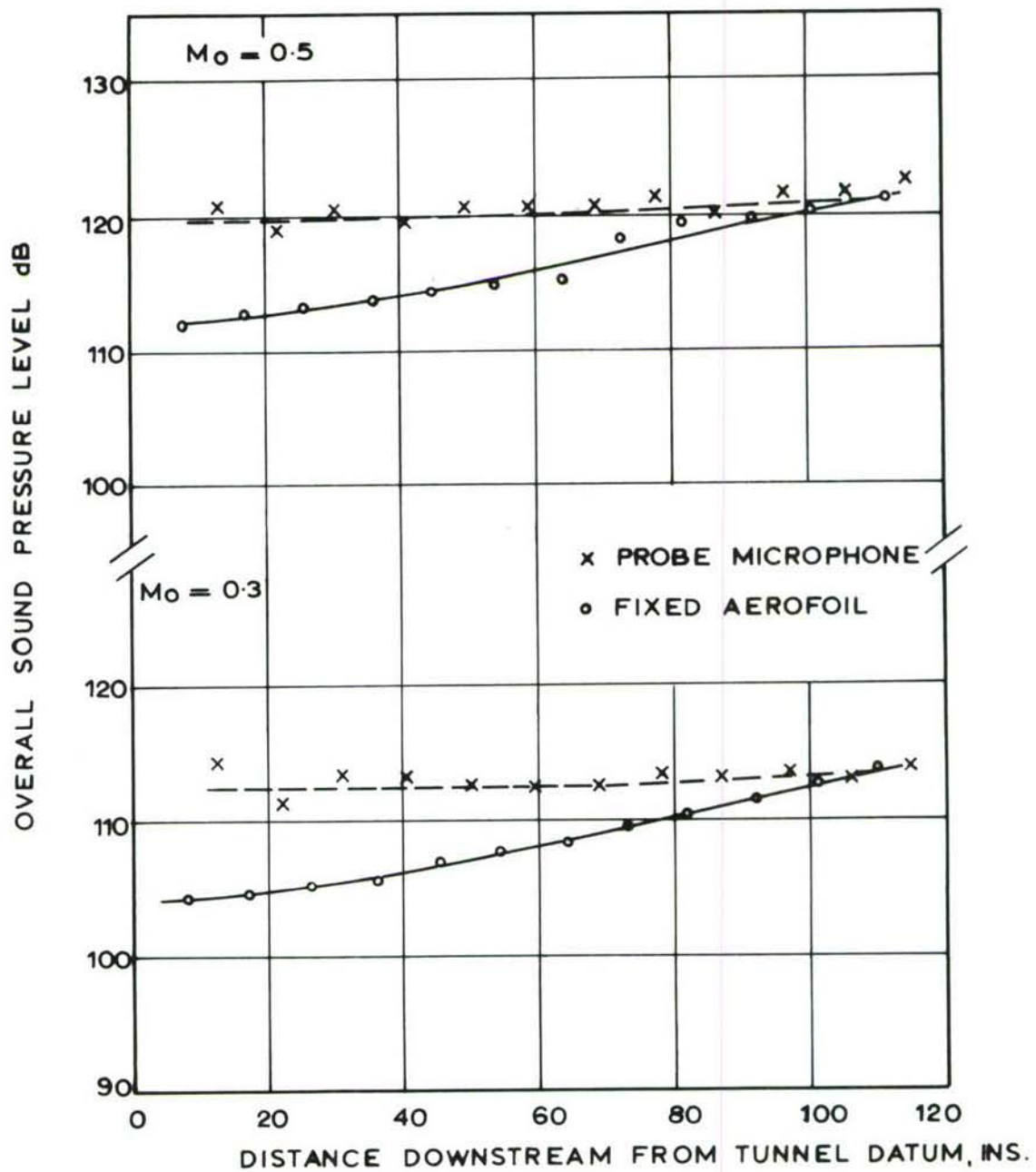


Fig. 15. Variation of sound pressure level along tunnel working section centre line.

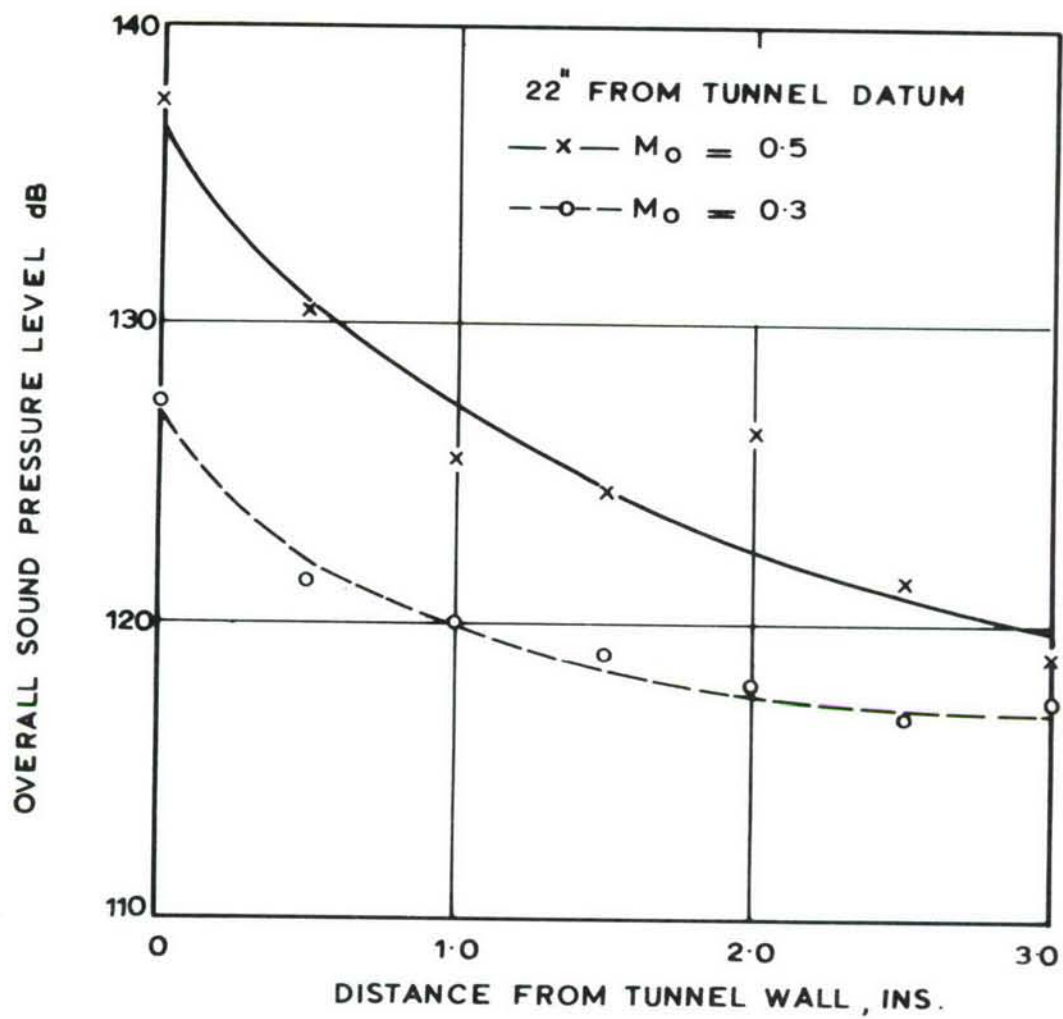


Fig. 16. Variation of sound pressure level across the tunnel working section.

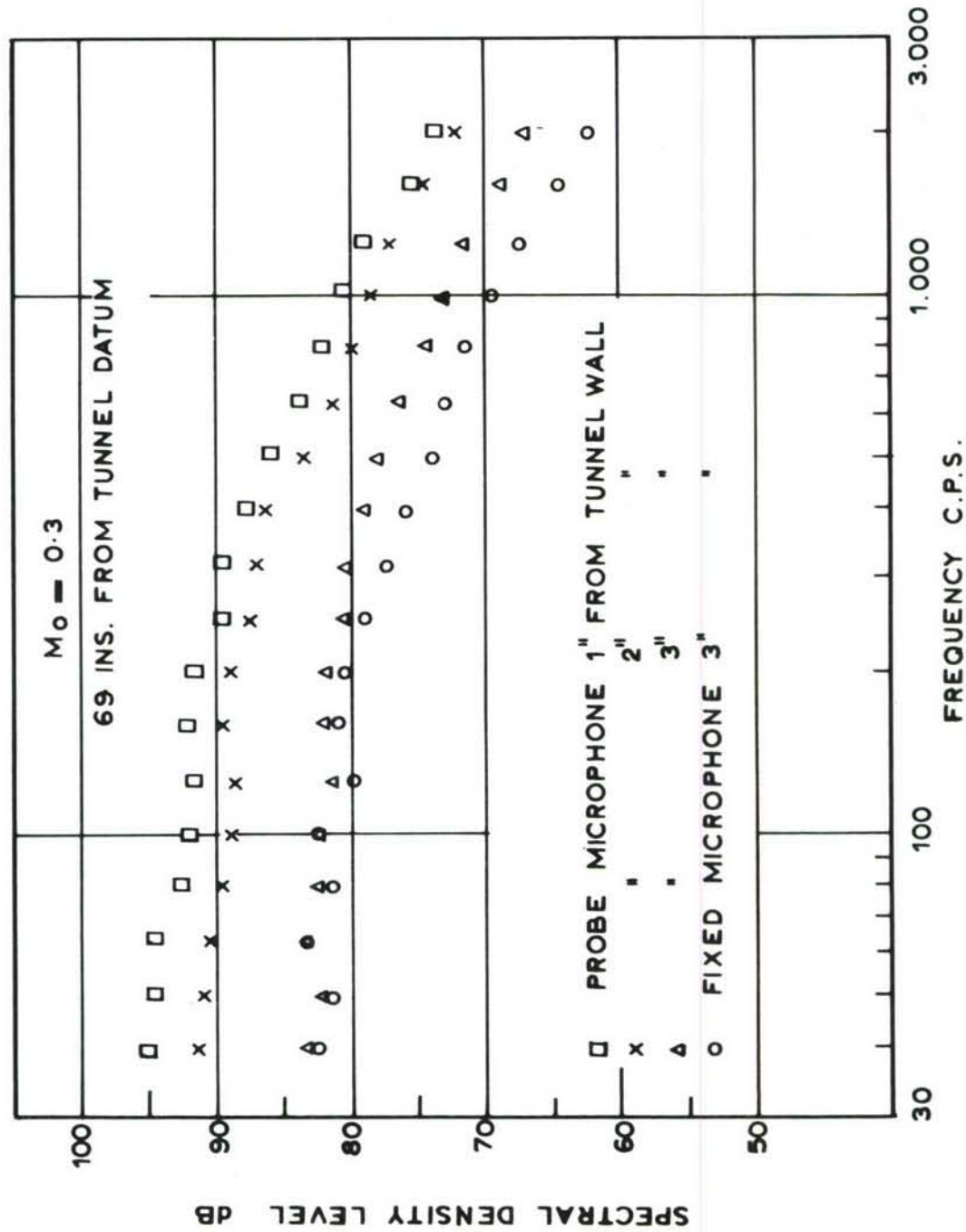


Fig. 17. Noise spectra in tunnel working section .

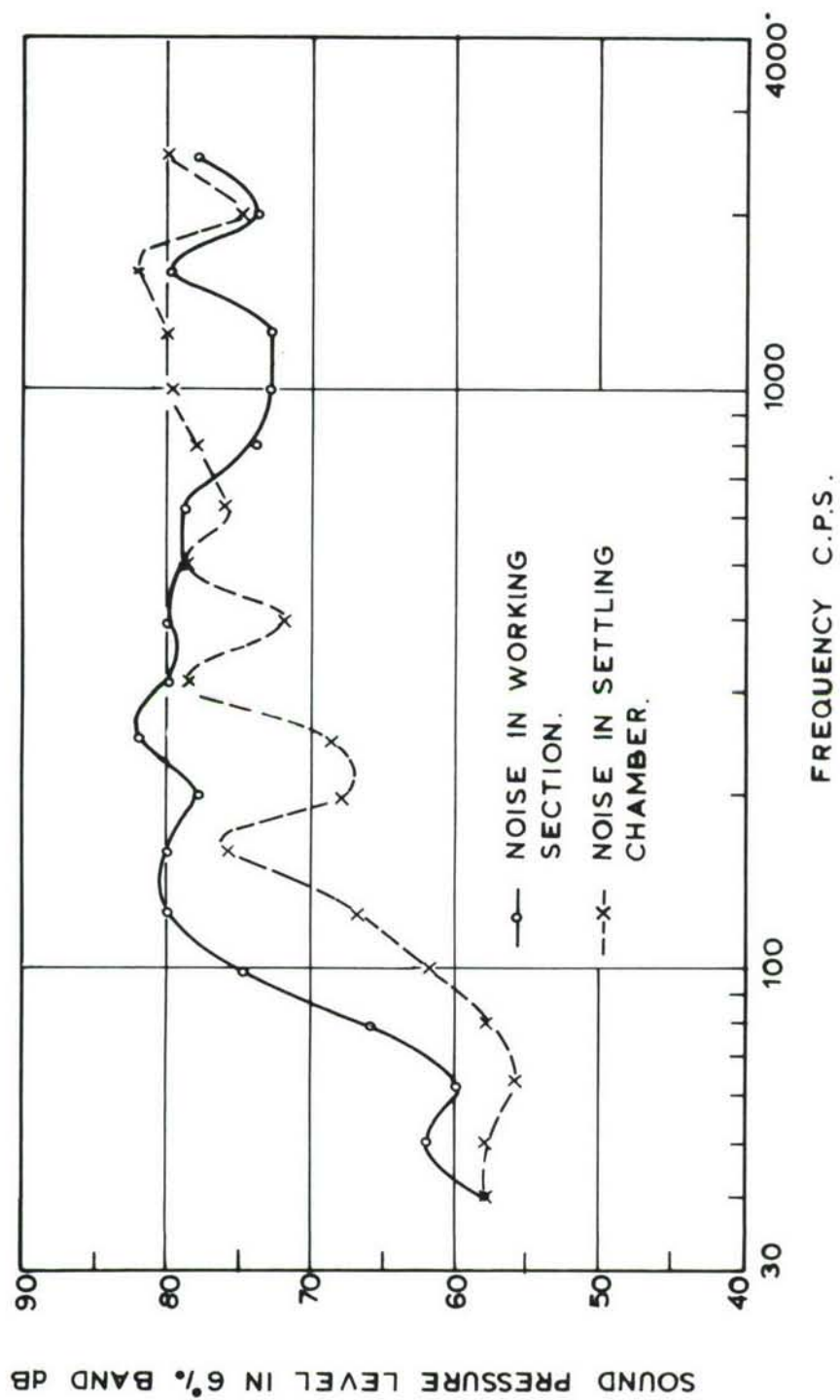


Fig. 18. Noise amplification through inlet contraction

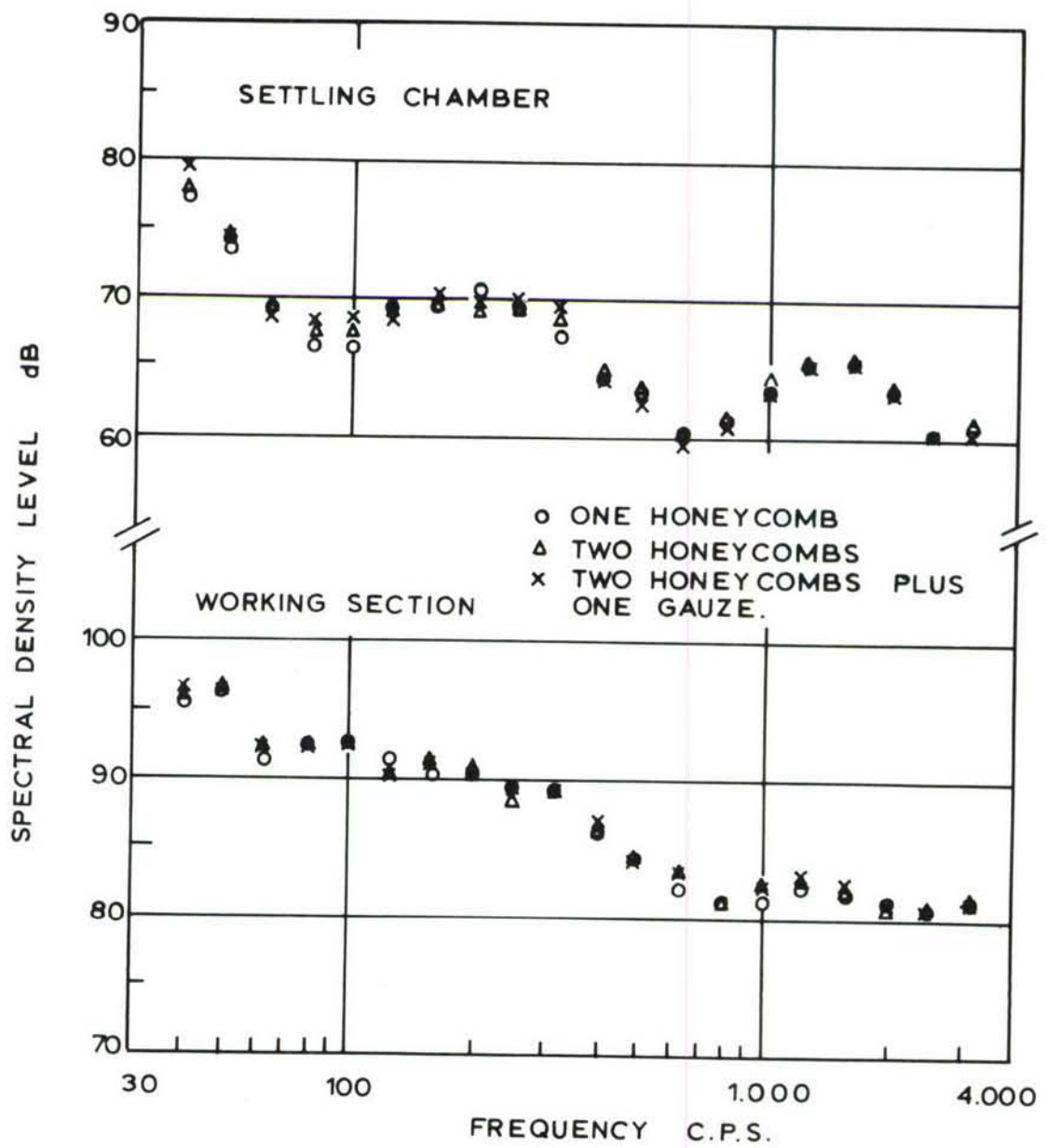


Fig. 19. Effect of tunnel inlet conditions on noise field.

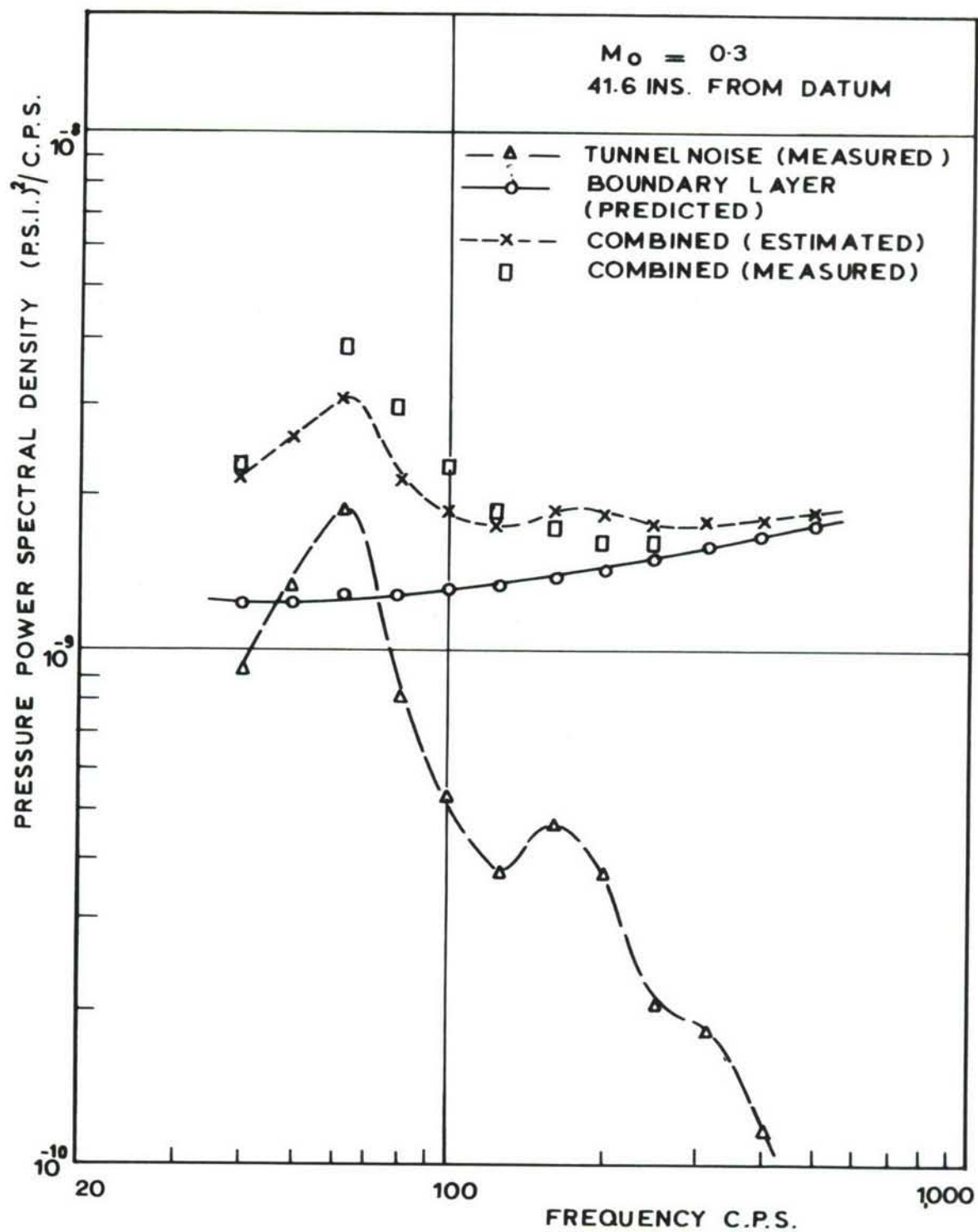


Fig 20. Boundary layer and tunnel noise spectra.

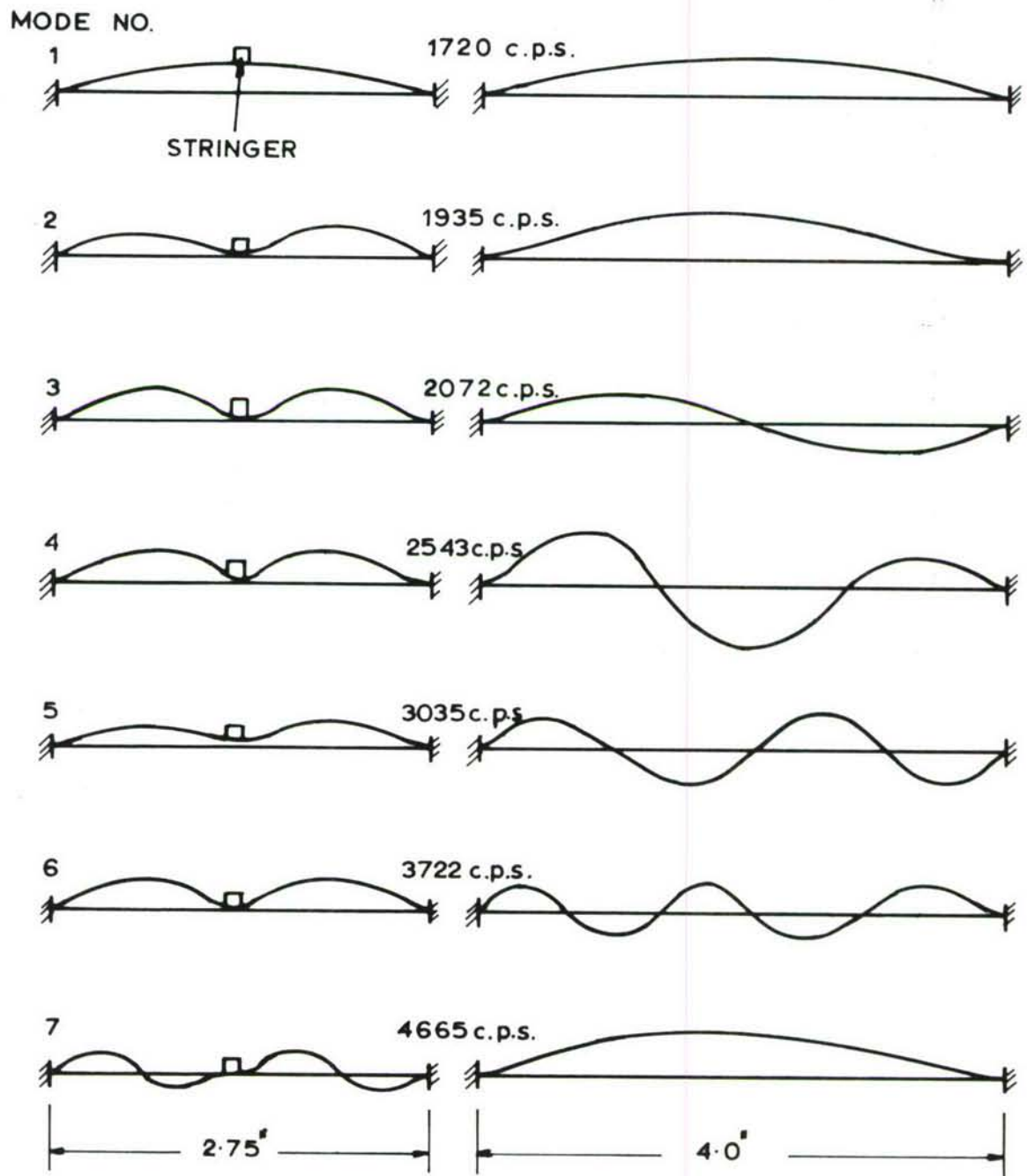


Fig. 21. Mode shapes and frequencies for stiffened panel.

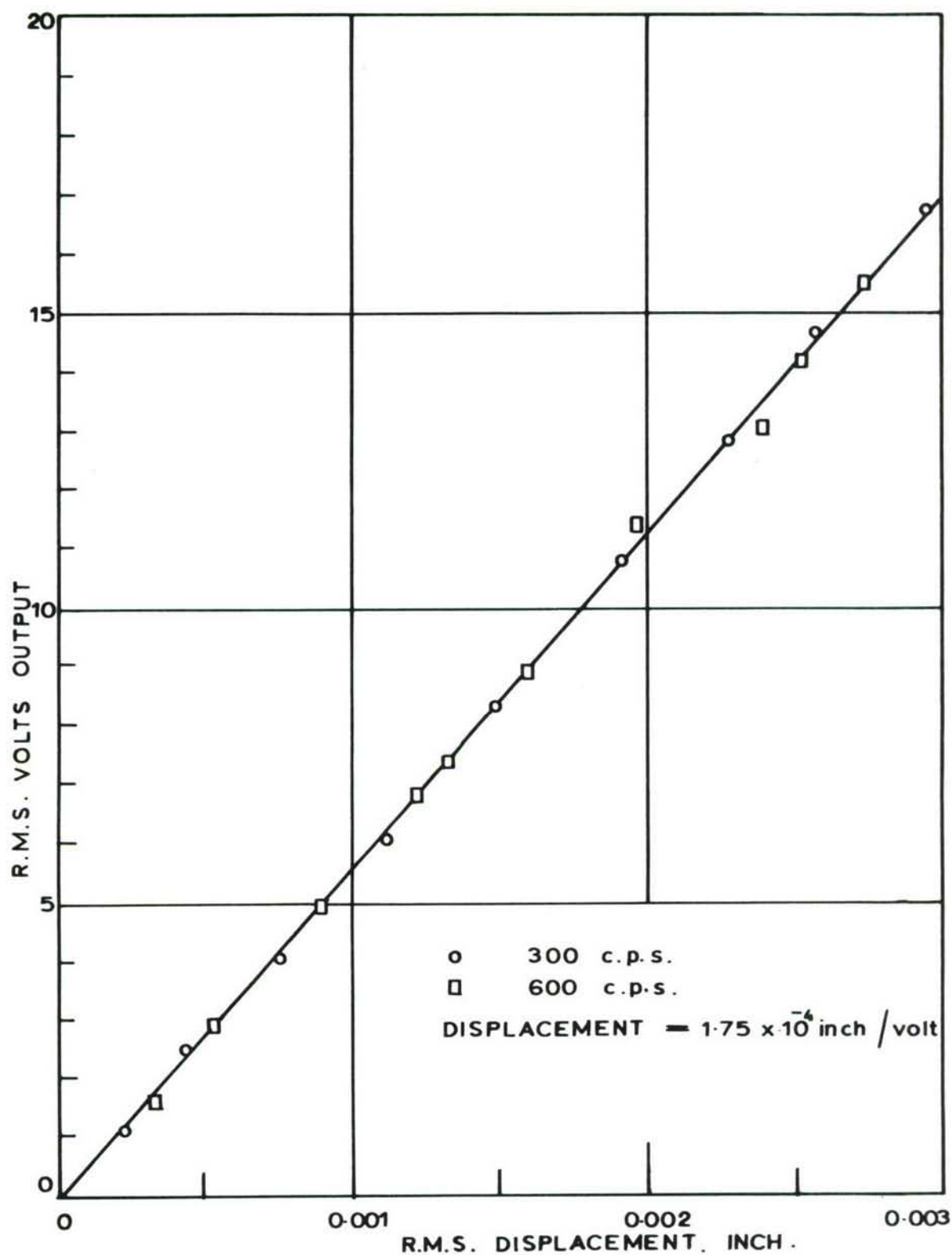


Fig. 22. Exciter-probe calibration with Wayne Kerr meter on normal scale.

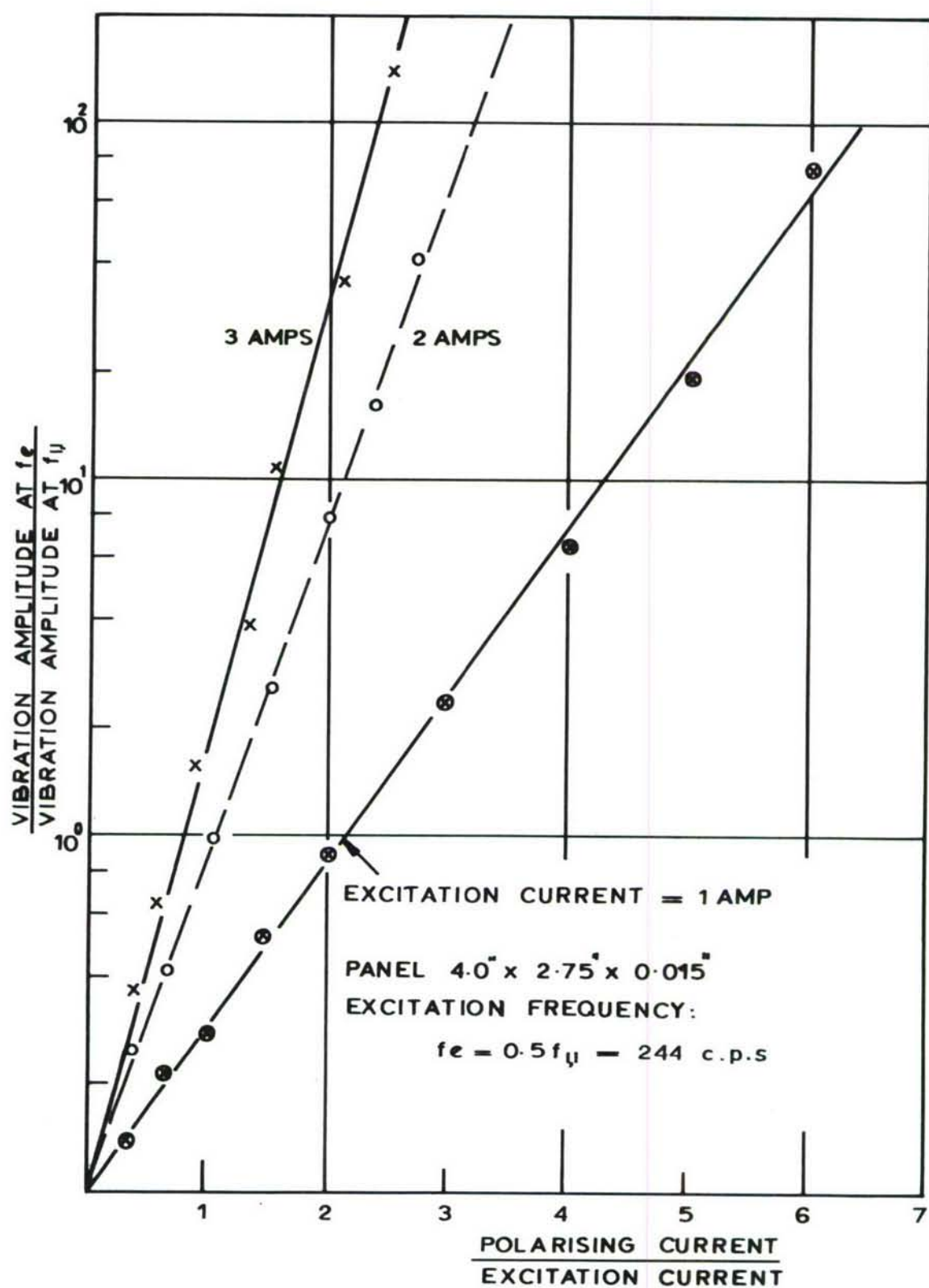


Fig. 23. Effect of polarising current on panel response.

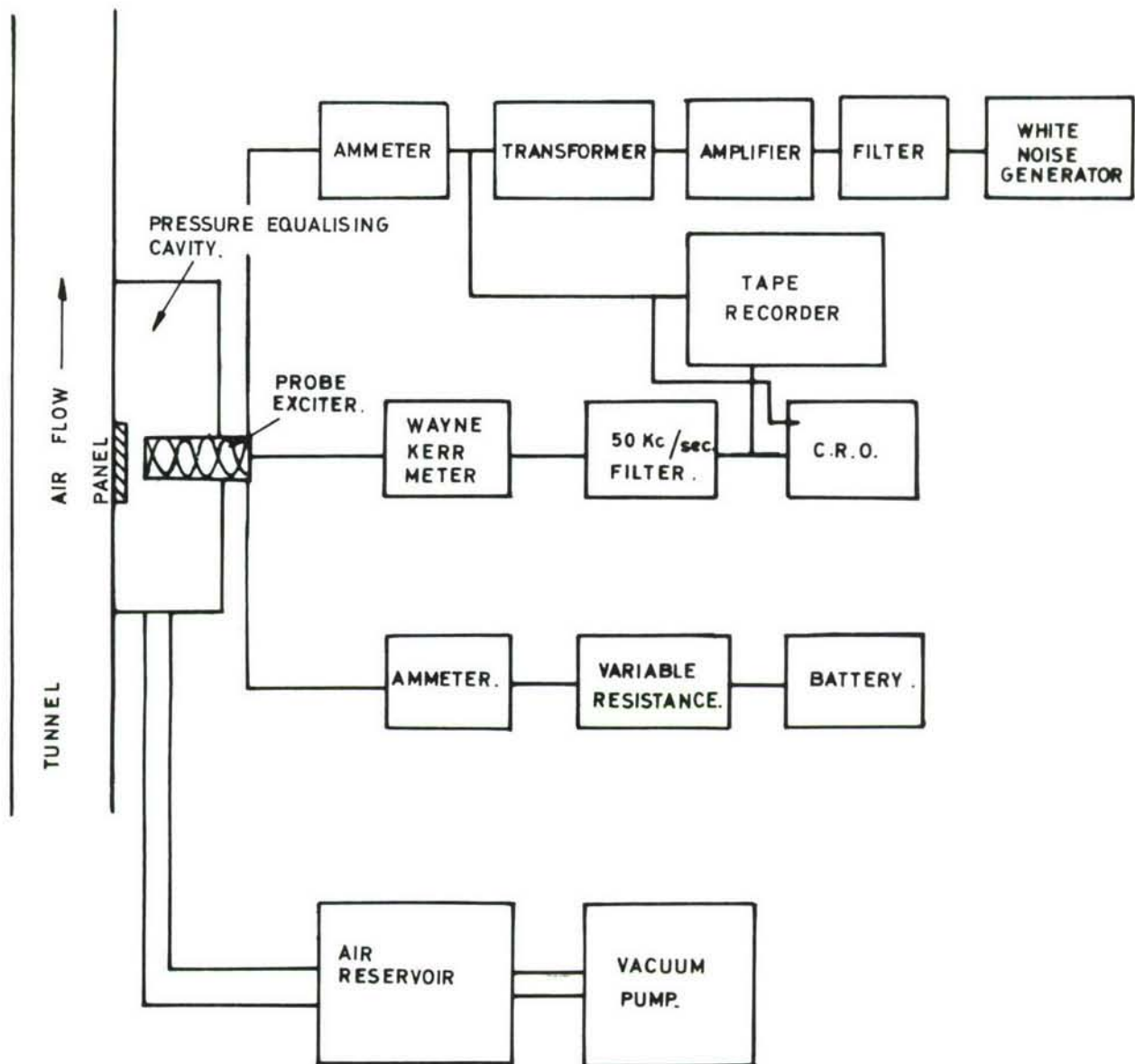


Figure 24 Schematic diagram of instrumentation for cross-correlation measurement of damping using exciter-probe.

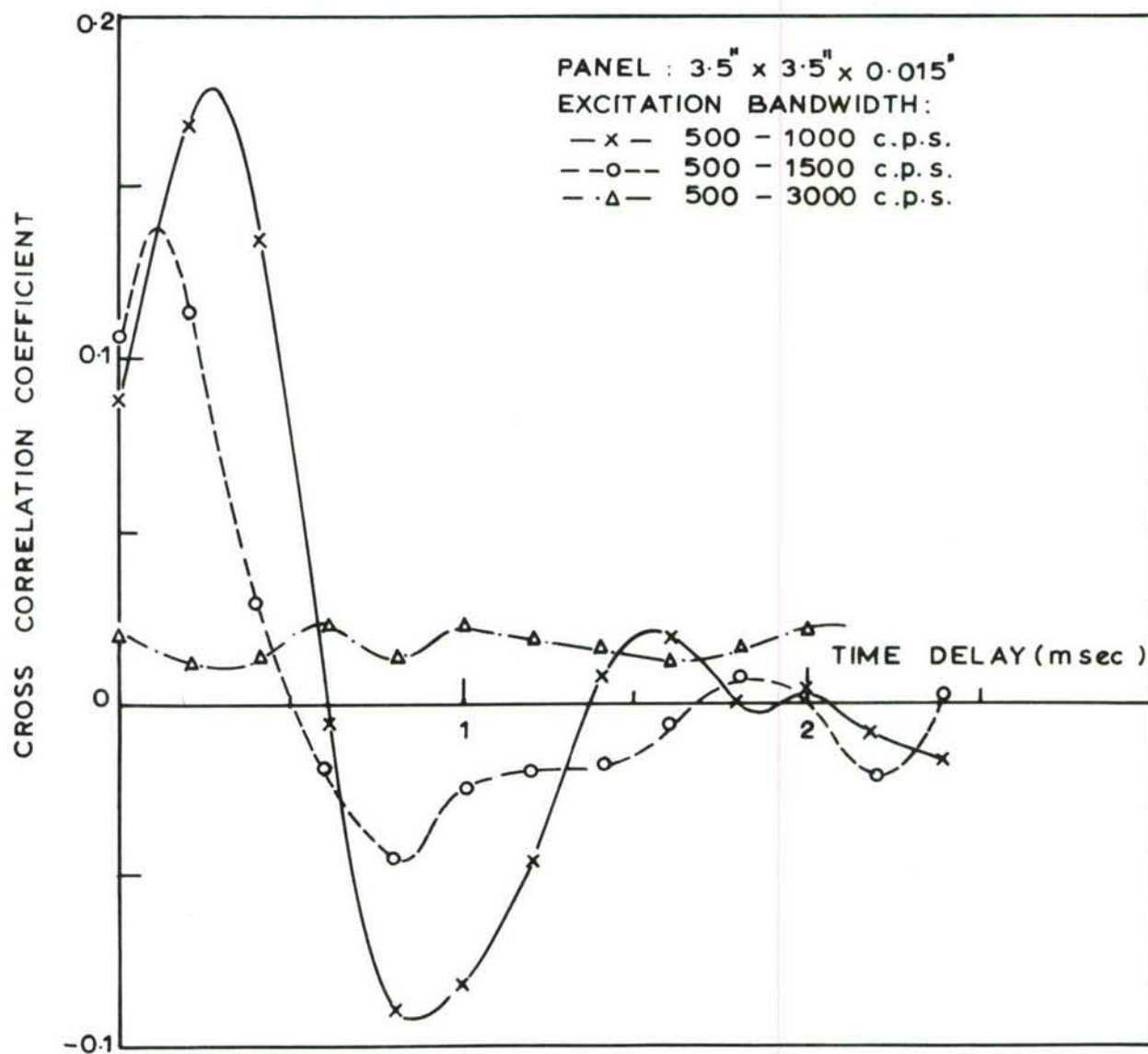


Fig. 25 Effect of excitation bandwidth on cross correlation between excitation and response.

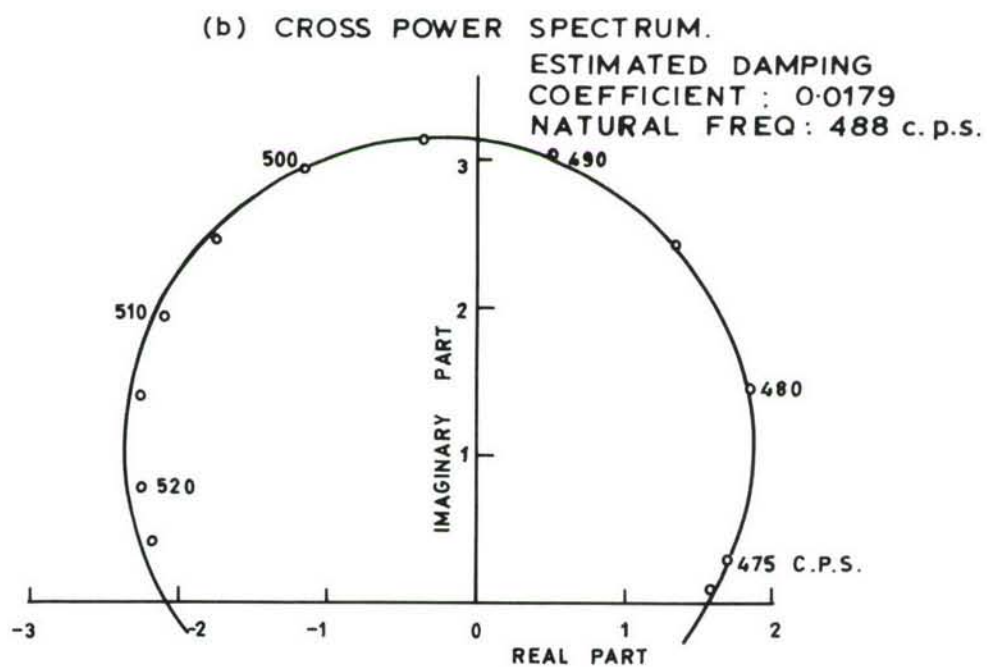
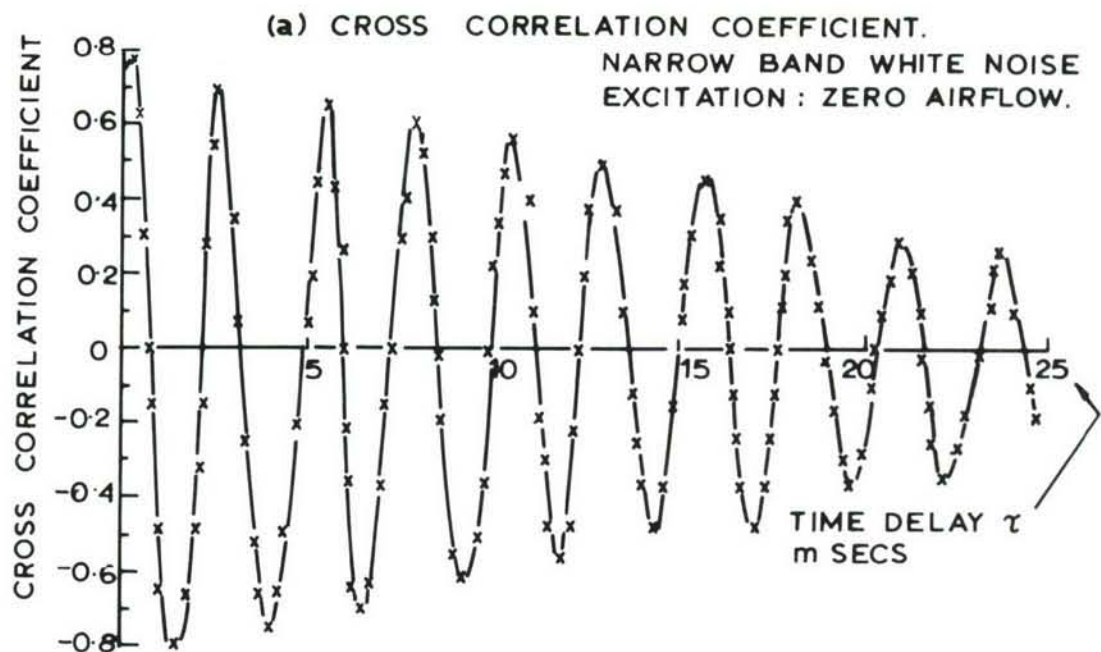
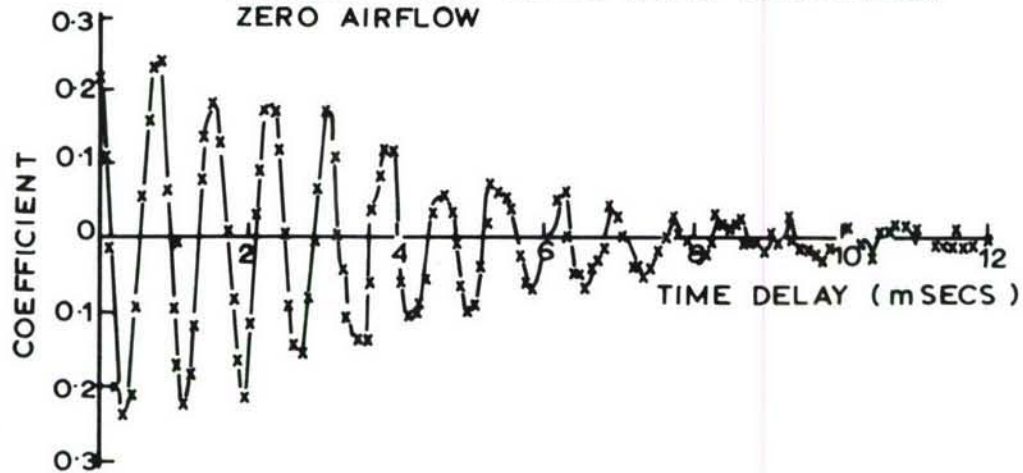


Fig. 26. Excitation - response cross power spectrum:
medium damping.

(a) CROSS CORRELATION COEFFICIENT.

NARROW BAND WHITE NOISE EXCITATION.
ZERO AIRFLOW



(b) CROSS POWER SPECTRUM

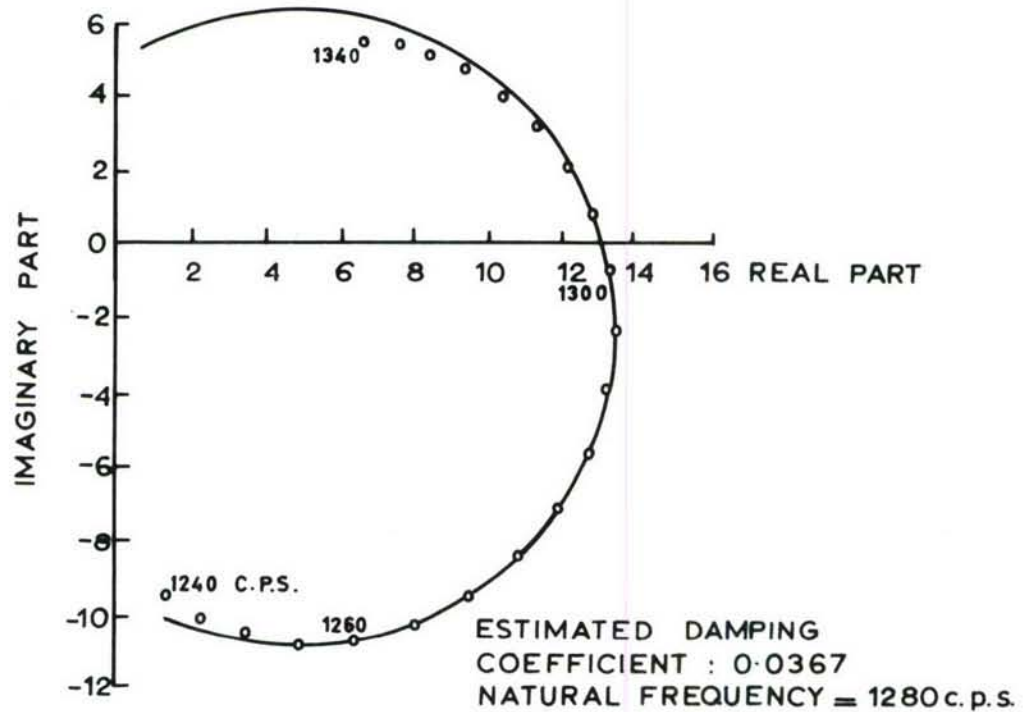


Fig. 27. Excitation-response cross power spectrum : light damping.

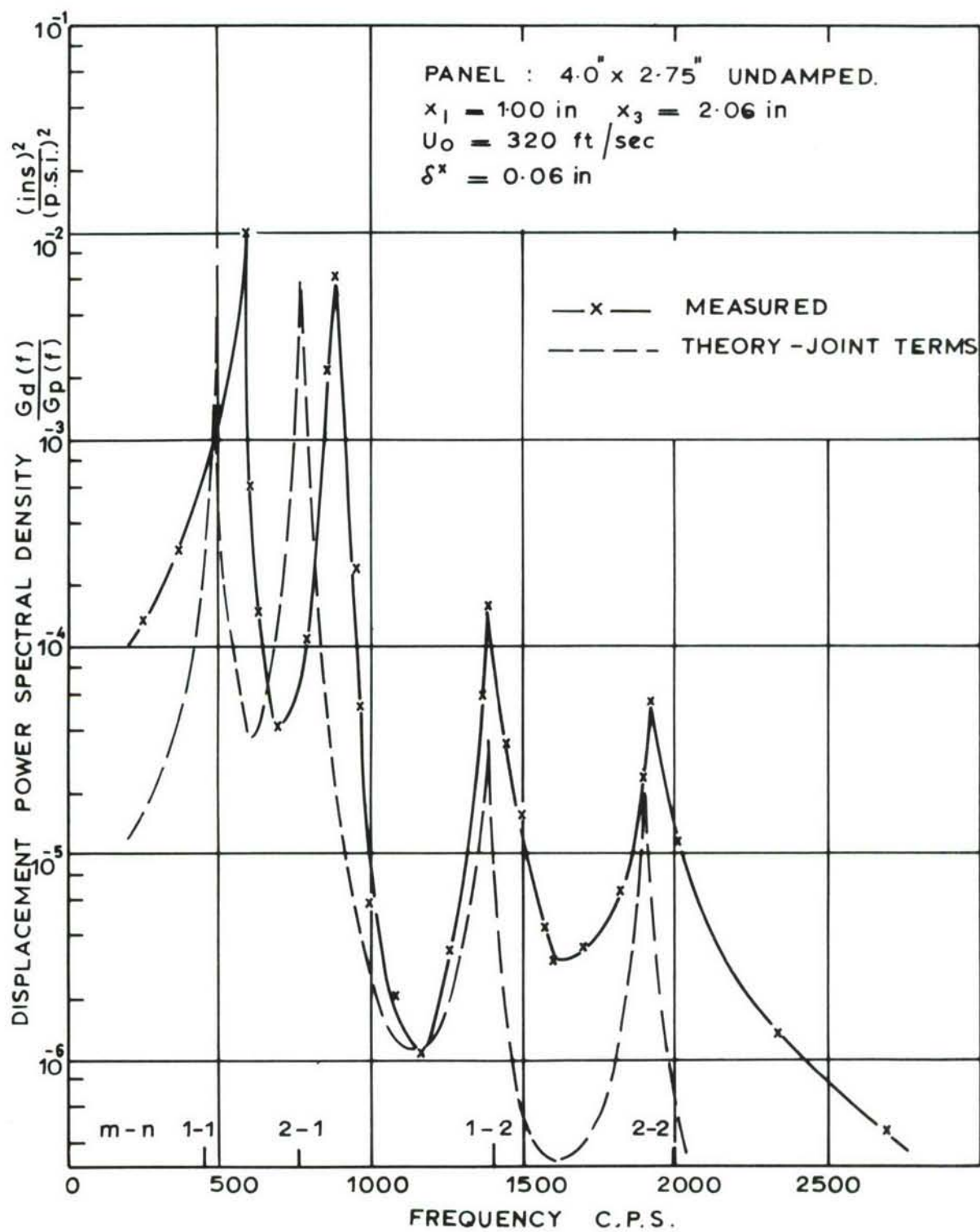


Fig. 28. Displacement spectra for undamped panel:
 $\delta^x = 0.06$ in

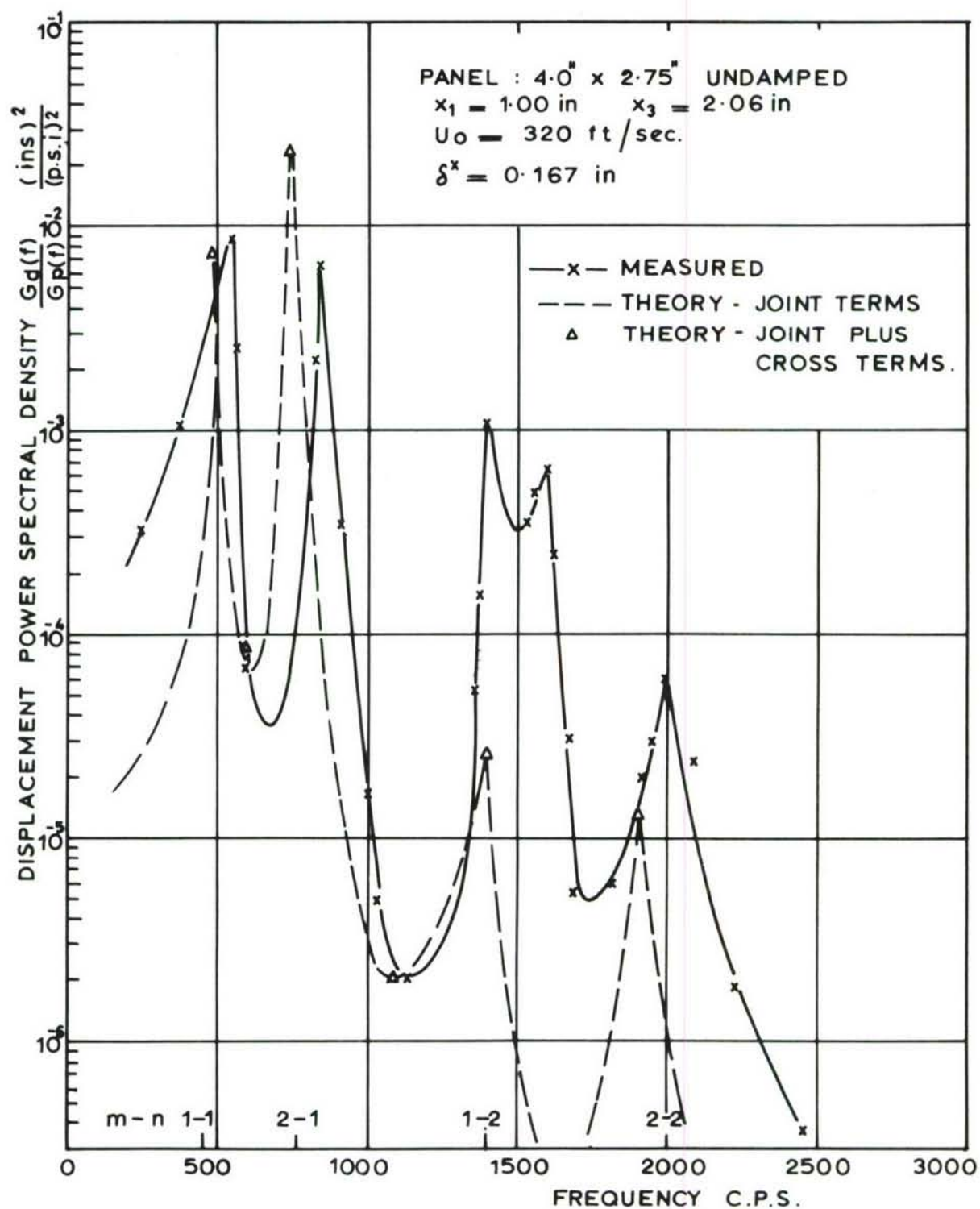


Fig. 29. Displacement spectra for undamped panel :
 $\delta^x = 0.167$ in .

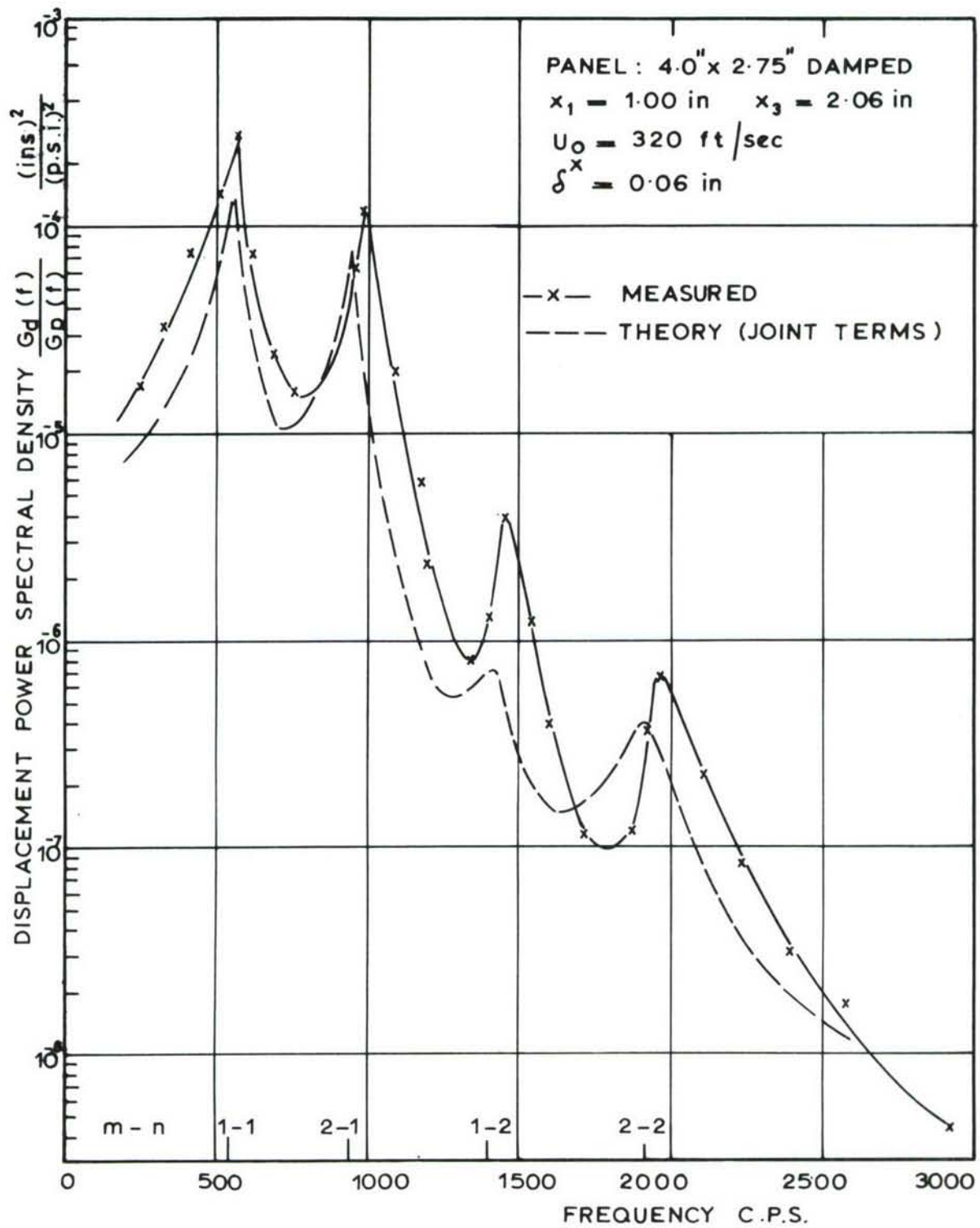


Fig. 30. Displacement spectra for damped panel:
 $\delta^x = 0.06$ in

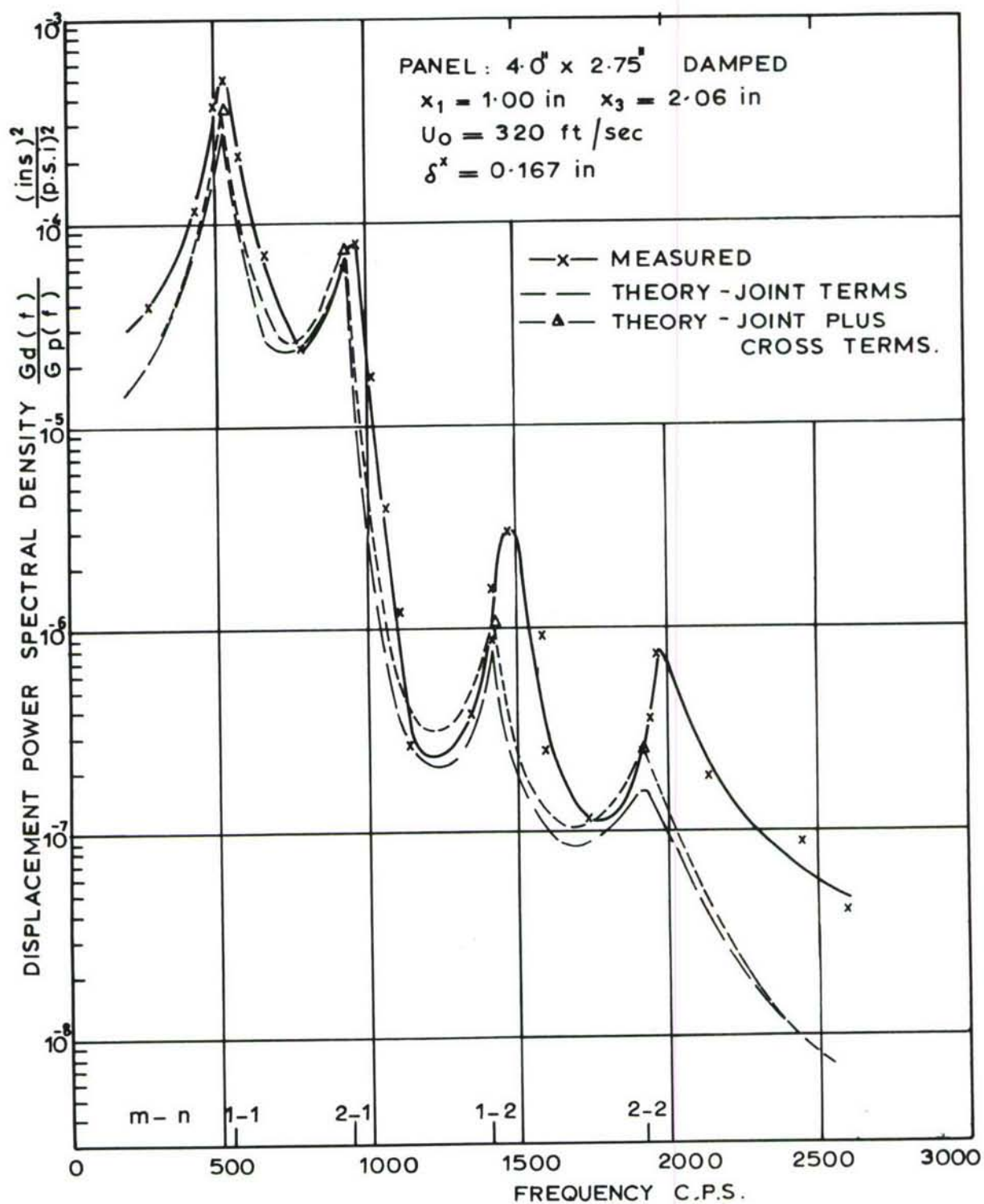


Fig. 31. Displacement spectra for damped panel :
 $\delta^x = 0.167$ in.

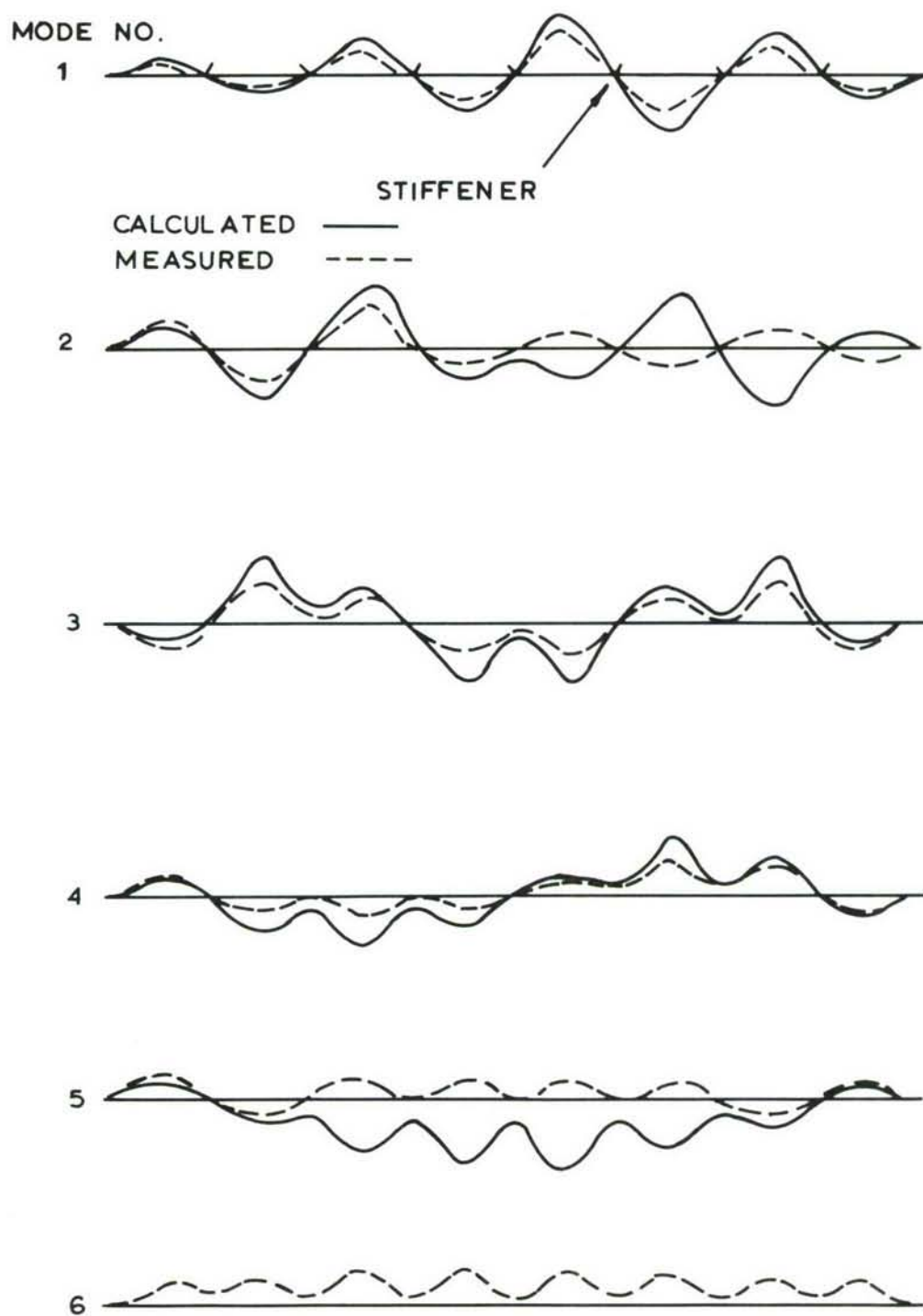


Fig. 32. Mode shapes for 8-bay array .

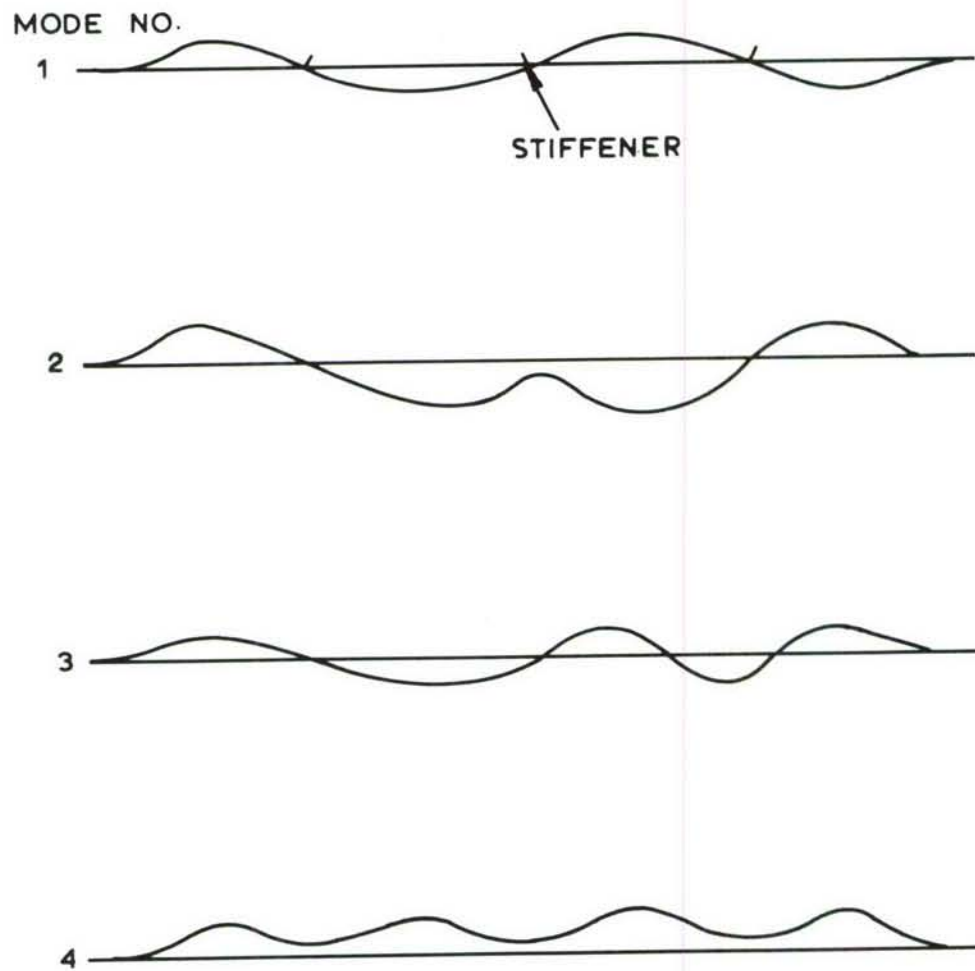


Fig. 33 Measured mode shapes for 4-bay array .

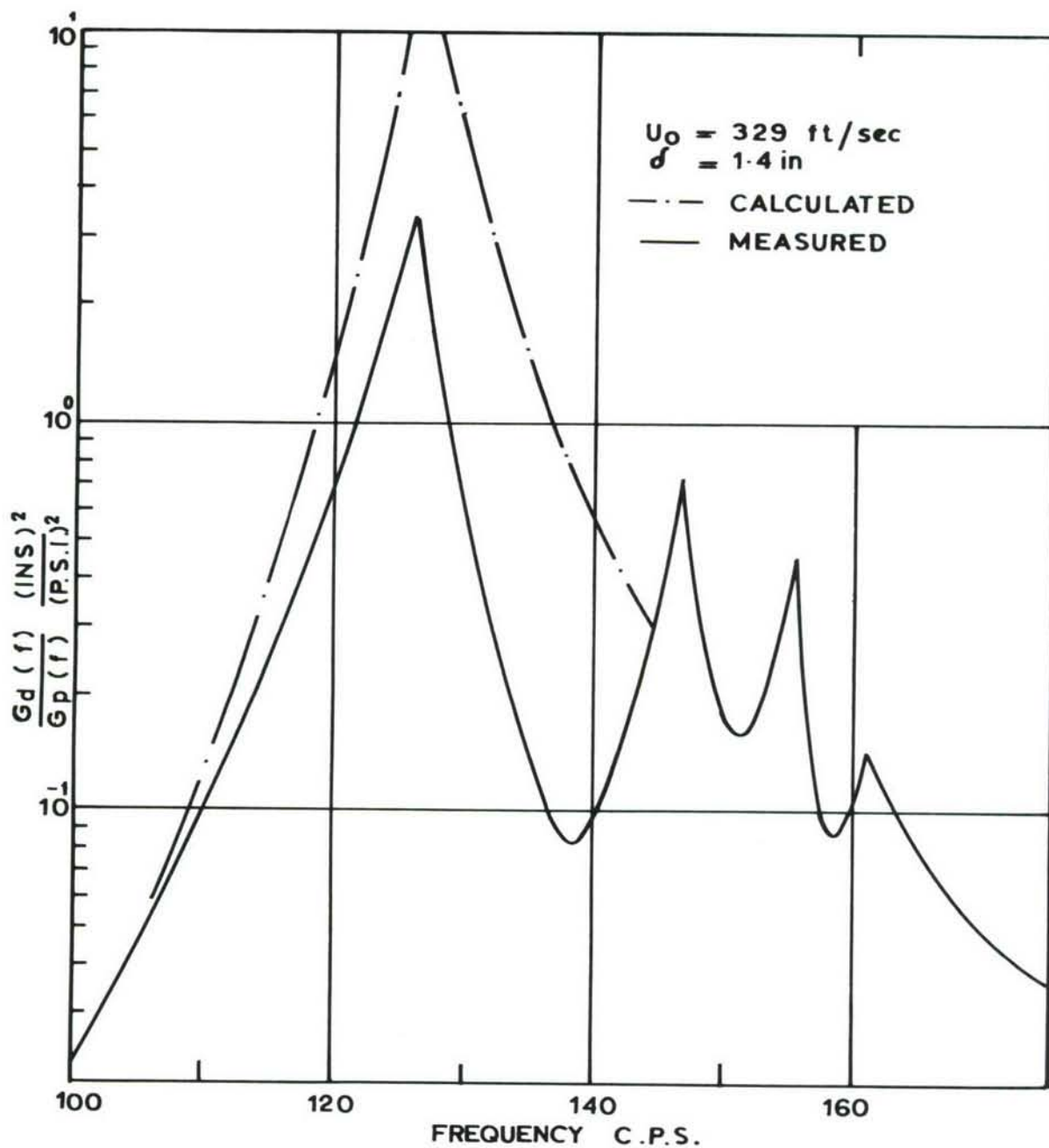


Fig. 34 Response spectra for 4 bay array: boundary layer excitation.

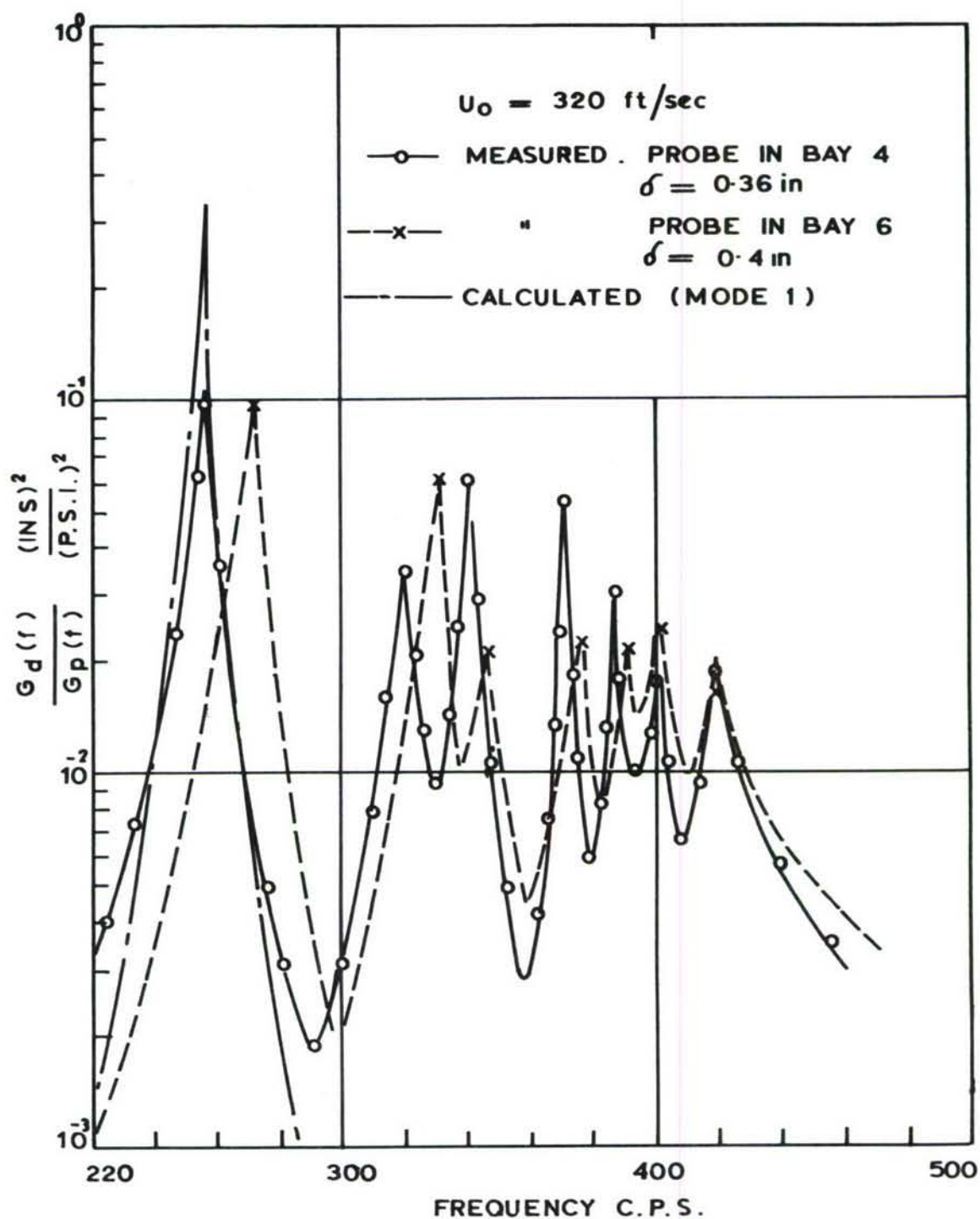


Fig. 35. Response spectra for 8-bay array :
boundary layer excitation.

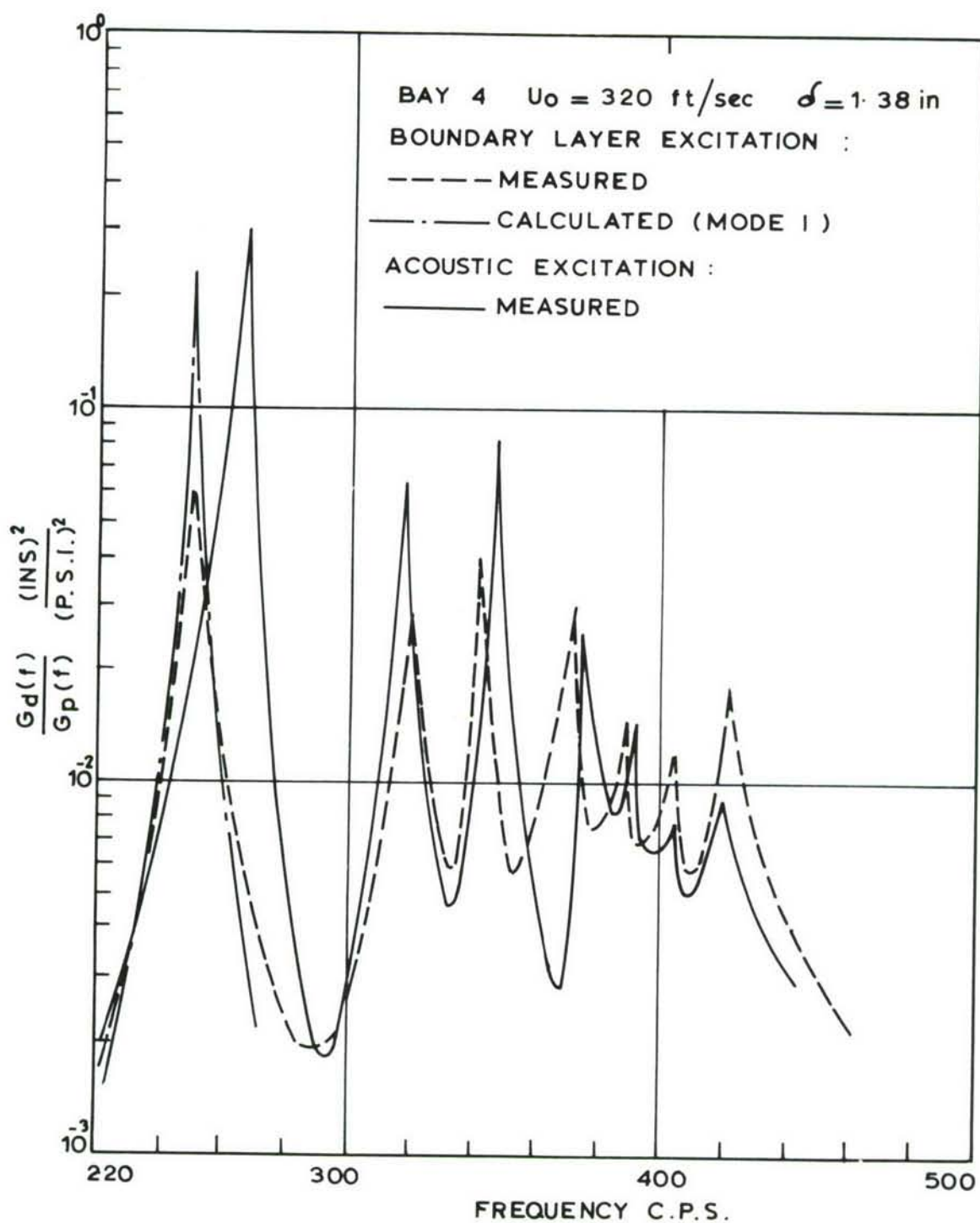


Fig. 36 Response spectra for 8 bay array :
boundary layer and acoustic excitation.

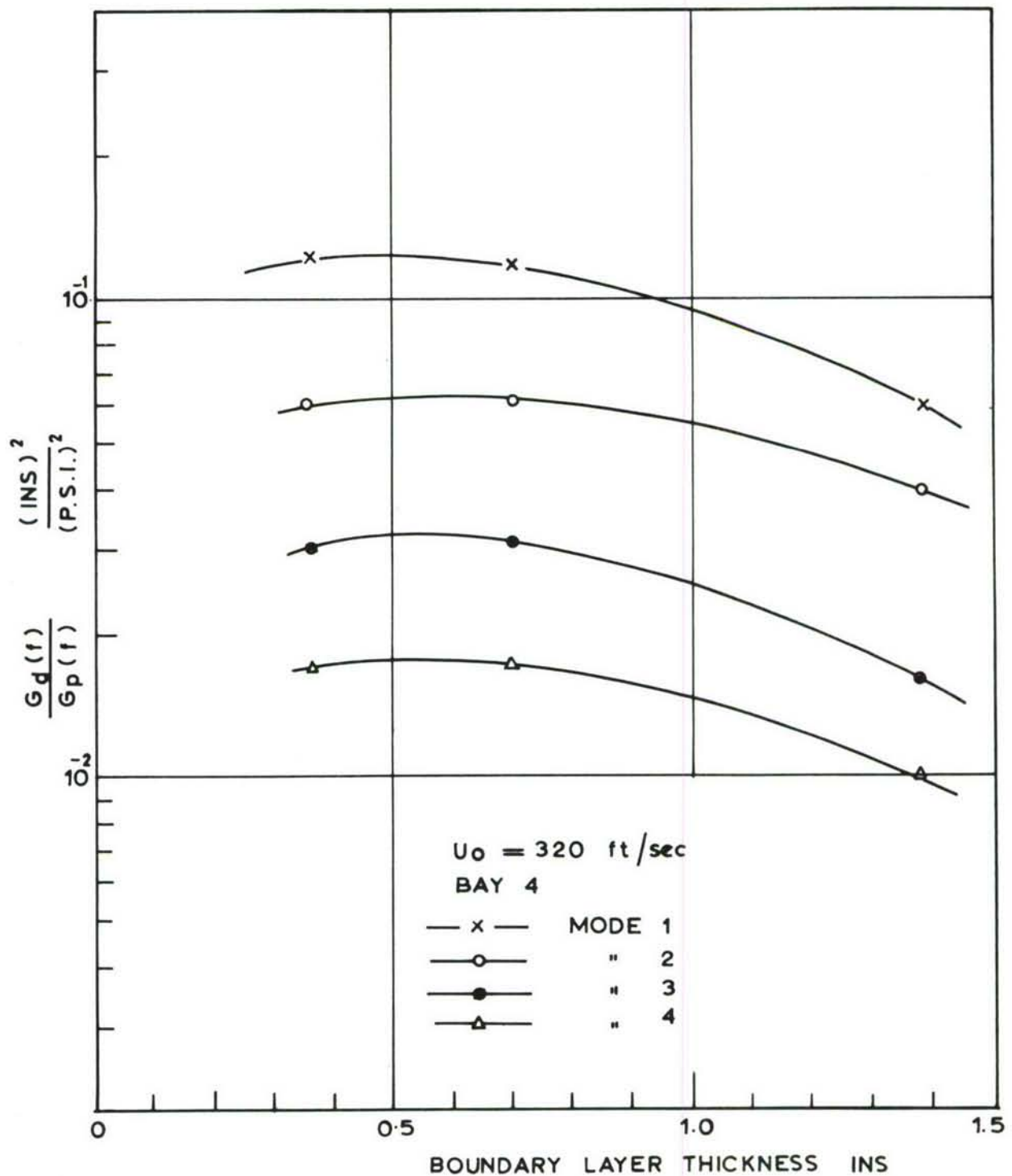


Fig. 37 Measured variation of modal response with boundary layer thickness: eight-bay array.

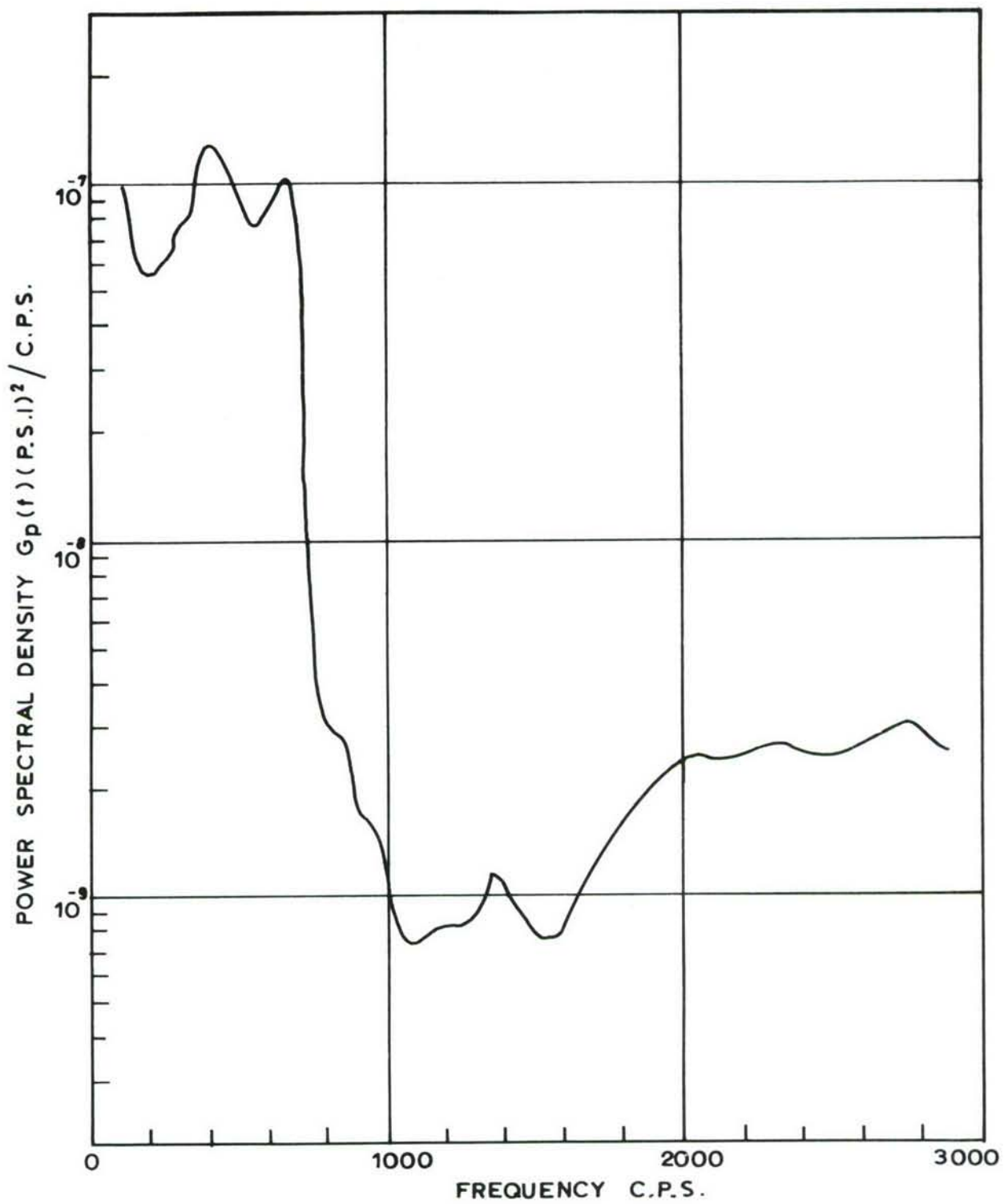


Fig. 38. Noise spectrum in the siren tunnel.

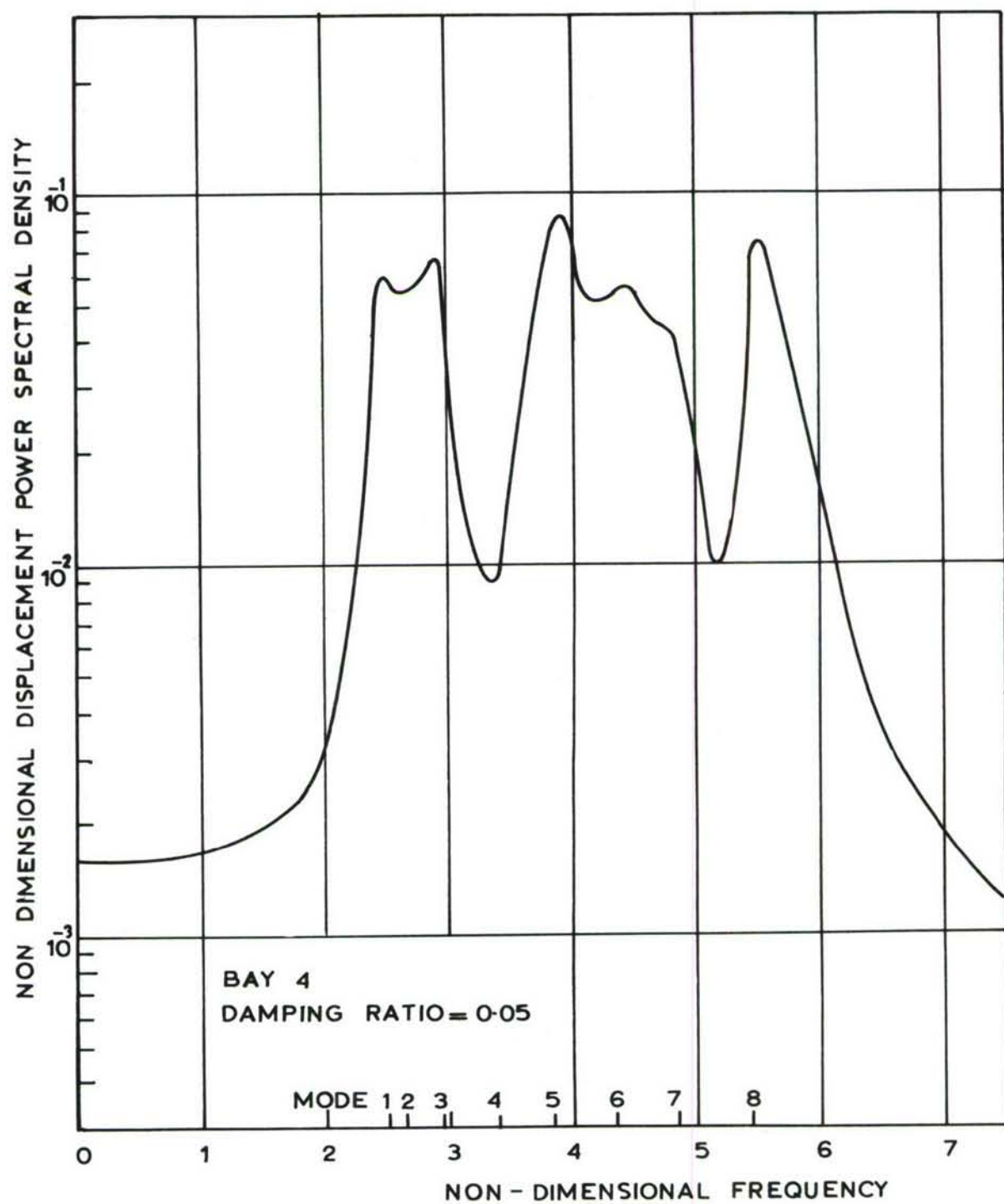


Fig.39 Theoretical response of 8-bay array to acoustic excitation.

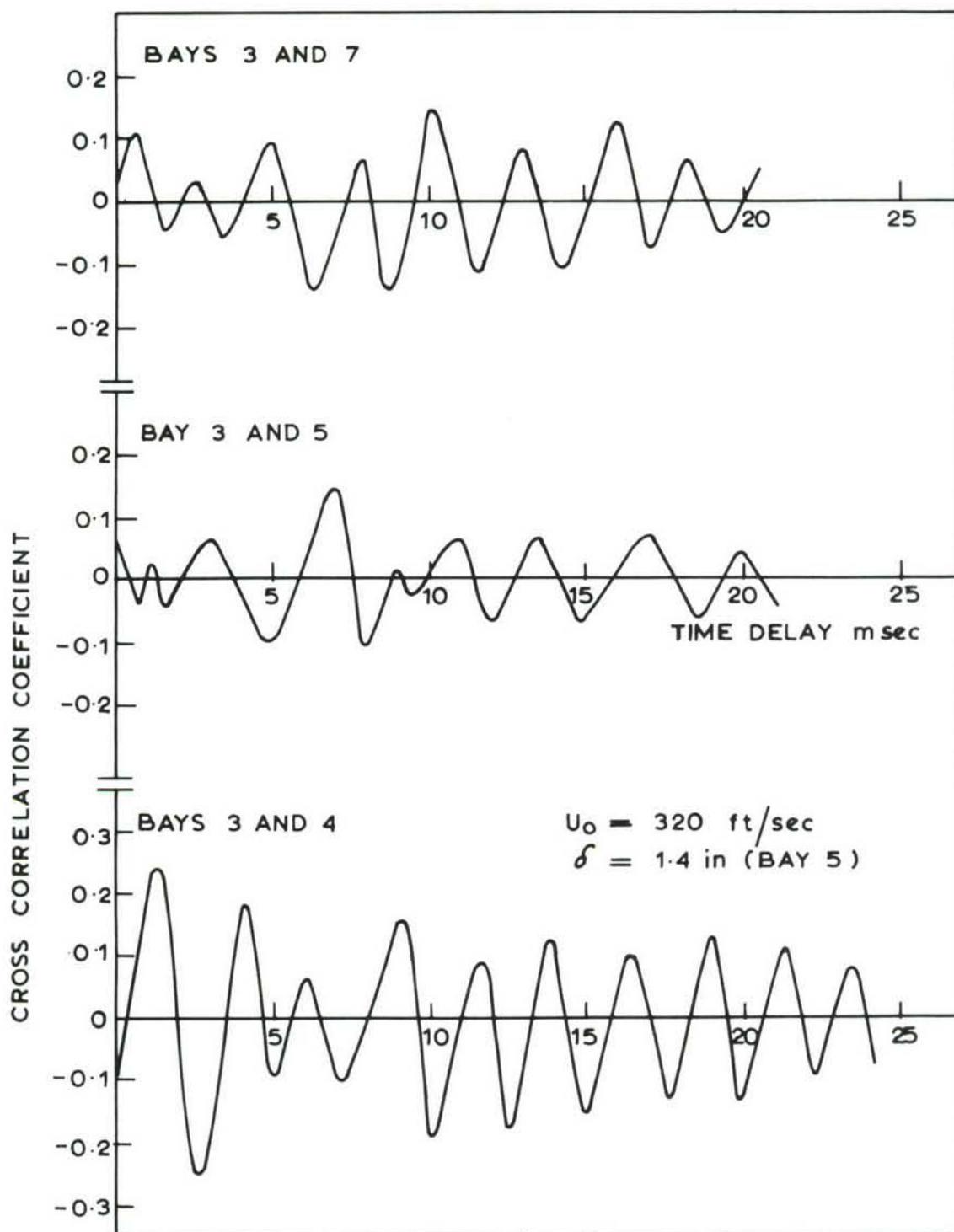


Fig. 40. Displacement cross correlation coefficient for 8-bay array : datum bay 3 .

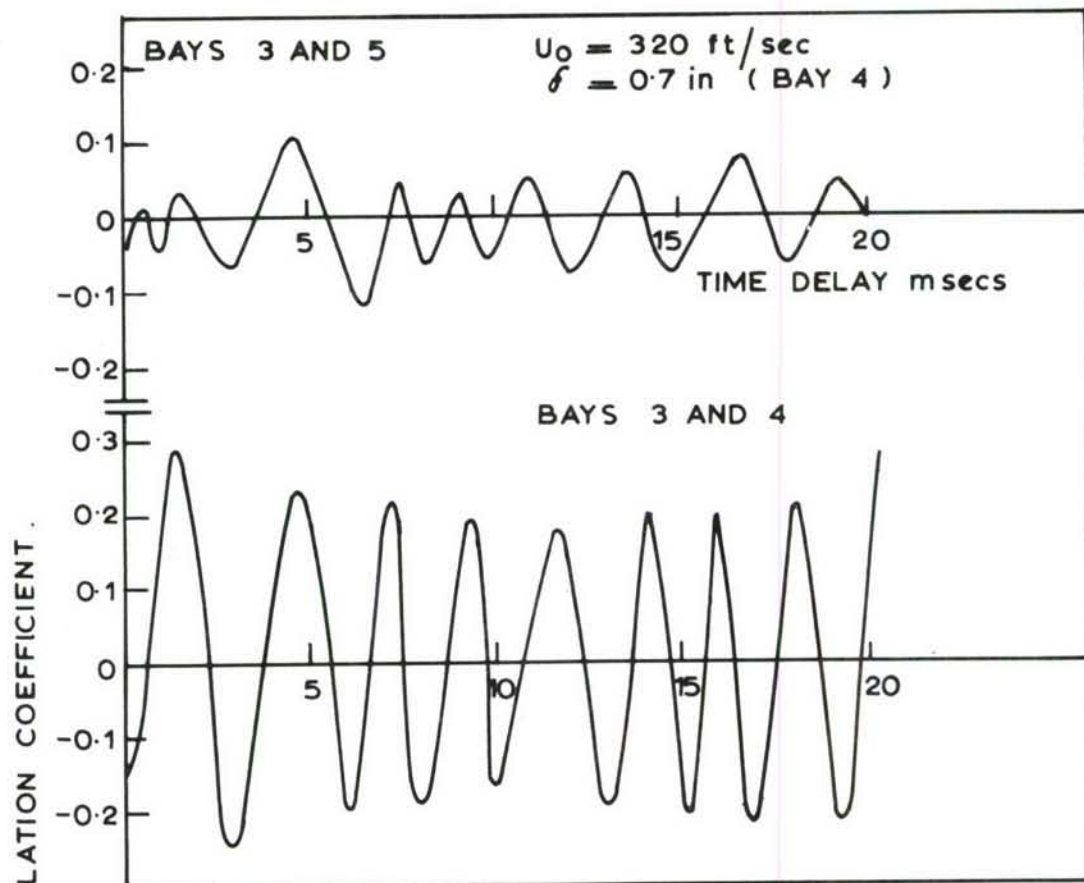


Fig. 41. Displacement cross correlation coefficient for 8 bay array: datum bay 3.

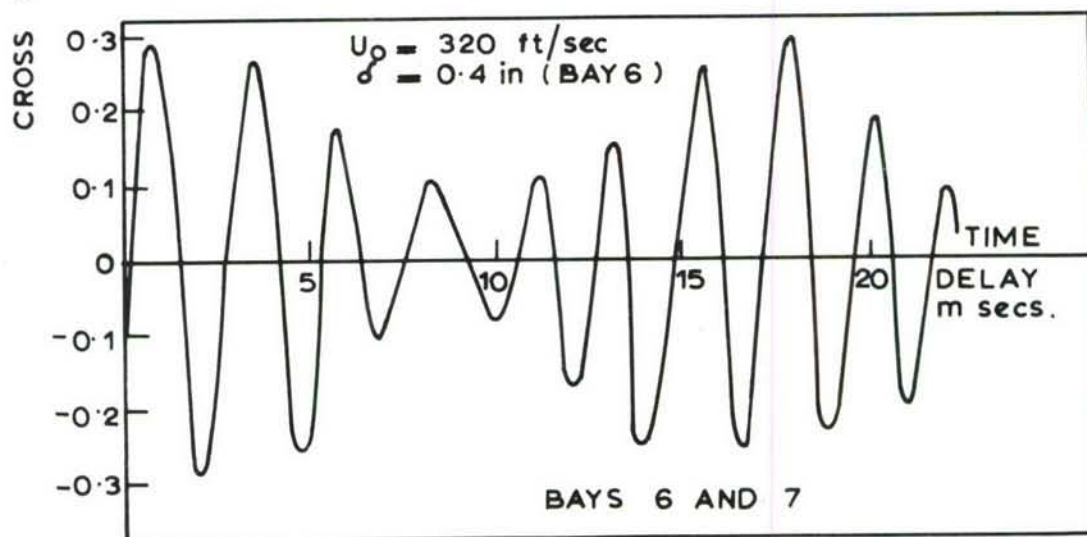


Fig. 42. Displacement cross correlation coefficient for 8-bay array: datum bay 6.

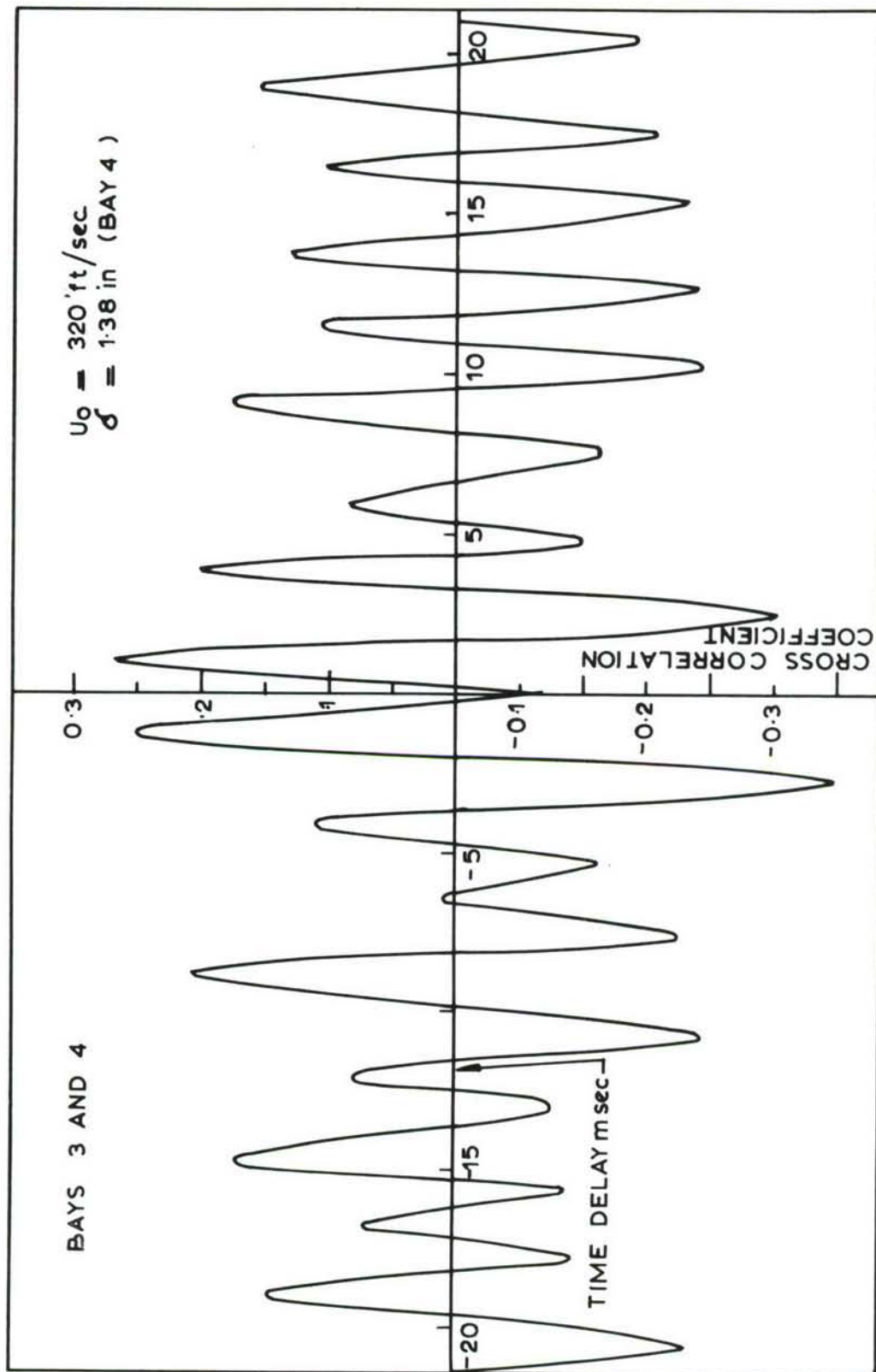


Fig.43 . Displacement cross correlation coefficient for 8 bay array :
 one bay separation

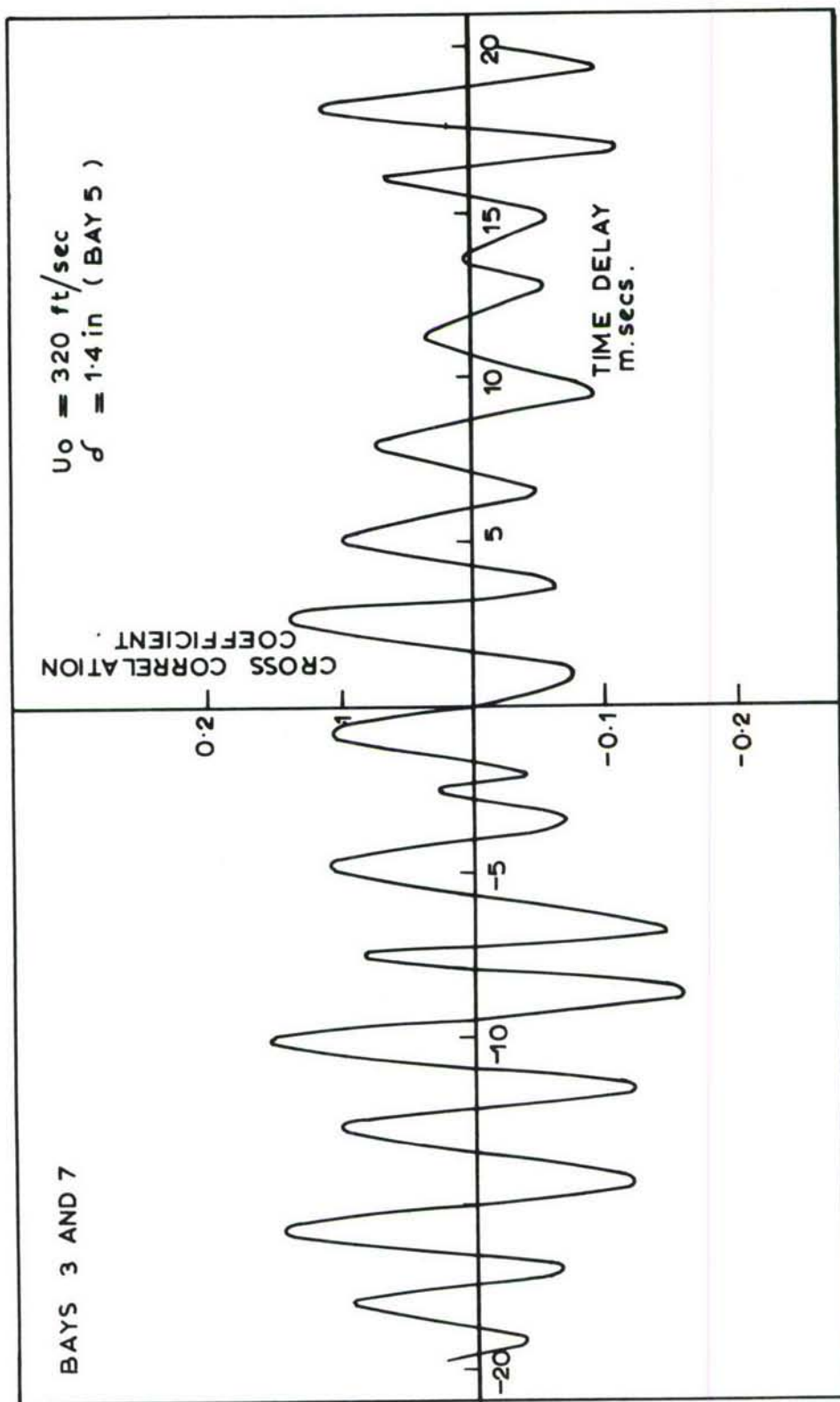


Fig. 44 . Displacement cross correlation coefficient for 8-bay array :
four bay separation.

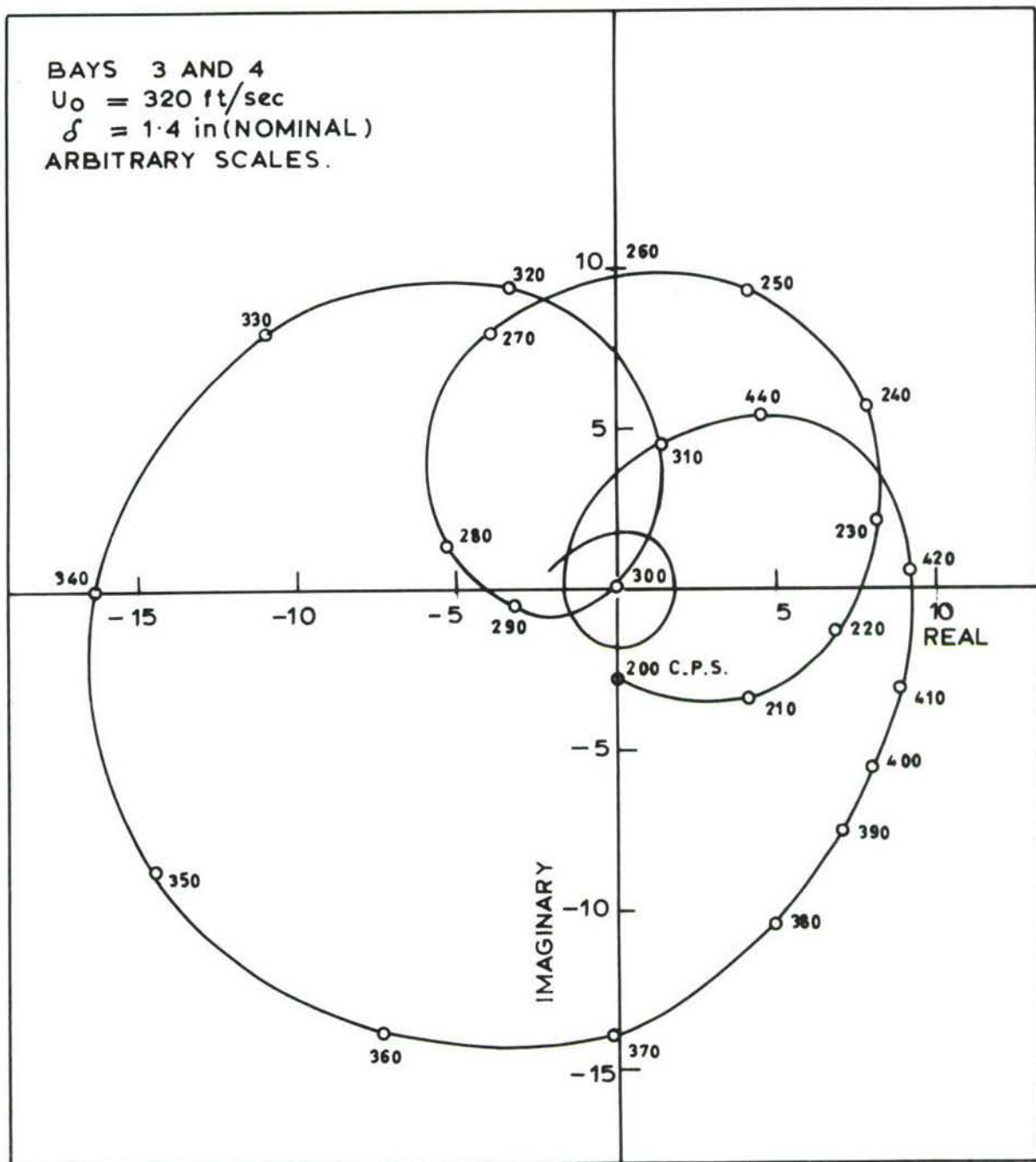


Fig. 45 Displacement cross power spectrum for bays 3 and 4 of 8 bay array : boundary layer excitation.

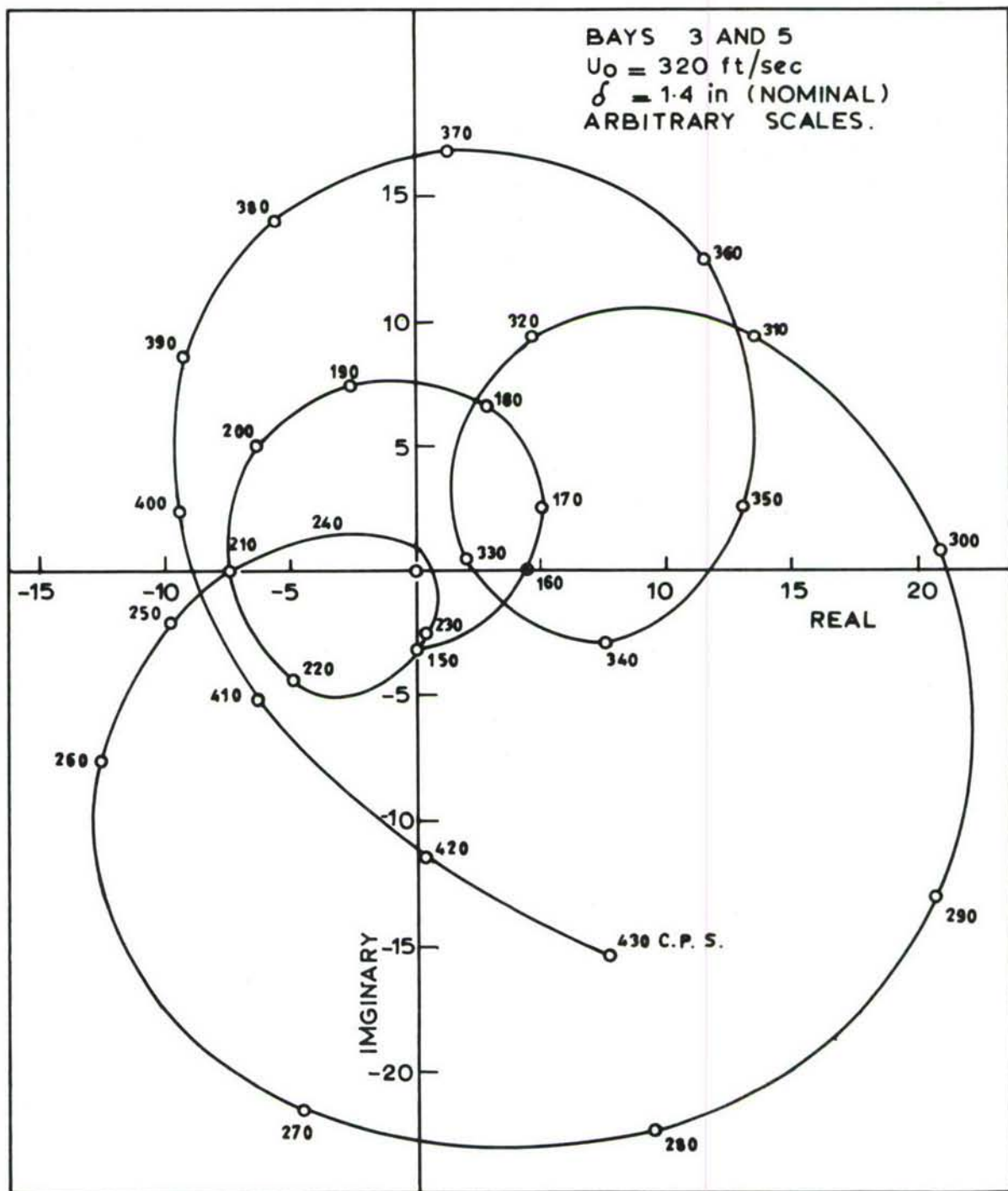


Fig. 46. Displacement cross power spectrum for bays 3 and 5 of 8-bay array: boundary layer excitation.

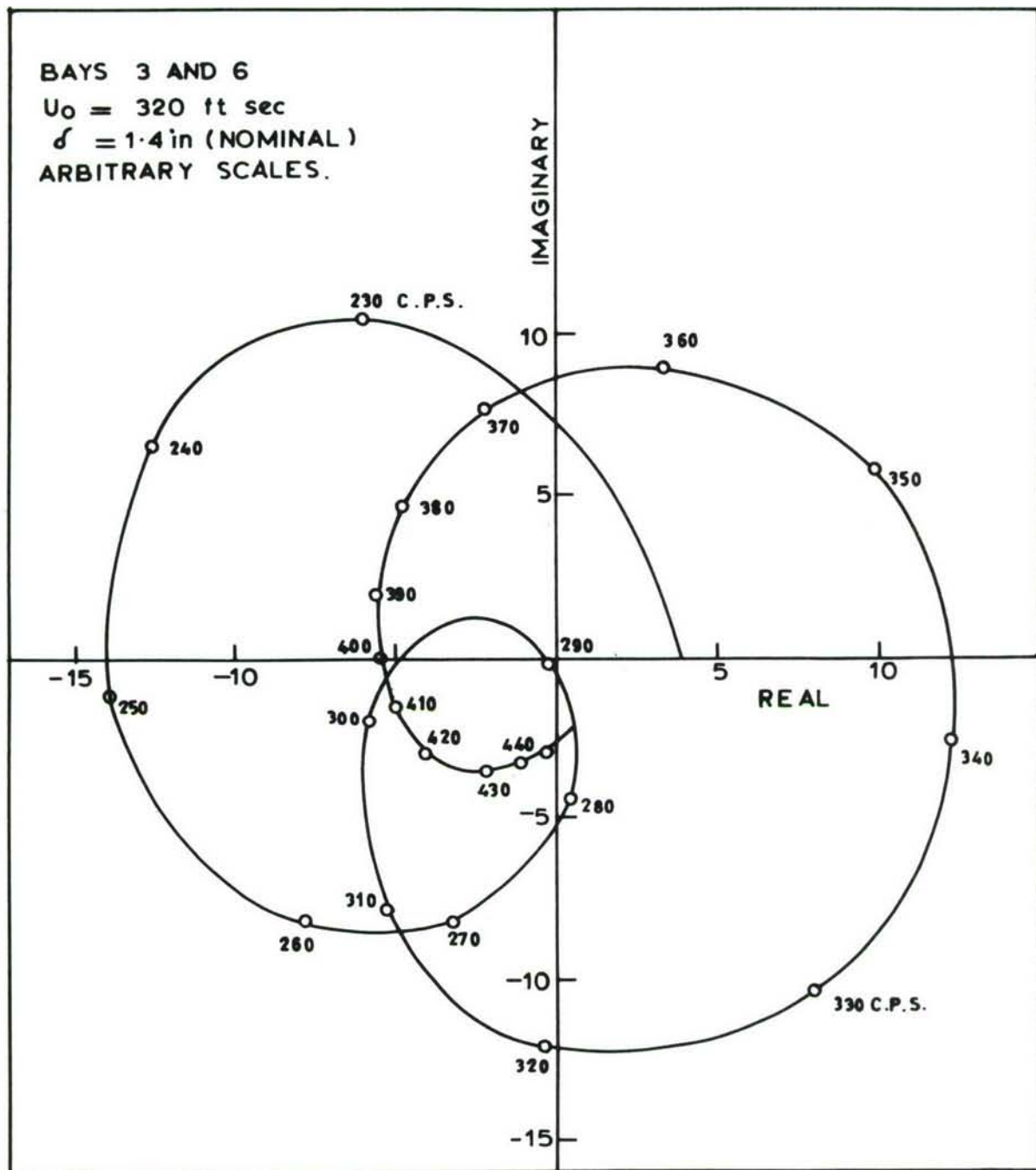


Fig. 47. Displacement cross power spectrum for bays 3 and 6 of 8-bay array : boundary layer excitation.

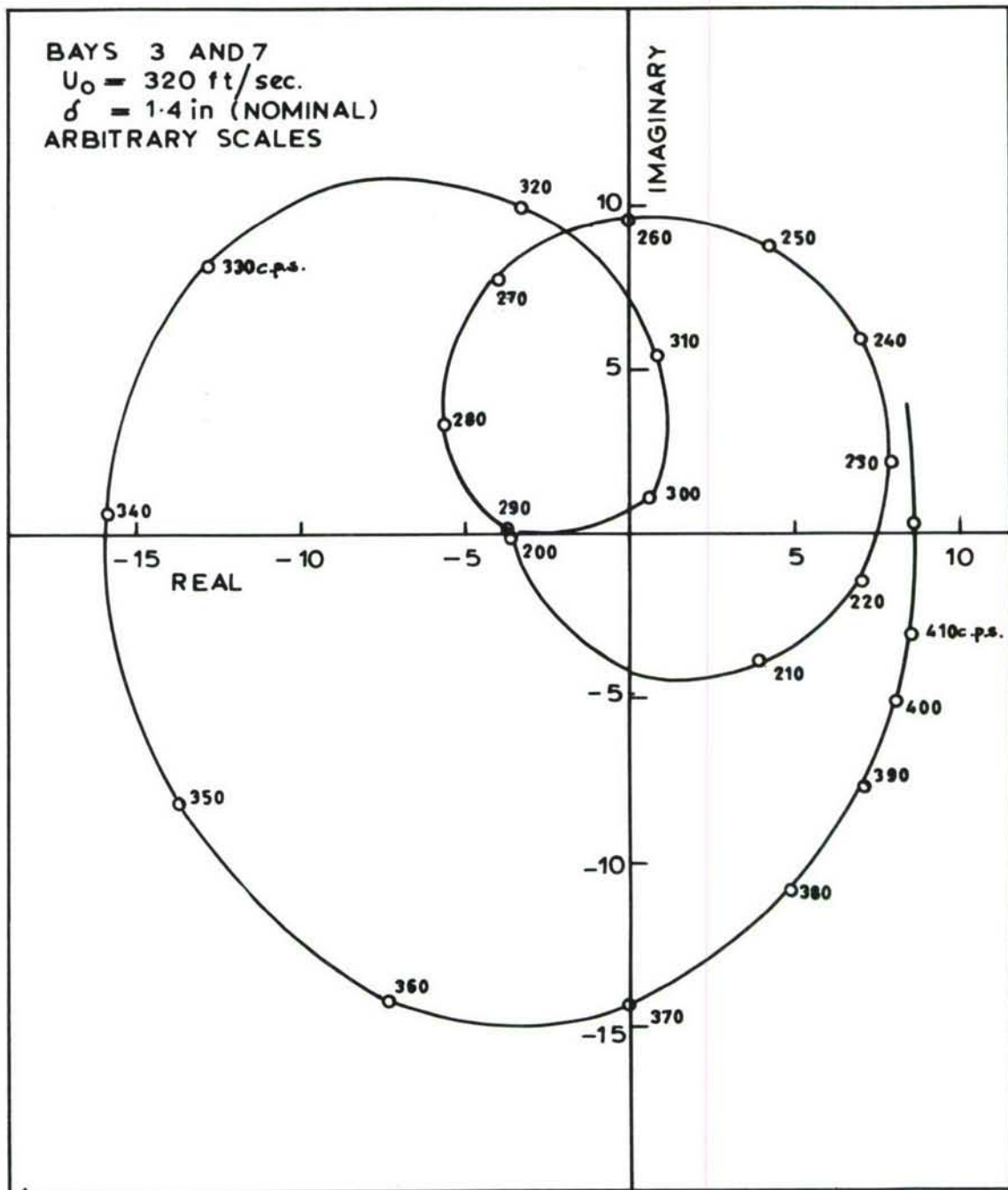


Fig. 48. Displacement cross power spectrum for bays 3 and 7 of 8-bay array: boundary layer excitation.

Unclassified

Security Classification

DOCUMENT CONTROL DATA - R&D

(Security classification of title, body of abstract and indexing annotation must be entered when the overall report is classified)

1. ORIGINATING ACTIVITY (Corporate author) Institute of Sound and Vibration Research, University of Southampton, Hampshire, England.		2a. REPORT SECURITY CLASSIFICATION Unclassified	
		2b. GROUP	
3. REPORT TITLE BOUNDARY LAYER PRESSURE FLUCTUATIONS AND STRUCTURAL RESPONSE			
4. DESCRIPTIVE NOTES (Type of report and inclusive dates) Final Scientific Report 1 November 1963 - 30 November 1966.			
5. AUTHOR(S) (Last name, first name, initial) Blackman, Deane R., Clark, Duncan M., McNulty, George J., and Wilby, John F.			
6. REPORT DATE October 1967		7a. TOTAL NO. OF PAGES 117	7b. NO. OF REFS 29
8a. CONTRACT OR GRANT NO. Contract AF61(052)-756		8a. ORIGINATOR'S REPORT NUMBER(S) AFFDL-TR-67-97	
b. PROJECT NO. 1471		8b. OTHER REPORT NO(S) (Any other numbers that may be assigned this report)	
c. Task No. 147102			
10. AVAILABILITY/LIMITATION NOTICES This document is subject to special export controls and each transmittal to foreign government or foreign nationals may be made only with prior approval of AF Flight Dynamics Laboratory (FDDA), WPAFB, Ohio			
11. SUPPLEMENTARY NOTES		12. SPONSORING MILITARY ACTIVITY Air Force Flight Dynamics Laboratory Wright-Patterson AFB, Ohio 45433	
13. ABSTRACT Investigations of the pressure fluctuations under a turbulent boundary layer, and the resultant vibration of simple panels, have been extended to consider the vibration of stringer-panel arrays and the intermittent pressure field in the boundary layer transition region. The response of multi-panel arrays to turbulent boundary layer excitation has been measured for a flow speed of 320 ft./sec.* Displacement spectra for the first band of modes, measured at the bay centres, have been compared with results due to acoustic excitation at grazing incidence. The vibration in the lower order modes is greater for the acoustic excitation but the converse is true for the higher order modes. Displacement cross correlation measurements show the presence of standing waves for distances up to three bay lengths but the wave system breaks down over larger distances. A comparison of random techniques used in structural damping measurements shows the autocorrelation decay method to be the most reliable. Using specially constructed gating apparatus, pressure measurements in the laminar-turbulent transition region show that the turbulent spots are autonomous regions of turbulent boundary layer, with similar pressure spectra. In addition there are low frequency pressure fluctuations due to the disturbances produced by the pressure steps on the mean flow. The background noise levels in the wind tunnel have been measured.			

DD FORM 1473

Distribution of this Abstract is
Unlimited

Unclassified

Security Classification

14. KEY WORDS	LINK A		LINK B		LINK C	
	ROLE	WT	ROLE	WT	ROLE	WT
Boundary Layer Transition Turbulent spots Pressure fluctuations Wind tunnel noise Damping Random analysis Panels Panel-stiffener arrays Vibration spectra Vibration correlation						

INSTRUCTIONS

1. **ORIGINATING ACTIVITY:** Enter the name and address of the contractor, subcontractor, grantee, Department of Defense activity or other organization (*corporate author*) issuing the report.

2a. **REPORT SECURITY CLASSIFICATION:** Enter the overall security classification of the report. Indicate whether "Restricted Data" is included. Marking is to be in accordance with appropriate security regulations.

2b. **GROUP:** Automatic downgrading is specified in DoD Directive 5200.10 and Armed Forces Industrial Manual. Enter the group number. Also, when applicable, show that optional markings have been used for Group 3 and Group 4 as authorized.

3. **REPORT TITLE:** Enter the complete report title in all capital letters. Titles in all cases should be unclassified. If a meaningful title cannot be selected without classification, show title classification in all capitals in parenthesis immediately following the title.

4. **DESCRIPTIVE NOTES:** If appropriate, enter the type of report, e.g., interim, progress, summary, annual, or final. Give the inclusive dates when a specific reporting period is covered.

5. **AUTHOR(S):** Enter the name(s) of author(s) as shown on or in the report. Enter last name, first name, middle initial. If military, show rank and branch of service. The name of the principal author is an absolute minimum requirement.

6. **REPORT DATE:** Enter the date of the report as day, month, year; or month, year. If more than one date appears on the report, use date of publication.

7a. **TOTAL NUMBER OF PAGES:** The total page count should follow normal pagination procedures, i.e., enter the number of pages containing information.

7b. **NUMBER OF REFERENCES:** Enter the total number of references cited in the report.

8a. **CONTRACT OR GRANT NUMBER:** If appropriate, enter the applicable number of the contract or grant under which the report was written.

8b, 8c, & 8d. **PROJECT NUMBER:** Enter the appropriate military department identification, such as project number, subproject number, system numbers, task number, etc.

9a. **ORIGINATOR'S REPORT NUMBER(S):** Enter the official report number by which the document will be identified and controlled by the originating activity. This number must be unique to this report.

9b. **OTHER REPORT NUMBER(S):** If the report has been assigned any other report numbers (either by the originator or by the sponsor), also enter this number(s).

10. **AVAILABILITY/LIMITATION NOTICES:** Enter any limitations on further dissemination of the report, other than those

imposed by security classification, using standard statements such as:

- (1) "Qualified requesters may obtain copies of this report from DDC."
- (2) "Foreign announcement and dissemination of this report by DDC is not authorized."
- (3) "U. S. Government agencies may obtain copies of this report directly from DDC. Other qualified DDC users shall request through _____."
- (4) "U. S. military agencies may obtain copies of this report directly from DDC. Other qualified users shall request through _____."
- (5) "All distribution of this report is controlled. Qualified DDC users shall request through _____."

If the report has been furnished to the Office of Technical Services, Department of Commerce, for sale to the public, indicate this fact and enter the price, if known.

11. **SUPPLEMENTARY NOTES:** Use for additional explanatory notes.

12. **SPONSORING MILITARY ACTIVITY:** Enter the name of the departmental project office or laboratory sponsoring (paying for) the research and development. Include address.

13. **ABSTRACT:** Enter an abstract giving a brief and factual summary of the document indicative of the report, even though it may also appear elsewhere in the body of the technical report. If additional space is required, a continuation sheet shall be attached.

It is highly desirable that the abstract of classified reports be unclassified. Each paragraph of the abstract shall end with an indication of the military security classification of the information in the paragraph, represented as (TS), (S), (C), or (U).

There is no limitation on the length of the abstract. However, the suggested length is from 150 to 225 words.

14. **KEY WORDS:** Key words are technically meaningful terms or short phrases that characterize a report and may be used as index entries for cataloging the report. Key words must be selected so that no security classification is required. Identifiers, such as equipment model designation, trade name, military project code name, geographic location, may be used as key words but will be followed by an indication of technical context. The assignment of links, rules, and weights is optional.